Contribution to the understanding of the poromechanical behavior of cement-based materials and geomaterials

Thèse présentée pour l'obtention de

l'**Habilitation à Diriger des Recherches**

Spécialité : Génie Civil

UNIVERSITÉ PARIS-EST

Université Paris-Est

École doctorale : Sciences, Ingénierie et Environnement

par

Matthieu VANDAMME

soutenue le 21 janvier 2019 devant le jury composé de :

Pietro LURA,	rapporteur
Noushine SHAHIDZADEH,	rapporteur
Christopher J. SPIERS,	rapporteur
Jan CARMELIET,	examinateur
Benoit COASNE,	examinateur
Jean-Michel PEREIRA,	examinateur
Gilles PIJAUDIER-CABOT,	examinateur

“Что делать?”
What is to be done?
– В. И. Ульянов (Lenin).

“Мы не сделаем вас умнее, мы научим вас думать”
We will not make you smarter, we will teach you to think.
– Motto of Novosibirsk State University.

A Marina, Misha, et Muse.

Acknowledgements

I would like first of all to thank my scientific mentors. Alain Ehrlacher was the director of my master internship, and I remember his intellectual skills and how quickly, when meeting with his various students, he could switch from one scientific topic to another. I am grateful to Franz-Josef Ulm for giving me the opportunity to perform a Ph.D. at MIT under his direction. The work I performed then was a great hands-on and experimental complement to my French studies, which were more oriented toward theory. Among other things, I have always been impressed by his ability to analyze experimental data and to make interesting and meaningful trends pop out of them, as well as by his intuition. Finally, I think of Olivier Coussy, who helped me a lot upon my arrival in France after my Ph.D. studies, and made me familiar with poromechanics and thermodynamics of porous materials. I would like to thank him for that, but also for having founded Laboratoire Navier: even though Olivier passed away more than half a decade ago, the dynamics he impulsed is still lasting, which makes Laboratoire Navier a great environment to work in, of which I benefit every day.
I want to thank my colleagues and collaborators: at Laboratoire Navier, in particular, Jean-Michel Pereira and Patrick Dangla. Likewise, co-advising students or working with Jean-Michel Torrenti, Henri Van Damme, Kim Kurtis, Zdeněk Bažant, Ippei Maruyama, or Roland Pellenq has always been a pleasure and taught me a lot.
I would like also to thank my actual and former industrial partners: Total, Schlumberger, EdF, and LafargeHolcim. I am grateful to them for their financial support, but also for the opportunity they give me to work on problems of societal interest and to interact with experts of their applications. Special thanks go to Lafarge (now LafargeHolcim), which has been supporting me continuously since my Ph.D. studies. At Lafarge, my thoughts go to Gilles Chanvillard, and in particular to his expertise and his kindness.
Finally, I would like to thank all my students for their work. I wish I would spend more time with them, but I hope they learned something with me.

Paris, France, November 2018
Matthieu VANDAMME

Abstract

I wrote this memoir to obtain my 'Habilitation à Diriger des Recherches'. It contains an overview of my main research results. After a brief description of my research profile, I describe in detail two themes on which I have worked significantly: adsorption-induced variations of permeability of coal seams, and time-dependent deformations of cement-based materials. I then turn to other topics more briefly to give an overview of the range of materials and physical processes that I have encountered. After having mentioned throughout the manuscript conclusions and perspectives related to each individual topic, I conclude this thesis with some reflections of synthesis and some more general perspectives.

Résumé

J'ai écrit ce mémoire en vue de l'obtention de mon Habilitation à Diriger des Recherches. Il contient un aperçu de mes principaux résultats de recherche. Après une brève description de mon profil de recherche, je décris en détail deux thématiques sur lesquelles j'ai travaillé significativement: les variations de perméabilité des veines de charbon associées aux phénomènes d'adsorption, et les comportements différés des bétons. J'aborde ensuite plus brièvement d'autres thématiques, afin de donner un aperçu de l'éventail des matériaux et processus physiques auxquels je me suis confronté. Après avoir explicité tout au long du manuscrit conclusions et perspectives relatives à chaque thématique individuelle, je termine ce mémoire par quelques réflexions de synthèse et de perspective plus générales.

Contents

List of Figures

List of Tables

1 Introduction

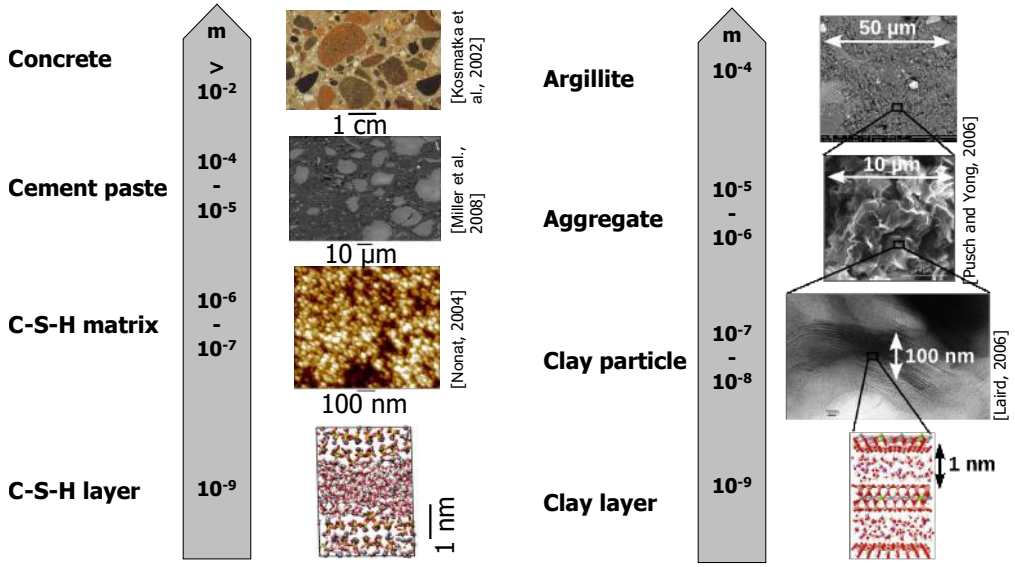

Figure 1.1 – Multiscale structure of (left) concrete and (right) argillite. C-S-H stands for calcium silicate hydrates. Subfigures are adapted from Kosmatka et al. (2002); Miller et al. (2008); Nonat (2004); Pusch and Yong (2006); Laird (2006).

Research profile

A civil engineer, I focus on materials relevant for civil engineering applications in the broad sense of the term (i.e., for construction, but also for energy applications). I am interested in, namely, cement-based materials, soils, or rocks. All those materials have a lot in common (see Fig. 1.1 for the example of concrete and argillite): they are disordered, heterogeneous, multiscale, and their porosity spans several orders of magnitude down to the nanometer scale.

I am particularly interested in the fact that those materials are porous, and in the study of how in-pore processes impact the mechanical behavior of porous materials. This field of study is called poromechanics.

I am rather a modeler, but with an experience in experiments. Most of the projects I co-advised contained some experimental work.

Although a mechanician, I have a keen interest in physics, and take great pleasure in interacting with colleagues with complementary skills, such as physicists or physical chemists, with whom thermodynamics often provides the lingua franca.

Research background

I started my research during my master internship in 2003, which was devoted to the study of piezoelectric multilayer plates. I worked under the supervision of Alain Ehrlacher and Jean-François Caron, at École des Ponts ParisTech (École Nationale des Ponts et Chaussées at

the time). My master research was dedicated to modeling: I aimed at deriving state equations for such plates, based on an energy approach.

My Ph.D. studies lasted from 2004 to 2008. I worked on the "nanogranular origin of concrete creep: A nanoindentation investigation of microstructure and fundamental properties of calcium-silicate-hydrates". Those Ph.D. studies, performed under the supervision of Franz-Josef Ulm, were mostly experimental. They gave me a taste for cement-based materials, and for the study of what occurs at the small scales.

After my Ph.D. studies, I readily took a position in 2008 as research scientist at École des Ponts ParisTech. I arrived in the newly formed Laboratoire Navier, founded and first directed by Oliver Coussy, who was a leading expert in poromechanics. He mentored me in this field, and gave me the opportunity to collaborate with him on his research projects.

A significant part of my research is linked to the industry. My Ph.D. studies were funded by Lafarge. Since then, I kept a permanent link with this company (now LafargeHolcim). When I arrived at Laboratoire Navier, Olivier Coussy integrated me in a research project he was undertaking with Schlumberger on CO_2-enhanced coal bed methane recovery and adsorption-induced deformations. Once Schlumberger decided to stop working on CO_2 storage in coal beds, Brice Lecampion at Schlumberger redirected Total toward us, and I went on working on this topic with Total. I also worked with EDF, on the concrete containment of nuclear power plants, in a project led by Jean-Michel Torrenti.

Organization of manuscript

This memoir aims at providing an overview of my research activities. Rather than aiming at exhaustiveness, I made the choice to present 2 topics in more depth, as they are quite representative of my main scientific skills and interests. Those 2 topics are adsorption-induced variations of permeability of coal seams (see chapter 2) and time-dependent deformations of cement-based materials (see chapter 3).

In contrast, chapter 4 provides a briefer description of other topics, namely freeze-thaw resistance of cement-based materials (see section 4.1), crystallization-induced expansion of cement-based materials (see section 4.2), drying shrinkage of cement-based materials (see section 4.3), drying-induced collapse of partially saturated sand (see section 4.4), and impact of moisture on mechanical properties of clay (see section 4.5). I thus aim at giving an idea of the variety of materials (coal, cement-based materials, clay, sand) and of physical processes (adsorption, drying, crystallization,...) on which I worked.

In addition to the conclusions and perspectives provided at the end of each section, chapter 5 provides some general synthesis and more global perspectives.

On each topic, I aimed at presenting the results that I deemed the most interesting. I also use the opportunity of this memoir to try to underline the approach chosen to tackle each topic,

and the reasons why we made some of the choices that we had to make along the way. I also provide perspectives that I consider of interest.

The related Ph.D. students or post-doctoral students, articles, and colleagues involved are indicated at the beginning of each relevant section.

2 Adsorption-induced variations of permeability of coal seams

2.1 Context of study

Ph.D. students: Laurent BROCHARD, Saeid NIKOOSOKHAN.

Postdoctoral student: D. Nicolas ESPINOZA.

Colleagues involved: Olivier COUSSY, Patrick DANGLA, Jean-Michel PEREIRA, Brice LECAMPION (Schlumberger), Sandrine VIDAL-GILBERT (Total), Roland J.-M. PELLENQ (UMI CNRS-MIT, Aix-Marseille Université).

When I arrived at Laboratoire Navier in 2008, Oliver Coussy invited me to work with him and educated me in poromechanics. He involved me in the Ph.D. project of Laurent Brochard that he directed, co-advised by Roland Pellenq and in collaboration with Brice Lecampion at Schlumberger, on CO_2 storage in coal seams. Olivier had seen the potential in making poromechanics (i.e., him) interact with molecular simulations (i.e, Roland Pellenq). In the continuity of Laurent Brochard's Ph.D. studies, I obtained funding for a Ph.D. from École des Ponts ParisTech to go on working on CO_2 storage in coal seams (Ph.D. thesis of Saeid Nikoosokhan, directed initially by Olivier Coussy and then by Patrick Dangla). When Schlumberger decided to stop working on underground CO_2 storage, Brice Lecampion kindly redirected Sandrine Vidal from Total toward us, as Total was still interested in the topic. Total funded the 2 years of post-doc of Nicolas Espinoza on CO_2-enhanced coal-bed methane recovery.

The application of this study is CO_2-enhanced coal-bed methane recovery, or CO_2-ECBM (see Fig. 2.1). Deep underground coal seams naturally contain CH_4 (i.e., methane), which the energy industry wants to produce. To recover more methane and recover it faster, one can drill an injection well, through which a fluid is injected, to "push" methane toward the production well. Such process is known as enhanced coal-bed methane recovery (or ECBM) in general, and as CO_2-enhanced coal-bed methane recovery (or CO_2-ECBM) when the injected fluid is CO_2 (i.e., carbon dioxide). Coal beds could also contribute to store CO_2 in the underground, up to 20 Gt (Gale, 2004).

Upon production of methane, significant variations of permeability are observed over time (Moore et al., 2011), as can be seen in Fig. 2.2: these field data show that production of methane initially increased the apparent permeability of the reservoir by more than 1 order of magnitude. Injections of carbon dioxide during CO_2-ECBM also induce significant variations of permeability, but in an opposite manner: over the injection, the permeability of the reservoir decreases significantly. The aim of the study was to model those variations of permeability and provide state equations that could be implemented into a reservoir code. The motivation for the industry was better management of the well and estimation of the economic viability of the exploitation of the reservoir.

Coal is a material that is natural fractured (Laubach et al., 1998): those fractures are called cleats, vary in size, are mostly vertical, and are spaced by about a centimeter (see Fig. 2.3). Cleats govern the permeability of the bed (Mazumder et al., 2006; Pan and Connell, 2007).

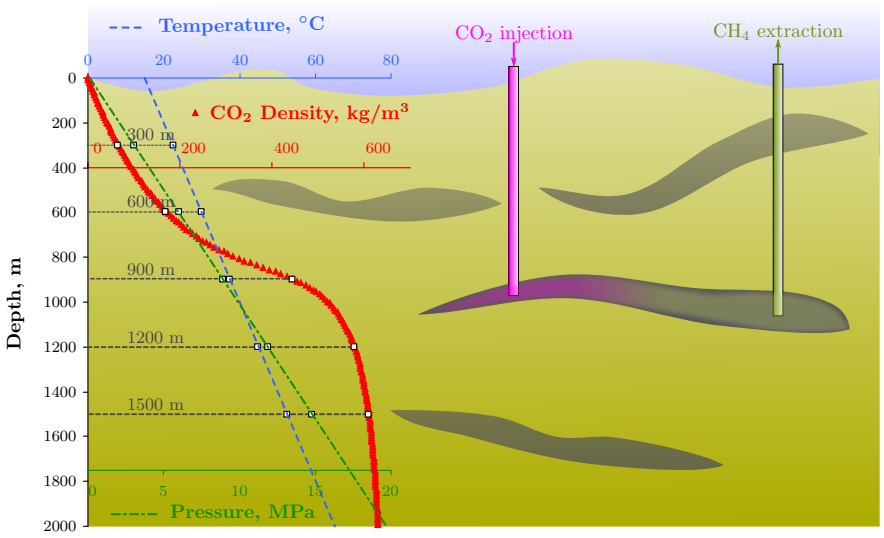

Figure 2.1 – Coal bed methane recovery enhanced with carbon dioxide injection. Figure from Brochard (2011).

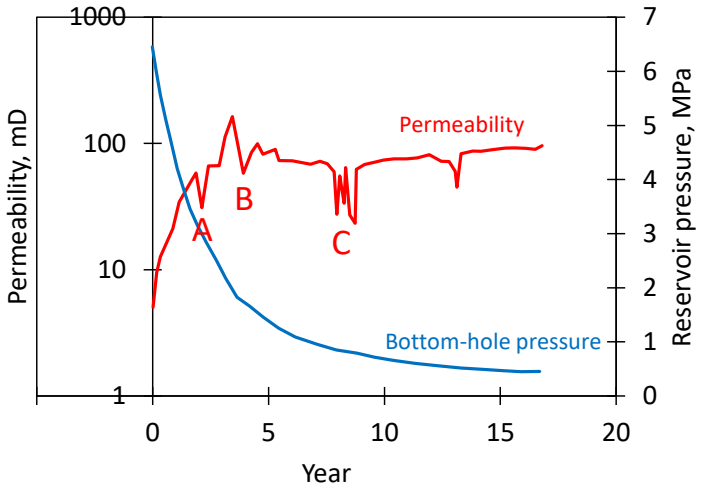

Figure 2.2 – Coal bed reservoir response during depletion: bottom-hole pressure and apparent permeability of the reservoir versus time. Note that sudden permeability reductions (indicated as A, B, and C) take place as bottom-hole pressure is reduced. The permeability drops are associated with coal failure events. The last permeability drop (C) is recovered after wellbore clean-up operations only. Figure adapted from field experimental data by Moore et al. (2011).

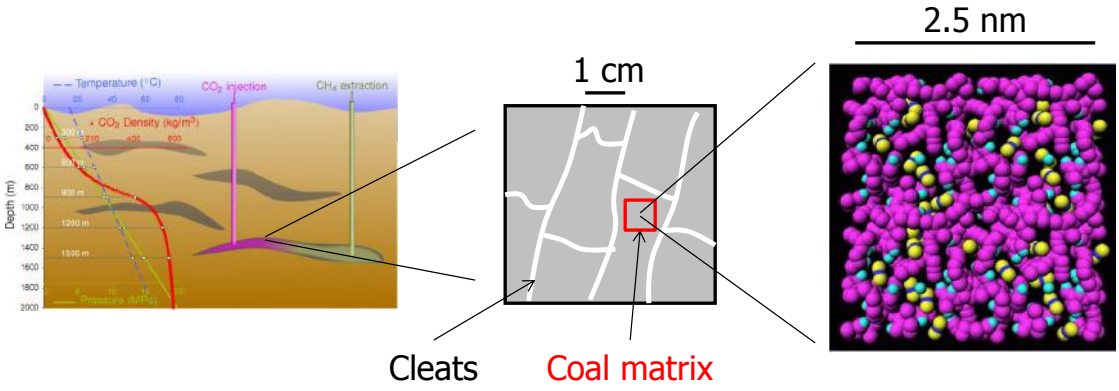

Figure 2.3 – Multiscale structure of coal beds. (left) Subfigure from Brochard (2011), (right) courtesy of L. Brochard.

In-between cleats, one finds the coal matrix, which is porous and contains pores down to a sub-nanometric size. The variations of permeability observed during production and/or injection are due to the opening or closure of the cleats, consecutive to respectively a shrinkage or swelling of the coal matrix. Dimensional variations of the coal matrix observed upon variations of pressure of the fluid it contains are known to be due to adsorption effects (Levine, 1996; Mazumder et al., 2006). In the smallest pores of the material, most of the fluid it contains is indeed said to be adsorbed, i.e., to be in intermolecular interaction with the atoms of the solid skeleton. Because of those intermolecular interactions, as observed in Fig. 2.4, upon an increase of pressure of fluid, an unconstrained piece of coal matrix tends to swell (Reucroft and Sethuraman, 1987; Ceglarska-Stefańska and Czapliński, 1993), even though contraction is observed at pressures larger than our pressures of interest (Hol and Spiers, 2012)[1]. The magnitude of those pressure-induced dimensional variations depends on the fluid. Upon the production of methane displayed in Fig. 2.2, production induces a decrease of pressure of methane in the bed, which translates into a shrinkage of the coal matrix, hence in an opening of the cleats, and finally into an increase of permeability[2]. We aimed at modeling those variations of permeability.

To model those adsorption-induced induced variations of permeability, we first considered the permeability law of coal. Permeability of coal can equivalently be interpreted as depending on the aperture of the cleats, or as depending on the stresses to which the material is submitted (indeed, a compressive stress tends to close the cleats and hence lowers the permeability, see Fig. 2.5). Consequently, for coal, both strain-based permeability laws (i.e., in which permeability depends on the geometry of the cracks, and hence on strains and/or porosity) (Levine, 1996; Robertson, 2005; Palmer and Mansoori, 1998) and stress-based permeability laws (i.e., in which permeability depends on stresses and/or pore pressure) (Seidle et al., 1992;

[1] Contraction is also possible at low fluid pressure for materials less disordered than natural coal and with specific pore sizes (Kowalczyk et al., 2008).

[2] The permeability is observed to increase only during the initial stage of production. During later stages, drops of permeability are observed, which, as we will see in section 2.5, are associated to failure of the coal bed.

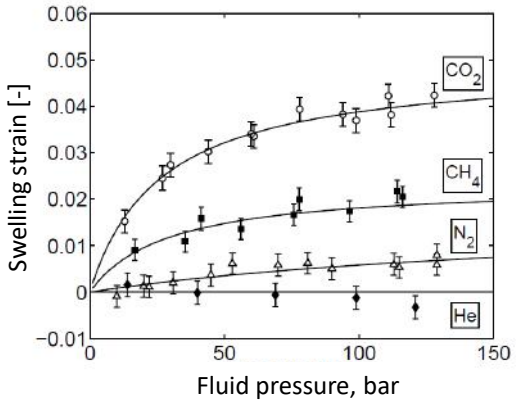

Figure 2.4 – Swelling of coal sample in presence of various fluids. Figure from Pini (2009).

Shi and Durucan, 2005; Cui and Bustin, 2005; Connell et al., 2010; Wu et al., 2010) exist. We chose to use a stress-based permeability law for the following pragmatical reason: when considering a coal sample in a triaxial experiment, we know the stresses and pore pressures, since we apply them. In contrast, even though we can determine the strains by measuring them, we cannot measure the porosity easily, as we do not know what part of the total pore volume must be attributed to the cleats and what part must be attributed to the pores of the coal matrix. Moreover, as we will see later, the notion of porosity is quite ambiguous for the microporous coal matrix. This difficulty incited us to use a stress-based permeability law, which relates the permeability k to the permeability k_0 in the state of reference of effective stresses $(\sigma'_{\parallel 0}, \sigma'_{\perp 0})$ through (Enever and Hennig, 1997):

$$k = k_0 \exp[\alpha_\parallel(\sigma'_\parallel - \sigma'_{\parallel 0}) + \alpha_\perp(\sigma'_\perp - \sigma'_{\perp 0})] \tag{2.1}$$

where $\sigma'_\parallel$ and $\sigma'_\perp$ are the actual effective stresses parallel and normal to bedding, respectively, and where $\alpha_\parallel$ and $\alpha_\perp$ are fracture compressibility coefficients.

Once the permeability law chosen, our aim was to derive state equations (i.e., relations between stresses, strains, porosity or amount of fluid, pore pressure or chemical potential of the fluid) which are applicable to coal. A variety of models existed in the literature (for a review, see, e.g., Pan and Connell (2012)), but most were not based on the Biot-Coussy framework of poromechanics (for an exception, see Wu et al. (2010)). We aimed at deriving such a model in that framework, as poromechanics is firmly grounded in thermodynamics, provides a framework that is suitable for the introduction of further complexities (e.g., anisotropy, non-linearity, viscoelasticity), and whose relevance to tackle geomechanical energy-related problems is well demonstrated (Selvadurai and Suvorov, 2016).

Follow some results obtained within the framework of this study. In section 2.2, the principle

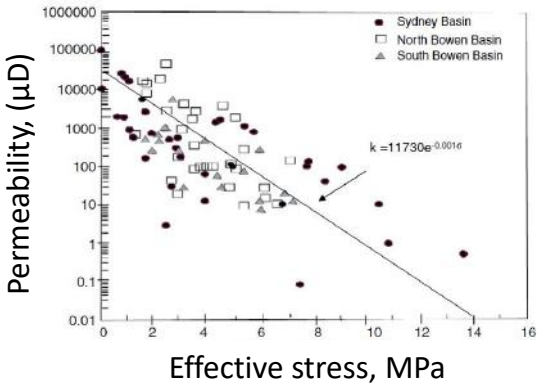

Figure 2.5 – Dependence of permeability of coal on effective stress. Figure adapted from Enever and Hennig (1997).

of the modeling is presented. Section 2.3 is devoted to an introduction of some complexity (namely, dual porosity and transverse isotropy) aiming at making the model more relevant. The model is calibrated in section 2.4. Finally, in section 2.5, we focus specifically on adsorption stresses and on their impact, both on the permeability and on the mechanical behavior of the coal.

2.2 Extension of poromechanics to microporous solids

Related journal article: Brochard et al. (2012)

Context

The specificity of the poromechanical modeling of coal is that, as explained earlier, coal is microporous, meaning that it contains pores with a sub-nanometric size. Because of this microporosity, adsorption effects are significant, which, as already mentioned, is the reason why a piece of coal immersed in a fluid swells when the pressure of the fluid is increased (see Fig. 2.4). For a macroporous material, in which adsorption effects are negligible, and whose volumetric behavior is governed by $\sigma = K\varepsilon - bp$ (where σ is the volume stress, ε the volume strain, p the pressure of the pore fluid, K the bulk modulus, and b the Biot coefficient), once the material is immersed and saturated, any increase of pressure of fluid leads to a shrinkage. Consequently, capturing adsorption effects and the swelling of coal in presence of fluid required an extension of the basic equations of poroelasticity.

This extension, performed here in the case of coal, can in fact be of value for all microporous materials, related to civil engineering applications (e.g., clay or clay-based rocks, cement-based materials) or not (e.g., zeolites or metal-organic frameworks).

Derivation

The principle of the modeling will be presented in the case of an isotropic material in small transformations, whose mechanical behavior in absence of fluid is linear elastic, and whose pore distribution is generic (and therefore can include micropores).

The derivation is performed by considering the thermodynamic equilibrium of a representative elementary volume (REV). Around this equilibrium, a combination of the first and second principles of thermodynamics yields the following energy balance in the reversible case:

$$df = \sigma d\varepsilon + \tau_{ij} de_{ij} + \mu dn, \quad \text{or} \quad d(f - n\mu) = \sigma d\varepsilon + \tau_{ij} de_{ij} - n d\mu \tag{2.2}$$

where f is the Helmholtz free energy (per unit volume of reference of the REV) of the sample and the fluids it contains, τ_{ij} the shear stress, e_{ij} the shear strain, μ the chemical potential of the fluid, n the total amount of fluid in the system. In the adsorption community, n is referred to as the total adsorbed amount, even though not all the fluid in the system may be adsorbed (indeed, in a macropore, most fluid in the pore is in a bulk state). The existence of the total differential (2.2) allows to write the following Maxwell symmetry relation:

$$\left.\frac{\partial \sigma}{\partial \mu}\right|_{\varepsilon, e_{ij}} = -\left.\frac{\partial n}{\partial \varepsilon}\right|_{\mu, e_{ij}}. \tag{2.3}$$

Integrating this Maxwell symmetry relation over μ and invoking the symmetries of the system for what concerns the shear behavior make it possible to obtain the poromechanical state equations of the material:

$$\sigma = K\varepsilon - \int_{p=0}^{p} \left[\left.\frac{\partial n}{\partial \varepsilon}\right|_{\mu, e_{ij}} \frac{1}{\rho_b} \right] dp = K\varepsilon - s^a(\varepsilon, p) \tag{2.4}$$

$$\tau_{ij} = 2G e_{ij} \tag{2.5}$$

$$n = n(\varepsilon, p) \tag{2.6}$$

where G is the shear modulus of the porous material, and ρ_b is the molar density of the bulk fluid. $s^a(\varepsilon, p) = \int_{p=0}^{p} \left[\left(\partial n / \partial \varepsilon|_{\mu, e_{ij}} \right) / \rho_b \right] dp$ is called 'adsorption stress', as proposed in the theory formulated by Ravikovitch and Neimark (2006). In presence of fluid, this adsorption stress is the opposite of the volumetric stress that must be applied to the system to prevent it from deforming.

The model readily recognizes that the total adsorbed amount $n(\varepsilon, p)$ is a function not only of the thermodynamic pressure p of the fluid (as is usually considered in the adsorption community), but also on the strain ε of the solid (or, equivalently, on the stress applied to the solid, as observed experimentally (Hol et al., 2011; Liu et al., 2016)). It is through this dependence that the fluid can deform the porous material. Within the limits of the initial assumptions under which they were derived, those state equations are generic: considering for instance that the material is macroporous makes it possible to retrieve the classical equations of linear poroelasticity (i.e., $\sigma = K\varepsilon - bp$ and $\varphi = b\varepsilon - p/N$, where φ is the variation of Lagrangian porosity, b the Biot modulus, and N the Biot modulus).

For the sake of simplicity, we consider that the total adsorbed amount $n(\varepsilon, p)$ can be well-approximated by its first-order expansion with respect to strains, i.e.:

$$n(\varepsilon, p) = n_0(p)(1 + C(p)\varepsilon), \tag{2.7}$$

where $n_0(p)$ is the adsorbed amount in the rigid porous material, and $C(p)$ is a coupling coefficient.

Discussion of some choices

The spirit of our model is to be based only on parameters that are well defined. In particular, we wanted to avoid the use of porosity, which, for a microporous solid, is ill-defined. Indeed, if one considers that the pore volume is equal to the volume of fluid that penetrates into the pores upon saturation, one understands that the apparent pore volume will be larger if probed with a fluid whose molecules are sufficiently small to penetrate into the micropores, than if probed with a fluid whose molecules are too large to penetrate into the micropores. Consequently, for microporous materials, pore volume is fluid-dependent, and thus ill-defined. Other authors made a different choice: Pijaudier-Cabot et al. (2011); Vermorel and Pijaudier-Cabot (2014); Perrier et al. (2015) chose to work with this apparent porosity. They also decided to work with excess adsorbed amounts (rather than total adsorbed amounts like we did): an advantage of their approach is that the excess adsorbed amount is the parameter that is directly obtained from adsorption measurements. The two approaches can essentially yield identical results (Gor et al., 2017).

We chose to express the adsorbed amount n as a function of strain ε and fluid bulk pressure p (or, equivalently, chemical potential μ). By using a Legendre-Fenchel transform different from the one we used in Eq. 2.2, we could have expressed the chemical potential μ as a function of stress σ and adsorbed amount n. This approach, in the spirit of the one used by Kulasinski et al. (2015), is equivalent to our. For the sake of simplicity, we also considered that the adsorbed amount $n(\varepsilon, p)$ can be reasonably approximated by its first-order expansion with respect to strain, and that the drained material behaved in a linear elastic manner. But, if justified by

the data, going to higher-order expansions (as was done by Kulasinski et al. (2015)) can be necessary. Also, such a thermodynamic approach can be adapted to capture phase transitions induced by adsorption, as was done by Neimark et al. (2010).

2.3 Enrichment of modeling: double porosity, fluid mixtures, and anisotropy

Related journal articles: Espinoza et al. (2013, 2014); Nikoosokhan et al. (2014)

Context and approach

Coal is a dual-porosity material (see Fig. 2.3), as it contains the pores of the coal matrix (down to micropores) and cleats (which are macropores). An advantage of the thermodynamic/-poromechanical approach presented in section 2.2 is that it can easily be extended to such dual-porosity case. Still in the case of an isotropic linear poroelastic medium, in such a dual-porosity case, we showed that the state equation that governs the volumetric behavior is:

$$\sigma = K\varepsilon - bp_c - (1-b)s^a(p_m) \tag{2.8}$$

$$\varphi_c = (p_c - s^a(p_m))/N + b\varepsilon, \tag{2.9}$$

where φ_c is the variation of the Lagrangian porosity of the cleats, K is the bulk modulus of the coal, b is the Biot coefficient associated to the cleat system, N is the Biot modulus associated to the cleat system, p_c is the thermodynamic pressure of the fluid in the cleats and p_m the thermodynamic pressure of the fluid in the coal matrix. These equations clearly show that the mechanical effect of the fluid in the cleats is its pressure p_c (since cleats are macropores), while fluid in the coal matrix impacts mechanically the material through the adsorption stress $s^a(p_m)$ it induces.

Another complexity that must be taken into account by a model for it to be applicable to the practical case of CO_2-ECBM is the presence of mixtures of fluids. Indeed, during CO_2-ECBM, a representative elementary volume will contain both carbon dioxide and methane. Moreover, coal seams also contain water, and moisture content is known to impact CO_2 selectivity (Clarkson, 2000), so that, in practice, CO_2-ECBM requires considering at least ternary mixtures. In Nikoosokhan et al. (2014), we considered the case of a coal seam saturated with a binary mixture of methane and carbon dioxide. The poromechanical framework presented in section 2.2 still holds, but with an adsorption stress s^a which now depends on the fugacities f^{CH_4} and f^{CO_2} of methane and carbon dioxide, respectively, i.e.: $s^a = s^a(f^{CH_4}, f^{CO_2})$.

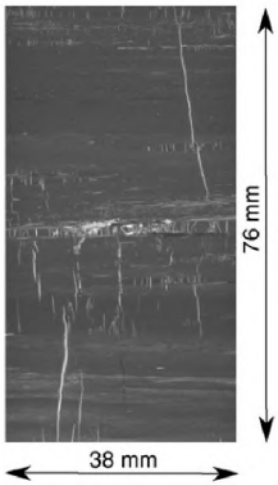

Figure 2.6 – Vertical slice of an X-ray microtomography volume of tested coal core. Vertical cleats are visible and appear white because they are filled with calcite. Horizontal layering induced by bedding is also visible. Figure adapted from Espinoza et al. (2016).

The microstructure of coal is anisotropic, as can be observed in Fig. 2.6. On this vertical slice of an X-ray microtomography volume, one clearly observes the horizontal bedding planes and the cleats: both bedding processes (Cody et al., 1988; Hol and Spiers, 2012) and the presence of mostly vertical cleats (Hu et al., 2010) are expected to confer some anisotropy to the hydro-mechanical behavior of the coal. From the presence of the vertical cleats (i.e., of cracks), one could also expect some nonlinearity in the mechanical behavior of the dry material. Therefore, after the extension to dual porosity, we had to choose between extending the model to first include anisotropy, or to first include mechanical non-linearities. We chose to consider anisotropy first.

Results

Anisotropy can originate from various scales: 1) anisotropy of the adsorption-induced stresses, or 2) anisotropy of the material itself. Given the multi-scale structure of coal, anisotropy of the material could originate from the scale of the coal matrix itself, or rather be due to the cleats. The coal matrix is quite isotropic, and we showed (Espinoza et al., 2013) that anisotropy of swelling in coal is primarily due to anisotropy of the coal sample itself, while the adsorption-induced stresses are, at the microscopic scale, rather isotropic (probably as a consequence of the isotropy of the coal matrix).

Based on this and on conventional anisotropic poroelasticity (Cheng, 1997; Coussy, 2004; Cowin, 2004), we extended the dual-porosity model to the case of a coal core that is transversely isotropic, and derived the poromechanical state equations for this case (see Eq. 1 in Espinoza et al. (2014)). After calibration on a sample of interest for our study (provided by Total, cored

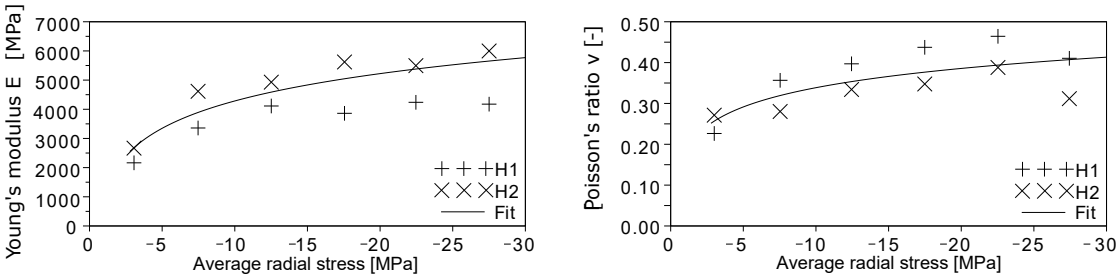

Figure 2.7 – Drained tangent elastic Young's modulus E and Poisson's ratio ν measured in the horizontal direction, as a function of axial stress and radial stress. Lines are fitted functions of the form: Elastic coefficient = cst_1 + cst_2 ln(-Stress/1 MPa). Figure from Espinoza et al. (2014).

from a coal block extracted from a mine in Forzando, South Africa), we found that, for this sample, anisotropy was quite limited, yielding Young's moduli equal to 2.74 GPa and 2.55 GPa parallel to bedding and normal to bedding, respectively, and Poisson's ratio equal to 0.267 and 0.198 parallel to bedding and normal to bedding, respectively. While we had expected a more pronounced anisotropy, the material exhibited strong mechanical non-linearities (see Fig. 2.7). A posteriori, when we had to choose between extending the model toward mechanical anisotropy or mechanical non-linearity, I now consider that we should rather have aimed at extending it toward non-linearity first.

2.4 Triaxial experiments as a tool to calibrate the model

Related journal article: Espinoza et al. (2014)

With the aim of providing a model usable by the engineer, we wanted to show that the most complex state equations that we derived, which, after the enrichment presented in section 2.3, took into account dual porosity and transverse isotropy, could be calibrated. To this effect, we employed a triaxial cell specifically designed for CO_2 testing at levels of stresses realistic for rock mechanics (see Fig. 2.8).

We showed experimentally that the model can be calibrated with the following 3 characterizations: an adsorption isotherm (measured on coal powder with a classical adsorption apparatus), mechanical testing of the dry specimen (see Fig. 2.7), and a swelling experiment in which the swelling of the sample submitted to a constant stress was measured as a function of the pressure of fluid (see Fig. 2.9). This swelling experiment consisted in injecting CO_2 from one extremity of the sample while keeping the stresses applied to the sample constant. Very quickly (i.e., in about 0.01 day), the pressure of fluid became homogeneous throughout the height of the sample. However, one observes that we needed to wait much longer than 0.01 day to reach equilibrium: after having first flowed by convection through the cleat system (up to about 0.01 day), CO_2 needed much more time to diffuse from the cleats to the coal matrix.

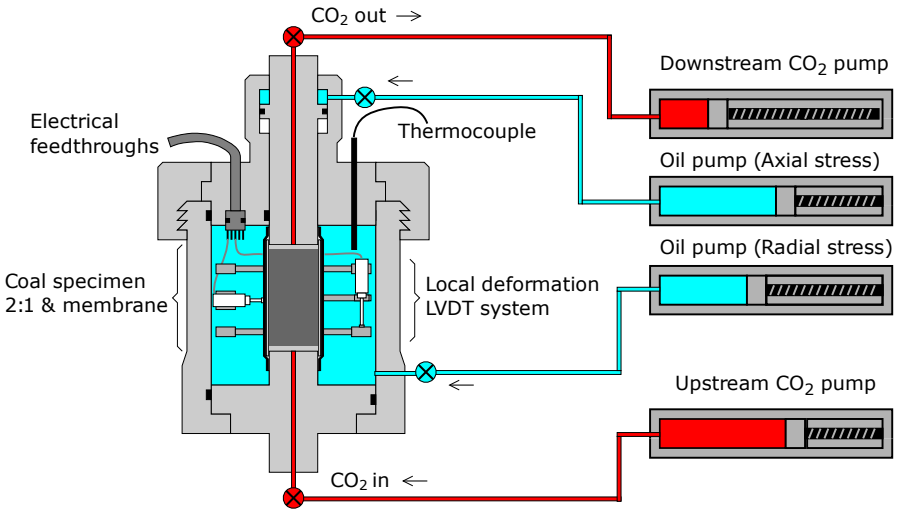

Figure 2.8 – Schematics of triaxial apparatus used for measurement of adsorptive–poromechanical properties of coal cores exposed to CO_2. Main characteristics include: maximum radial stress 40 MPa, maximum axial stress 60 MPa, measurement of local strains through LVDTs, temperature control and ability to handle pressurized pore-fluids. Figure from Espinoza et al. (2014).

2.5 Adsorption stresses: direct measurement and their impact

Related journal articles: Espinoza et al. (2014, 2015)

Motivation

An originality of the modeling that we developed is that, in contrast to many models which focus on adsorption swelling strain, our model naturally introduces an adsorption stress (which is the function s^a in Eq. 2.4). Experimentally as well, most studies of the mechanical effect of adsorption focus on adsorption-induced deformations. Motivated by our modeling, we decided to focus experimentally on a direct measurement of adsorption stress, which was original.

We also aimed at checking whether these adsorption stresses are sufficient to explain the variations of permeability (i.e., initial increase of permeability by more than 1 order of magnitude during methane production) and failure events displayed in Fig. 2.2. Those failure events induce a decrease of permeability because they lead to a production of fine coal particles which plug the well (Okotie and Moore, 2010).

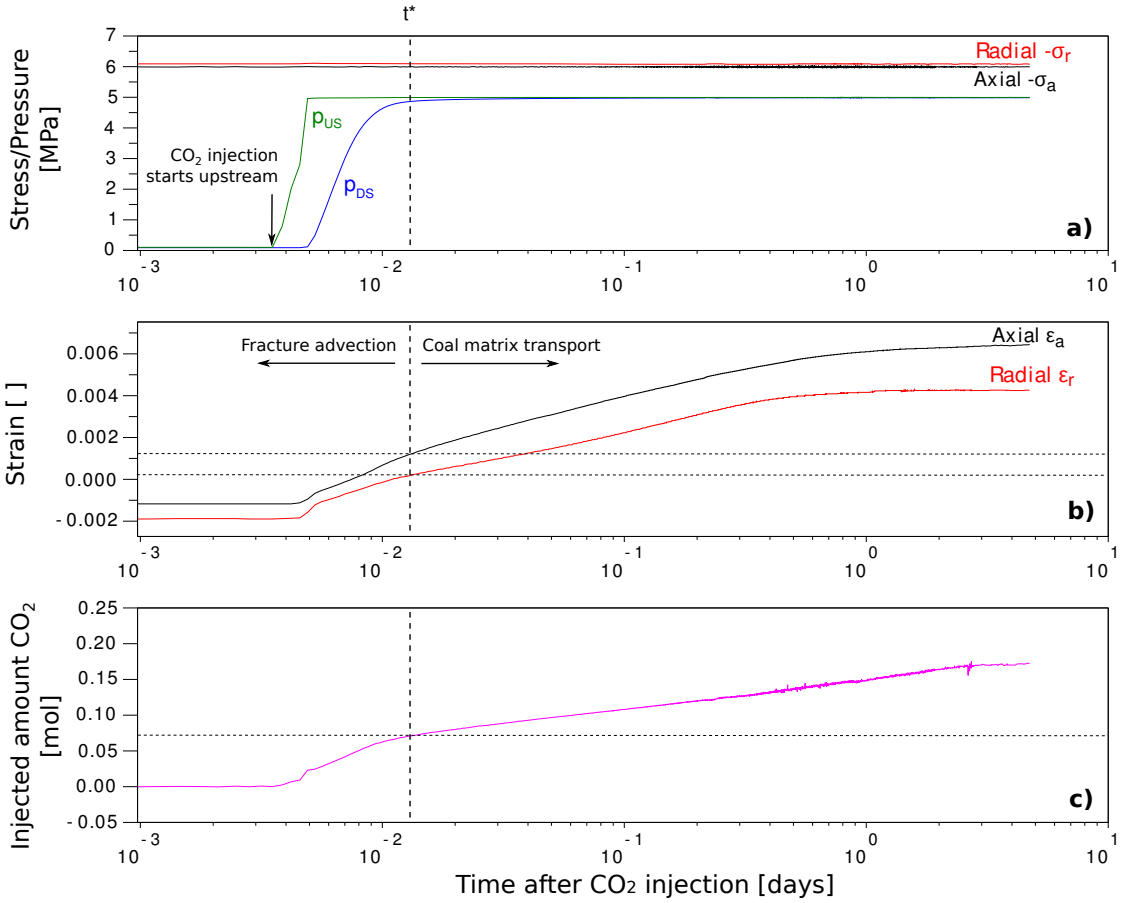

Figure 2.9 – Example of swelling experiment under constant confining stresses $\sigma_r = \sigma_a = -6$ MPa and an objective injection pressure of CO_2 of 5 MPa. Time evolutions of (top) fluid pressure, (center) strains, and (bottom) injected amount of CO_2. Two regimes are observed: 1) before about 10^{-2} days, fluid penetrates mostly through the cleats, and 2) after about 10^{-2} days, pressure of the fluid is homogeneous throughout the cleat system and diffuses into the coal matrix. Figure from Espinoza et al. (2014).

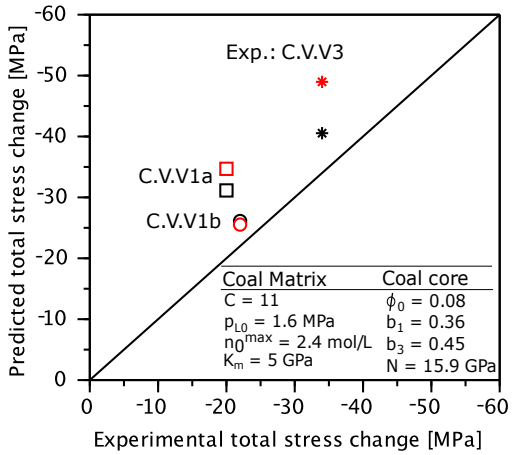

Figure 2.10 – Change of total stress in coal cores induced by CO_2 injection at near constant-volume conditions: comparison between experimentally measured values and model predictions. Experiments C.V.V1 and C.V.V3 were performed at pressures of CO_2 equal to 2 MPa and 5 MPa, respectively. Figure from Espinoza et al. (2014).

Results

Starting from a dry state of reference, when the sample is put in contact with a fluid at a certain bulk pressure, the adsorption stress is equal to the increment of total compressive stress that must be applied to the sample to prevent it from swelling. As can be observed in Fig. 2.10, at 2 MPa of CO_2 pressure (i.e., for experiment C.V.V1), the adsorption stress was around 20 MPa: said otherwise, when injecting the sample with CO_2 at 2 MPa, we needed to increase the compressive stresses by about 20 MPa to prevent the coal sample from swelling. By analogy with the classical poroelastic equation $\sigma = K\varepsilon - bp$, if we define an apparent Biot coefficient as $-\Delta\sigma/\Delta p$ in isochoric conditions, the measurement of an adsorption of about 20 MPa at 2 MPa of CO_2 pressure is interpreted as an apparent secant Biot coefficient of about 10, which is way out of the range [0;1] encountered classically for the Biot coefficient of macroporous materials: this surprising high value is a direct consequence of adsorption effects. Note however that several in the poromechanics community dislike defining a Biot coefficient as $-\Delta\sigma/\Delta p$ in isochoric conditions. They consider that the Biot coefficient should only be defined as $1 - K/K_S$, where K_S is the bulk modulus of the solid skeleton. But, for a microporous solid, the solid skeleton (and hence its stiffness) is quite ill-defined.

The variations of adsorption stresses are sufficient to explain the significant variations of permeability observed in the field (see Fig. 2.2), and we could indeed recreate those variations of permeability in the lab. For a sample in oedometric conditions, flushing it with CO_2 at 2 MPa led to a decrease of permeability of about 2 orders of magnitude (see Fig. 2.11). On this figure, the hard permeability of the coal is apparent (i.e., the fact that the logarithm of the permeability does not depend linearly on effective stress): this additional complexity could be captured by using a permeability law more complex than Eq. 2.1, as did Liu and Rutqvist

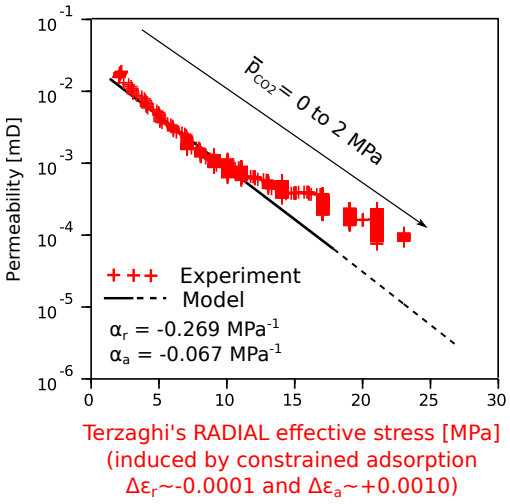

Figure 2.11 – CO_2 permeability evolution of coal core subjected to constrained adsorption under near constant-volume conditions. The specimen is subjected to increasing compressive stresses as a result of CO_2 injection and constrained swelling. Ensuing stresses lower measured permeability up to 100 times. The dashed line indicates values of permeability extrapolated out from the experimental fitting range. Time goes from top left to bottom right. Figure from Espinoza et al. (2014).

(2010) for instance.

The variations of adsorption stresses are also sufficient to induce failure of the coal. We showed it by desorbing fluid from a sample in oedometric conditions. Starting with a sample under a certain level of compression and containing fluid at a certain pressure, we decreased the fluid pressure. This decrease of pressure and the shrinkage of the coal matrix it induced led to an axial contraction and to a reduction of the compressive radial stress (see Fig. 2.12). At some point during the experiment (i.e., at time equal to 0.325 days in Fig. 2.12), the sample failed. We could show that this failure is a direct consequence of the evolution of the state of stresses. Indeed, as can be observed in Fig. 2.13, the sample failed right when Terzaghi effective stresses reached the failure envelope of the coal (which had been characterized beforehand by triaxial shear testing of dry samples). We believe that we recreated in the lab the mechanism through which coal failure can happen in the field during methane production.

2.6 Conclusions and perspectives

Conclusions

The work here performed combined modeling and experiments, with the aim of deriving, calibrating, and verifying a model that could be used by the reservoir engineer to predict evolutions of permeability during CO_2-ECBM. The poromechanical part of the model is valid

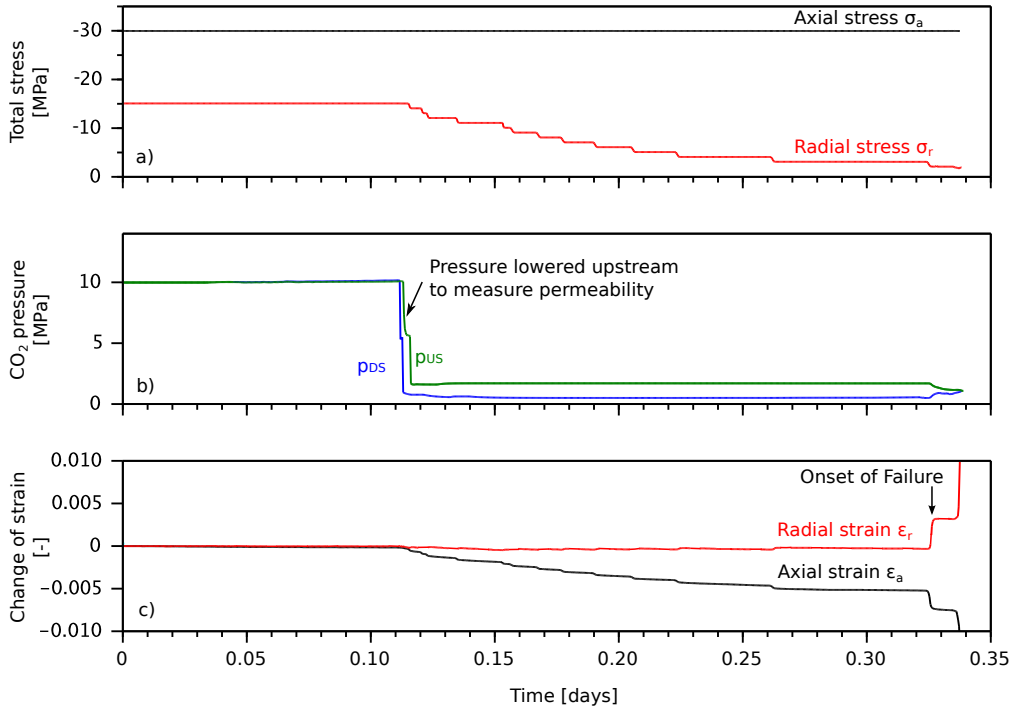

Figure 2.12 – Time history of experiment leading to coal failure: (top) total stresses, (center) fluid pressure measured at upstream and downstream loading caps (a pressure gradient is applied to measure permeability), and (bottom) change of strain with respect to equilibrium initial conditions. Failure occurred at 0.325 days. Figure from Espinoza et al. (2015).

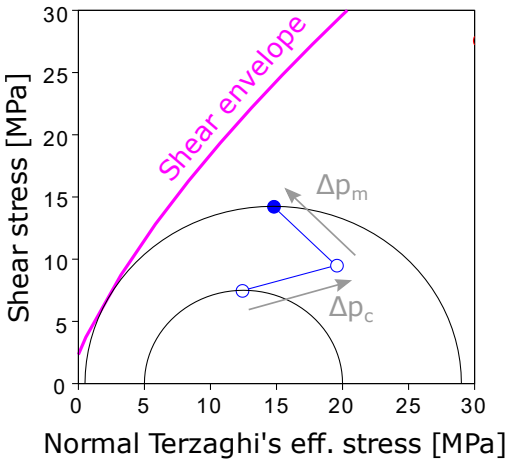

Figure 2.13 – Numerical simulation of coal core depletion–desorption of CO_2 in oedometric conditions. First the pressure p_c of the fluid in the cleats is decreased, and then the pressure p_m of the fluid in the coal matrix. Figure from Espinoza et al. (2015).

for a porous material that is linear elastic. It relies only on well-defined thermodynamic parameters and is based on the notion of adsorption stress. The model includes transverse isotropy, dual-porosity, and can be applied with a fluid mixture. However, it does not take into account mechanical non-linearities, which, based on the experimental characterizations performed, appear to be significant experimentally.

On top of permitting calibration, experiments yielded an original measurement of adsorption stresses. The variations of permeability and coal failure observed in the field have been successfully recreated in the lab.

Although not described here, the derived state equations have been successfully implemented in the finite-element/finite-volume package Bil by P. Dangla (Dangla, 2017).

Perspectives

Starting from the model I presented, many aspects could be improved. I discuss some of them next.

When we derived the poromechanical state equations for coal being considered as a dual-porosity material (see section 2.3 and Eqs. 2.8 and 2.9), pressures p_m of the fluid in the coal matrix and p_c of the fluid in the cleats were considered independent from each other. However, when we implemented the equations in the Bil finite-element/finite-volume package, we always made the assumption of local thermodynamic equilibrium, i.e., we assumed that at any time and any location in the coal bed, $p_c = p_m$. However, such condition may not be always satisfied. It is for instance not verified in the swelling experiment displayed in Fig. 2.9, in which we observe that transfer of fluid toward the coal matrix continues long after the pressure of fluid in the cleats reached its equilibrium value. To capture such transient differences between pressures in the cleats and in the coal matrix, one could introduce a kinetics of transfer between pressure of fluids in cleats and in coal matrix, in the spirit of what we did in Vandamme et al. (2014). Based on such kinetics, it would be interesting to determine what the time scales and/or length scales are, for which taking explicitly into account this kinetic of transfer is necessary, and which are the ones for which just considering local equilibrium is sufficient.

However, considering such kinetics of transfer between cleats and coal matrix is not sufficient to capture all transient phenomena occurring at the scale of a representative elementary volume. Let us for instance consider a piece of coal subjected to a constant state of stress, and into which some fluid is injected at some controlled pressure. Akin to what was observed in Fig. 2.9, what will happen in practice is that the injected fluid will first flow into the cleats and increase the fluid pressure in the cleats up to the control value, before diffusing toward the coal matrix. So, within the coal matrix, pressure of fluid will increase first in the vicinity of the cleats, and hence the coal matrix in the vicinity of the cleats will swell. This swelling localized around the cleats will tend to close the cleats and decrease the permeability. After waiting

longer, at equilibrium, the whole coal matrix will have swollen homothetically and cleats will have opened back. This transient closure of cleats induces a transient decrease of permeability, observed experimentally and referred to as 'permeability rebound' in the literature (Liu et al., 2011; Peng et al., 2014). Our present model, in which, inside a representative elementary volume, a unique pressure p_c is associated to the fluid in the cleats and a unique pressure p_m is associated to the fluid in the coal matrix, is unable to capture such permeability rebound, even if a kinetic of transfer of fluid between cleats and coal matrix is considered. Indeed, one can show that, with the model presented in section 2.3, under constant stresses, any increase Δp_c of pressure in the cleats and any increase Δp_m of pressure in the coal matrix leads to an increase of the volume of the cleats (see Eq. 2.9). Therefore, upon an injection of fluid in a sample under a constant stress state, independent of the kinetics that we assign to the transfer of fluid between cleats and coal matrix, our model will predict a monotonic increase of the volume of the cleats over time, and hence of the permeability. Therefore, capturing the 'permeability rebound' observed experimentally would require a conceptual modification of the model.

A fundamental question is related to the notion of representative elementary volume for coal. Indeed, cleats present a frequency of occurrence which depends on their aperture in a fractal manner (Laubach et al., 1998): a large sample may include a large cleat that would be unlikely to be present in a smaller sample. This observation brings up the question of whether it is possible to define a representative elementary volume for coal, and of whether properties measured on coal cores (like in section 2.4) are representative of properties of coal beds. The answer may depend on the property of interest: one could well imagine that adsorption properties of coal cores are representative of those of the coal bed (as they are not expected to be impacted by the presence of cleats), while stiffnesses of coal cores may be not representative of those of the coal bed (as they are likely to be significantly impacted by the presence of cleats). The case being, although I would expect the general form of the poromechanical equations introduced in section 2.3 to hold at the scale of the coal bed, some parameters of the model should be characterized directly at the scale of the coal bed (e.g., through ultrasound for what concerns stiffness properties) rather than on coal samples. For what concerns mechanical anisotropy in particular, lab experiments performed here or found in the literature (Day et al., 2010; Morcote et al., 2010) show that, at the scale of the coal sample, the Young's modulus $E_\perp$ in the direction perpendicular to the bedding plane is lower than the Young's modulus $E_\parallel$ in the direction parallel to the bedding plane. However, since most cleats are perpendicular to the bedding plane, we could expect a reversal of the mechanical anisotropy at the scale of the seam (i.e., $E_\perp > E_\parallel$). The same issue of representativity holds for permeability, knowing that permeability of the seam ranges from 0.1 to 100 mD (Scott et al., 2012), while that of coal samples ranges from 0.0001 to 0.01 mD (Lake and Srinivasan, 2004).

As explained in section 2.3, our model neglects mechanical non-linearities, while experiments show that those mechanical non-linearities are significant (see Fig. 2.7), probably as a consequence of the presence of cleats. Extending the model to the case of mechanical non-linearities seems necessary to correctly interpret our lab data. However, the relevance of

such extension for practical applications can be discussed, as mechanical non-linearities are especially pronounced at low effective stress, and as effective stresses in the field are not that low.

Finally, another point that could be improved is that of coal swelling induced by an adsorption of a fluid mixture. As mentioned in section 2.3, we already treated this case in Nikoosokhan et al. (2014). However, in that article, we made an assumption (namely that the adsorbed amount $n_i(p,x)$ of species i, where p and x are the pressure and mole fraction of species i of the bulk fluid mixture, respectively, can be expressed by separating variables, i.e., that $n_i(p,x) = n_i(p,x=0) * f(x)$). This assumption is not the one used in the Ideal Adsorbed Solution Theory (IAST) (Myers and Prausnitz, 1965), which is a theory that is widely employed (and with success) to model adsorption of mixtures on rigid adsorbents. It would be interesting to revisit our work in Nikoosokhan et al. (2014) to the light of the IAST theory. Such improvement could be of interest not only for the community working on coal, but also for the adsorption community working on adsorption in compliant networks in general. Extension to ternary mixtures (to model the swelling due to co-adsorption of water, methane, and carbon dioxide) would also be valuable for the modeling of CO_2-ECBM applications.

3 Time-dependent deformations of cement-based materials

Hydric condition \ Loading condition	No load	Under load
No water exchange with outside	**Autogenous shrinkage**	Autogenous shrinkage + **Basic creep**
Water exchange with outside	Autogenous shrinkage + **Drying shrinkage**	Autogenous shrinkage +Drying shrinkage +Basic creep + **Drying creep**

Table 3.1 – Time-dependent strains of cement-based materials in function of loading condition and hydric condition.

The amount of concrete produced every year in the world (roughly 35 billion tons per year, or about 2 cubic meters per year and per capita) has never been as high as today, and still goes on increasing, at a rate that was only matched for a few years right after World War II (Van Damme, 2018). Much more concrete is produced than all others building materials combined (Van Damme, 2018). The cement industry is usually considered to contribute about 5% to anthropogenic CO_2 emissions (Worrell et al., 2001).

Concrete is a multiscale heterogeneous material constituted of cement paste and aggregates (see Fig. 1.1-left). Cement paste is obtained by mixing clinker with water. The main hydration product obtained with regular Portland cement is called calcium silicate hydrates (noted C-S-H in short). C-S-H is a microporous gel which plays the role of the 'glue' of Portland cement pastes. Since C-S-H constitutes the matrix of the cement paste and of the concrete, C-S-H significantly impacts many of the properties of concrete.

3.1 Introduction to time-dependent deformations of concrete

Over time, concrete in the lab or in the field deforms, as a consequence of a variety of causes, among which hydration, mechanical stress, variations of water content, or variations of temperature (Chanvillard, 1999). Conventionally, under isothermal conditions, time-dependent strains of cement-based materials are decomposed into the following four components (see Tab. 3.1) (Neville et al., 1983): autogenous shrinkage, basic creep, drying shrinkage, and drying creep. Autogenous shrinkage is the time-dependent strain of a non-loaded specimen exchanging no moisture with its surroundings. Basic creep is the difference between the strain of a loaded specimen exchanging no moisture with its surroundings and the autogenous shrinkage: basic creep is regarded as the strain due to the applied load. Drying shrinkage is the difference between the strain of a non-loaded specimen exchanging water with its surroundings and the autogenous shrinkage: drying shrinkage is regarded as the strain due to drying of specimen. Finally, drying creep is the additional time-dependent strain of a loaded specimen exchanging

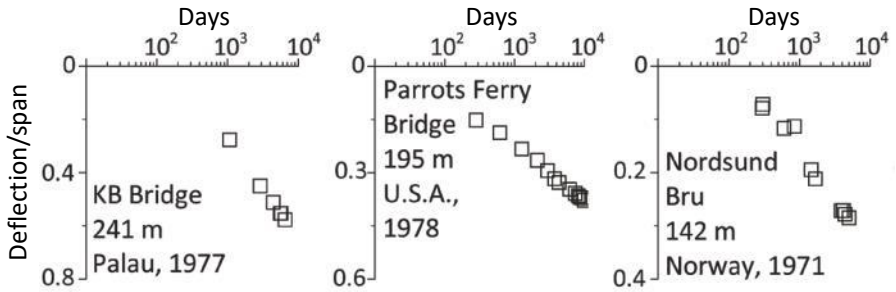

Figure 3.1 – Deflection of prestressed concrete bridges. Figure adapted from Bažant et al. (2011).

water with its surroundings, with respect to the sum of autogenous shrinkage, basic creep and drying shrinkage. Drying creep is also known as 'Pickett effect' as it was first reported by Pickett (1942), and can also be interpreted as an acceleration of load-induced creep when the load is concomitant with an increase or decrease of relative humidity.

For concrete, time-dependent deformations in general, and creep in particular, can extend over very long periods of time. Data of deflection of prestressed concrete bridges, gathered in Bažant et al. (2011), show that concrete still creeps after decades, with a clear logarithmic kinetics (see Fig. 3.1), which is recognized by some recent codes, e.g., the B4 model (RILEM Technical Committee TC-242-MDC, 2015) or the fib Model Code 2010 (Fib, 2012; Müller et al., 2013), while the Eurocode 2 still considers basic creep to be asymptotic (Eurocode, 2004). Creep can cause excessive deformations (Bažant et al., 2011), which, in prestressed structures, is being accompanied by a loss of prestress (Tadros et al., 2003). In the concrete community, a famous example of a catastrophe associated to creep of concrete is that of the Koror–Babelthuap Bridge in Palau in 1996 (Burgoyne and Scantlebury, 2006) [1].

With time-dependent deformations in general, and creep in particular, I identify the following points of interest for the cement and concrete industry:

- Contributing about 5% to global anthropogenic CO_2 emissions (Worrell et al., 2001), the cement industry aims at reducing the CO_2 footprint of hydraulic binders, by developing innovative "low-CO_2" binders (Gartner, 2004), which contain less Portland cement, or even no more Portland cement (e.g., BYF cements (Gartner, 2017)). Because of the novelty of those materials, we have very little feedback on their long-term time-dependent behavior. The industry is interested in innovative testing methods which could provide them with indicators of long-term performance in a relatively fast manner.

[1] After 18 years, as a consequence of creep, shrinkage, and prestress loss, deflection at mid-span had reached 1.2 m, which required retrofit. About 6 weeks after this retrofit, the bridge collapsed, killing 2 people. After an in-depth analysis of the case, Burgoyne and Scantlebury (2006) reached the conclusion that poor design did not provide the bridge enough robustness with respect to accidental damage, and proposed the following mechanism for the failure: resurfacing during the retrofit may have locally damaged the concrete in the top flange, such that creep behind the anchorages of the prestressing tendons could have occurred very fast, eventually leading to damage of the concrete between the prestressing tendons, and to the failure of the bridge.

- As we will see in section 3.3, there exist some infrastructures —typically the French nuclear power plants — which are now reaching the end of their design lifespan, and for which their owners aim at extending this lifespan. Justifying the safety of such extension requires a good modeling of the long-term time-dependent behavior of concrete.

- The physical origin of time-dependent deformations of concrete is still debated, being attributed among others to reorganization of intermolecular bonds (Bažant et al., 1997), jumping over energy barriers (Wittmann, 1982), free volume dynamics (Vandamme and Ulm, 2009), migration of water (Powers, 1968), or pressure-solution creep (Pachon-Rodriguez et al., 2014). I believe that understanding this physical origin, which sounds like a fundamental question, could have an interest for the industry. This belief comes from the example of gypsum, for which a direct proof of the physical origin of its creep has been brought only recently. Pachon-Rodriguez et al. (2011, 2014) showed that creep in gypsum is due to pressure-solution: under mechanical stress, stress concentration at contact points between gypsum needles leads to the dissolution of the ions involved in gypsum crystals (i.e., Ca^{2+} and SO_4^{2-}), which then diffuse and precipitate again, but further from the contacts. This process provides some apparent mobility at the contact between gypsum crystals, which translates macroscopically into creep. Once this has been identified, to control creep of gypsum (since you want your gypsum board to remain as flat as possible over time), one can envision to develop innovative agents that target the dissolution of the gypsum crystals, or the diffusion of its ions. In the same spirit, identifying the origin of time-dependent deformations in cement could pave the way for future innovative breakthroughs aiming at controlling the kinetics of those deformations.

The work which I performed on the time-dependent deformations of concrete is in the spirit of those points of interest. Section 3.2, devoted to the measurement of basic creep by micro-indentation, aims at providing a fast way of assessing the long-term kinetics of basic creep of concrete. Section 3.3 focuses on the modeling of the three-dimensional creep behavior of concrete, since, as we will see in that section, the three-dimensionality is important for some applications. Section 3.4 focuses on hypothesis testing on the physical origin of the long-term kinetics of autogenous shrinkage. Finally, in section 3.5, we present two models based on the idea of local microscopic relaxations which can explain basic creep of concrete.

3.2 Fast measurement of long-term kinetics of basic creep by micro-indentation

Ph.D. student: Qing ZHANG
Related journal article: Zhang et al. (2014)
Colleagues involved: Robert LE ROY, Jean-Noël ROUX, Bruno ZUBER (Lafarge)

Context

This study was performed in the continuity of my Ph.D. on the investigation of the creep properties of calcium silicate hydrates by nano-indentation. My Ph.D. studies were funded by Lafarge. When I came back to Laboratoire Navier, Lafarge proposed me to go on working on the topic and funded the Ph.D. project of Qing Zhang on a study by micro-indentation of the impact of microstructure and moisture content on mechanical properties (and creep properties in particular) of hydraulic binders.

Indentation is an experimental contact technique to probe the mechanical properties of volumes, by pressing an indenter probe of known geometry and mechanical properties into the sample whose mechanical properties need to be determined. During my Ph.D., I derived a formula to back-calculate a creep compliance from an indentation creep experiment (Vandamme et al., 2012). I showed at that time (Vandamme and Ulm, 2009) that minutes-long nano-indentation experiments yield a creep compliance which, after a few seconds, is logarithmic with respect to time. This logarithmic kinetics is reminiscent of the long-term creep kinetics observed after weeks on structures (see Fig. 3.1) or on concrete samples tested by regular macroscopic means. Our results also suggested that the rate of this logarithmic creep of calcium silicate hydrates was consistent, after upscaling, with the one observed macroscopically on concrete samples (Vandamme and Ulm, 2009). The aim of the study performed in the framework of the Ph.D. studies of Q. Zhang was to confirm this suggestion, through a methodical comparison between indentation creep experiments and macroscopic uniaxial creep experiments.

Approach

The final interest of the study being the assessment of creep properties at the macroscopic scale, we chose not to use nano-indentation (which probes volumes with a characteristic size below the micron, and thus can yield the properties of the individual hydration products in a cement paste), but to rather use micro-indentation (which probes volumes of a larger scale, with a characteristic size on the order of a few dozen microns, and thus can yield the properties of the cement paste). Micro-indentation creep experiments consisted in applying a constant load on the indenter tip and measuring the evolution of the indentation depth over time.

The study aimed at comparing creep results obtained by micro-indentation on cement paste with creep results obtained by regular uniaxial macroscopic creep testing on concrete. Given the complexity and duration of macroscopic creep experiments (which need to last for several months to a few years to yield a reliable measurement of the long-term creep kinetics), we chose not to perform our own macrosocopic creep experiments, but based our study on results available in the literature, namely the results of Le Roy (1996) obtained during his Ph.D. (see also (Torrenti and Le Roy, 2017) for a detailed analysis of these results), displayed in Fig. 3.2-left. In 2011, i.e., about 20 years after R. Le Roy manufactured his concrete samples in

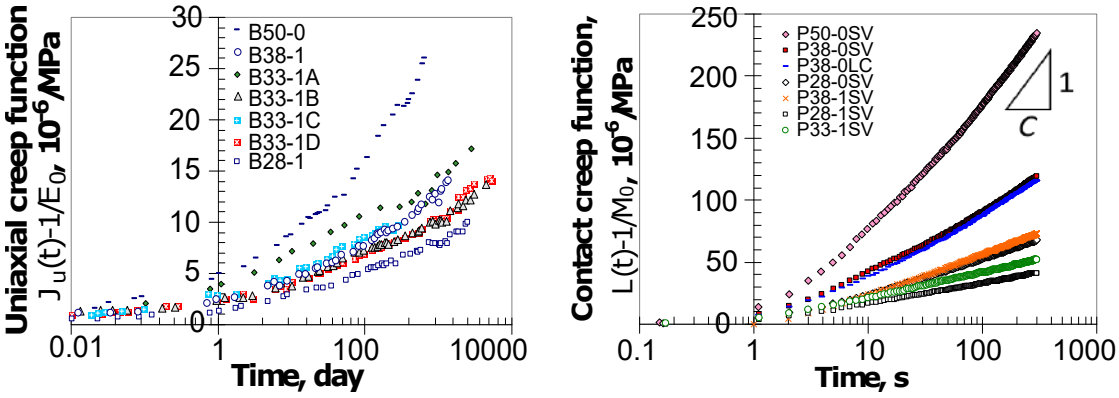

Figure 3.2 – (left) Uniaxial basic creep functions obtained on concrete with uniaxial compressive creep testing (Le Roy, 1996) and (right) contact creep functions $L(t) - 1/M_0$ obtained on cement paste samples with micro-indentation. When the creep function looks linear in a semi-log scale in the long term, as is the case here, the slope of the line is $1/C$, where C is the creep modulus defined in Eq. 3.1. Figures from Zhang et al. (2014).

1992, we manufactured cement pastes identical to the ones used in the concrete samples in Le Roy's thesis, and performed micro-indentation creep experiments on them. We compared our micro-indentation measurements with his macroscopic measurements. The results of this comparative study are presented next.

Main results

Le Roy manufactured 7 types of concrete samples, all based on the same clinker, but which differed in terms of water-to-cement mass ratio, amount of silica fumes added, and quantity of aggregates. Those 7 types of concrete samples were made of cement pastes with 4 different mix designs. We manufactured those 4 cement pastes.

Le Roy measured the basic creep of his concrete samples by classical uniaxial compression. His samples were cylinders with an height of 1 m and a diameter of 20 cm. The results of his experiments are displayed in Fig. 3.2-left: the longest experiment lasted for about 13 years. A logarithmic kinetics is observed, which kicks off after a few days.

For the study by micro-indentation, the cement paste samples were slices with a thickness of a few millimeters, cut from cement paste cylinders with a diameter of 2 cm. The results obtained by micro-indentation on the cement pastes are dispayed in Fig. 3.2-right. A clear logarithmic kinetics is observed for all samples, which kicks off after a few seconds.

The identical logarithmic kinetics supports the idea of comparing the two sets of measurement with each other. To perform a quantitative comparison, all creep functions $J(t)$ were fitted

with a function of the form:

$$J(t) = \frac{1}{C}\log(1 + t/\tau), \tag{3.1}$$

where we named the parameter C 'creep modulus', as it is homogeneous to a modulus, and where τ is a characteristic time. At large times (i.e., for $t \gg \tau$), the creep rate $\dot{J}(t)$ is equal to $1/(Ct)$: the creep modulus C governs the long-term creep rate and, the larger the creep modulus, the smaller the long-term creep rate. When the creep function is displayed on a semi-log axis (like in Fig. 3.2), the creep function looks like a line in the long term: the slope of this line is $1/C$.

To compare the creep moduli obtained by micro-indentation with those obtained by uniaxial macroscopic testing, a change of scale was necessary, as micro-indentations were performed on cement paste, while macroscopic creep experiments were performed on concrete samples, which are a mix of cement paste with aggregates. To perform this upscaling, from the scale of the cement paste to the scale of the concrete, we used a classical Eshelby-based homogenization scheme (namely, the Mori-Tanaka scheme (Mori and Tanaka, 1973)), which we extended to linear viscoelasticity for asymptotically large times. We considered that aggregates do not creep, and that paste and aggregates are perfectly bonded (i.e., that there is no interfacial transition zone, which is consistent with the microstructural observations of Scrivener et al. (2004)). Such upscaling makes it possible to infer, based on the measured creep modulus of the cement paste, what the creep modulus of the concrete of which it is made, should be. The results of the comparison are displayed in Fig. 3.3. The comparison is very good, which shows that we can estimate the long-term kinetics of concrete creep (governed by its creep modulus) based on minutes-long micro-indentation of its paste.

The characteristic times τ fitted on the uniaxial macroscopic creep experiments were on the order of a few days (see Fig. 3.2-left), which is very different from the characteristic times fitted on the micro-indentation creep experiments, which were on the order of a few seconds (see Fig. 3.2-right). The reason for this discrepancy cannot be attributed to the difference in scale as, upon upscaling, the characteristic time does not vary by orders of magnitude (at least in linear viscoelasticity) (Beurthey and Zaoui, 2000). We also checked experimentally (Vandamme and Ulm, 2013) that, between the scale of nano-indentation (i.e., with indentation depths on the order of 100 nm) and the scale of micro-indentation (i.e., with indentation depths on the order of 10 μm), the characteristic time did not evolve significantly. In section 3.5, I present a potential explanation of why characteristic times to reach a logarithmic kinetics of creep are so different between micro-indentation experiments and uniaxial macroscopic experiments.

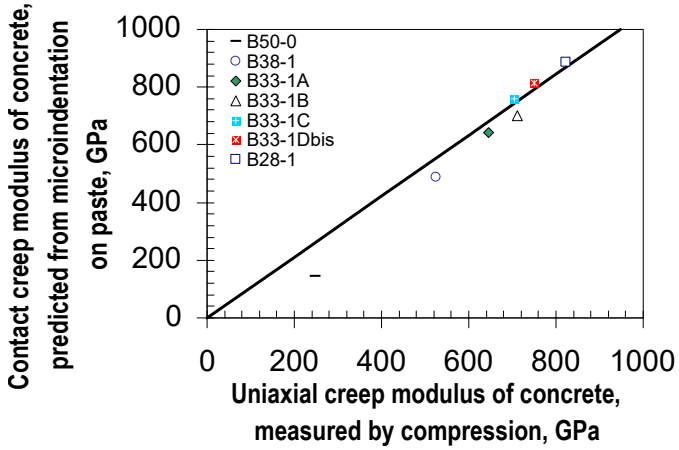

Figure 3.3 – Uniaxial creep modulus measured by uniaxial compression creep experiments on concrete versus contact creep modulus of concrete estimated from upscaled micro-indentation creep experiments performed on cement paste. Figure adapted from Zhang et al. (2014).

Conclusions and perspectives

We showed that the long-term creep kinetics of concrete, which is usually measured in months at the macroscopic scale, can be assessed by a combination of minutes-long micro-indentation creep experiments with analytical upscaling techniques. This result is of direct practical interest for the cement and concrete industry, which, to determine the full creep function of a material, can now combine a relatively short few-weeks-long macroscopic creep experiment (to determine the short-term creep) with micro-indentations (to determine the creep modulus and hence the long-term creep kinetics), instead of performing a months-long or years-long macroscopic creep experiment.

However, many questions remain. The good agreement between upscaled creep modulus measured in minutes by micro-indentation with the creep modulus measured in months at the macroscopic scale is surprising and, up to now, unexplained. Is this agreement a mere correlation, or is the creep after a few seconds in an indentation experiment really governed by the same physical processes as the ones governing long-term logarithmic creep at the macroscopic scale? If the latter, why would the characteristic time at which the long-term logarithmic creep kinetics kicks off be orders of magnitude smaller by micro-indentation testing than by uniaxial macroscopic testing? Indeed, as explained above, within the framework of linear viscoelasticity, this characteristic time should not depend significantly on the scale, which was confirmed by a comparison between nano-indentation and micro-indentation.

A potential candidate to explain the shift in characteristic time between micro-indentation and macroscopic creep testing could be the magnitude of the stresses at stake (see section 3.5 for more details). Indeed, most macroscopic creep experiments on concrete are performed at stresses below 30% of the compressive strength, so that the viscous behavior remains linear

with respect to the applied stress. For instance, Le Roy's experiments analyzed in this study were all performed at stresses lower than 30 MPa (Le Roy et al., 2017). In contrast, the stress below the indenter can be much larger. Typically, during micro-indentation on cement-based materials, those stresses, which depend principally on the shape of the indenter and on the mechanical properties of the indented material and not so much on the applied load, are on the order of a few hundred MPa. It may well be that the significant decrease in characteristic time is a consequence of the significantly higher stresses at stake during indentation testing than during regular macroscopic testing. It would be interesting to test this hypothesis further: one way of doing it could be to immerse a sealed concrete sample in a fluid and pressurize the fluid up to several hundred MPa, to make the sample creep volumetrically. Working with volumetric stresses could allow applying stresses significantly larger than 30% of the compressive strength without failing the material.

In any case, if we recognize that the indentation technique makes it possible to reach the long-term kinetics of creep much quicker than with conventional macroscopic testing, in return a drawback of the indentation technique is that it does not allow the assessment of short-term creep! Also, our application of the indentation technique to creep testing relies on the fact that, after some time, creep evolves logarithmically with respect to time, may it be at the macroscopic scale or at the scale of indentation. Indeed, our analysis relies on the notion of creep modulus (see Eq. 3.1), which is meaningful only when the long-term creep is logarithmic with respect to time. However, not all hydraulic binders creep logarithmically with respect to time. For instance, gypsum does not, and there is no reason why non-Portland cement pastes should. For such materials, how to use the indentation technique to assess long-term creep behavior remains unclear.

3.3 3-dimensional creep behavior of concrete and of C-S-H gel

Ph.D. student: Abudushalamu AILI
Related journal articles: Aili et al. (2015, 2016)
Colleagues involved: Jean-Michel TORRENTI (IFSTTAR), Benoit MASSON (EDF), Julien SANAHUJA (EDF)

Context

In France, in 2014, about 75% of electricity was produced from nuclear energy, by the 58 nuclear reactors owned by EDF (Cour des Comptes, 2016). The reactors were designed for a service life of 40 years (Cour des Comptes, 2016). In 2015, the average age for the 34 nuclear reactors of 900 MW, 20 nuclear reactors of 1 300 MW, and 4 nuclear reactors of 1 400 MW was 34, 28, and 18 years, respectively (Cour des Comptes, 2016). Consequently, in the following years, many nuclear power plants will reach the end of the service life for which they were initially designed. For their owner EDF, and for France in general, being allowed to extend

this service life bears tremendous economic implications. The main concern upon extending service life is to guarantee safety of the installations.

The reactor building of the 1 300 MW nuclear power plants consists of two concentric containments (Granger and Torrenti, 1995). The outer one, designed to withstand external aggressions, is made of reinforced concrete. The inner one is made of prestressed concrete: the prestress was designed to ensure tightness of the containment even in case of an internal pressure of 0.5 MPa. Indeed, the prestress (applied by the prestressing steel tendons) ensures that the concrete remains permanently compressed, hence keeping any crack or micro-crack closed. The prestress is therefore a key ingredient to ensure tightness of the confinement. However, because of creep of concrete (and of the prestressing tendons), the prestress decreases over time, at a rate which depends on the creep properties of the concrete. Predicting the evolutions of prestress over time requires an accurate knowledge of the creep behavior of the concrete.

A specificity of the concrete containment building is that the prestress of the concrete is biaxial (i.e., vertical and orthoradial). Consequently, predicting how this biaxial prestress of the concrete will relax over time requires the knowledge of the full three-dimensional creep behavior of concrete. Concrete being an isotropic material, its 3-dimensional elastic behavior is characterized by two elastic parameters, which can be for instance the Young's modulus E and the Poisson's ratio ν. By extension, for what concerns linear viscoelasticity, the 3-dimensional viscoelastic behavior of a mature (i.e., non-aging) concrete is characterized by two time-dependent relaxation moduli, for instance a Young's relaxation modulus $E(t)$ and a viscoelastic equivalent $\nu(t)$ of a Poisson's ratio (Christensen, 1982). The Young's relaxation modulus, which is the inverse (in the sense of the convolution product) of the uniaxial creep compliance, has been studied extensively, through uniaxial creep experiments. In contrast, very little is known about the viscoelastic equivalent of the Poisson's ratio of concrete.

Based on various studies available in the literature, Neville et al. (1983) gathered the following values for the viscoelastic equivalent of the Poisson's ratio of concrete: close to 0 (Ross, 1954; Furr, 1967), equal to 0.05 (L'Hermite, 1959), equal to the elastic Poisson's ratio (Duke and Davis, 1944; Polivka et al., 1963), increasing with time, or decreasing with time (York et al., 1972)! Although part of the variability may come from the variety of hydric conditions used in the various experimental campaigns, even for basic creep (i.e., in absence of any hydric transfer, see Table 3.1), no consensus existed. We aimed at bringing a clear answer to the question of the value of the viscoelastic equivalent of the Poisson's ratio of concrete.

Approach

Part of the scatter observed in the literature originates from the fact that there exist many different definitions for the viscoelastic equivalent of a Poisson's ratio, as mentioned by Hilton (2017) in his review paper. Consequently, a first step was to get a clear idea on how to define a viscoelastic equivalent of a Poisson's ratio. Then, we aimed at making a consistent use of this definition to perform an exhaustive analysis of all basic creep data from the literature for

which sufficient information was available (i.e., in which strain was measured in at least two directions) to back-calculate this Poisson's ratio.

Main results

Naturally, by analogy with elasticity, in viscoelasticity a Poisson's ratio can be defined, for a sample solicited uniaxially, as the ratio

$$-\frac{\varepsilon_l(t)}{\varepsilon_a(t)} \tag{3.2}$$

between a lateral strain $\varepsilon_l(t)$ and an axial strain $\varepsilon_a(t)$.

A first choice to be made is whether the strains considered in Eq. 3.2 must be creep strains or total strains (these latter being the sum of elastic strains and creep strains). In the spirit of the recommendation of Bažant et al. (1993), we chose to consider a definition based on total strains. Indeed, if only a parameter based on creep strains is reported, and if elastic stiffness is not reported in parallel (which often happens in the literature), the reported data is useless for the reader. For instance, when fitting his B4 model to an exhaustive set of creep data from the literature (RILEM Technical Committee TC-242-MDC, 2015), Bažant had to discard all data for which creep strains were provided but elastic stiffness was not.

Even when the choice of working with total strains is made, one can choose to apply definition 3.2 to a uniaxial creep test (in which the axial stress is kept constant over time) or to a uniaxial relaxation test (in which the axial strain is kept constant over time). The application of this definition to those two tests will provide two different time-dependent Poisson's ratios, which we named creep Poisson's ratio and relaxation Poisson's ratio, respectively.

Strictly speaking, creep and relaxation Poisson's ratio are not equal to each other, although their initial values (which is the elastic Poisson's ratio) and their long-term asymptotic values are identical. The creep Poisson's ratio is the one usually reported in the literature, as it can be directly calculated from strains measured in a creep experiment. However, when employing the elastic-viscoelastic correspondence principle (Christensen, 1982), the relaxation Poisson's ratio is the operator with which the elastic Poisson's ratio should be replaced. Although creep and relaxation Poisson's ratios are not equal, we showed, based on an analysis of creep experiments on cement pastes, mortars, and concretes, that those two Poisson's ratios differ in a negligible manner for cement-based materials. Consequently, we do not distinguish them and refer to them as to the viscoelastic Poisson's ratio.

We now present an example of the interest of using a definition based on total strains rather than on creep strains. By using a definition of Poisson's ratio based on creep strains rather than total strains, Gopalakrishnan et al. (1969) proposed that, for a concrete sample under

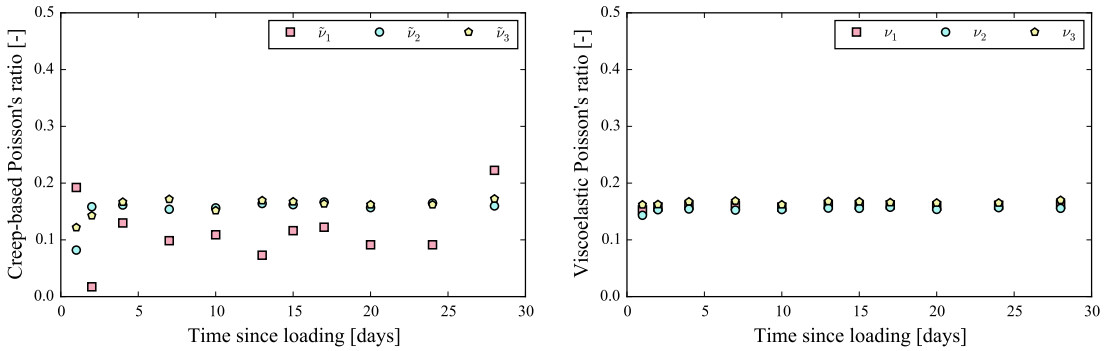

Figure 3.4 – Time-dependent Poisson's ratio in different directions, calculated from data of experiment TC10 of Gopalakrishnan et al. (1969), when using (left) creep strains or (right) total strains. Total strains are the sum of elastic strains and creep strains. Figures from Aili et al. (2016).

triaxial compression, creep properties are anisotropic, i.e., time-dependent Poisson's ratios are different in different directions (see Fig. 3.4-left). With the definition that we chose, based on total strains, a new analysis of the same set of data provides a creep behavior that is fully isotropic, i.e., time-dependent Poisson's ratios which are the same in all directions (see Fig. 3.4-right). This isotropy of the creep behavior is consistent with the fact that concrete is an isotropic material. Therefore, the anisotropy proposed by Gopalakrishnan et al. (1969) appears to have been an artifact induced by the way how the time-dependent Poisson's ratio was defined.

With a clear definition of viscoelastic Poisson's ratio in mind, we then analyzed all data available in the literature (found in a database gathered in Northwestern University by Bažant's group (Bažant and Li, 2008)) out of which we could calculate a viscoelastic Poisson's ratio. The results of the analysis are displayed in Fig. 3.5 in a condensed manner, where we only display the long-term asymptotic value of the viscoelastic Poisson's ratio versus its initial one (i.e., the elastic Poisson's ratio). Based on the few data available, we can conclude that the long-term value of the viscoelastic Poisson's ratio of concrete is equal to or smaller than its elastic Poisson's ratio, and comprised between 0.15 and 0.20. Importantly for the engineer, when the elastic Poisson's ratio of mature concrete is comprised between 0.15 and 0.20, for practical applications, one can consider that its viscoelastic Poisson's ratio is constant over time. Bažant had made this assumption all along his career (see., e.g., Bažant and Wittman (1982)), but had never justified it. Here we showed that his assumption was very reasonable!

By using Eshelby-based homogenization schemes (i.e., the Mori-Tanaka scheme (Mori and Tanaka, 1973)), we downscaled the viscoelastic Poisson's ratio of concrete down to the scale of C-S-H. Results of this downscaling are presented in Fig. 3.6. This figure shows that the long-term viscoelastic Poisson's ratio of the C-S-H gel has little effect on the long-term viscoelastic Poisson's ratio of concrete. We also find that the long-term viscoelastic Poisson's ratio of the

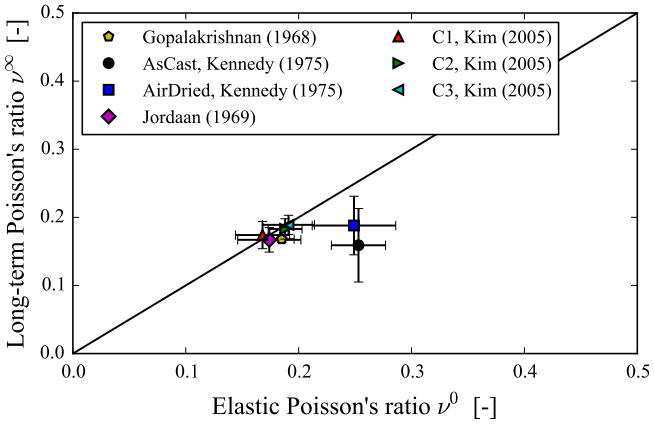

Figure 3.5 – Long-term asymptotic value of viscoelastic Poisson's ratio of concrete versus elastic Poisson's ratio of concrete, averaged over all experiments performed with a specific mix design. Figure from Aili et al. (2016).

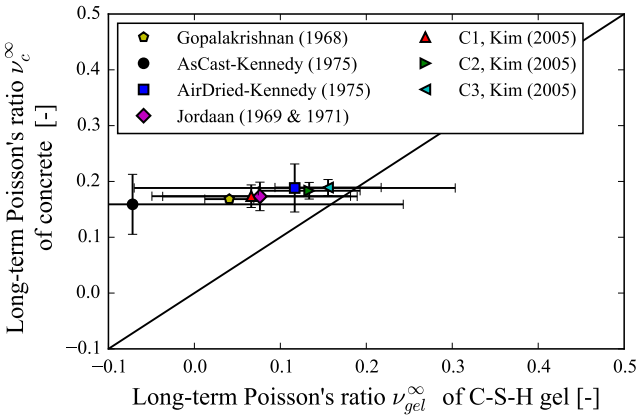

Figure 3.6 – Long-term value of viscoelastic Poisson's ratio of concrete versus long-term value of viscoelastic Poisson's ratio of C-S-H gel. Figure from Aili et al. (2016).

C-S-H gel is comprised between 0 and 0.2: any potential mechanism proposed to explain creep of C-S-H should be consistent with this observation.

Conclusions

We showed that, once properly defined, the viscoelastic Poisson's ratio is the same in all directions, which is consistent with the fact that the creep properties of an isotropic material should be isotropic. For regular concretes, for which the elastic Poisson's ratio is comprised between 0.15 and 0.2, considering for practical applications that their viscoelastic Poisson's ratio is constant over time is a very reasonable assumption. This result (already assumed by Bažant and many others) is of value for the engineer.

We downscaled the viscoelastic Poisson's ratio down to the scale of the C-S-H gel and found that, in the long term, the viscoelastic Poisson's ratio of concrete must be comprised between 0 and 0.2. Any mechanism proposed to explain the physical origin of creep in C-S-H should be confronted to this observation.

3.4 Kinetics of long-term autogenous shrinkage

Ph.D. student: Abudushalamu AILI
Related journal article: Aili et al. (2018)
Colleagues involved: Jean-Michel TORRENTI (IFSTTAR), Benoit MASSON (EDF)

Context and approach

As apparent in Table 3.1, time-dependent strains are decomposed into autogenous shrinkage, basic creep, drying shrinkage, and drying creep. Those 4 components are considered to add to each other to yield the total time-dependent strain of the concrete material under any type of mechanical and hydric conditions. This classical decomposition is fully legitimate phenomenologically, as it is directly associated to the various experiments that can be performed to assess time-dependent deformations of concrete. In practice, many design codes obtain the total delayed strain by summing the 4 components described above (e.g., Fib (2012) or ACI Committee 209 (2008)). However, from a physical point of view, this phenomenological decomposition is not fully satisfactory, in the sense that it does not recognize that those strains all result from the response of a porous material made of a solid skeleton which creeps to a complex combination of loads (induced by hydration, by the presence or absence of water, by the application of a mechanical load, or by the action of eigenstresses). Recognizing this unified physical origin, we envisioned to go beyond the classical phenomenological decomposition presented in Table 3.1 and propose a poromechanical model out of which the different time-dependent contributions could result, without being assumed a priori, in the spirit of the poromechanical model developed by Sellier et al. (2015).

In a first step toward this effort, we focused on autogenous shrinkage, and more precisely on the kinetics of long-term autogenous shrinkage. As already explained in section 3.1, autogenous shrinkage is the strain over time of a concrete sample that is sealed (i.e., exchanges no moisture with its surroundings) and is not loaded mechanically. Autogenous shrinkage is considered to be asymptotic with time in some models and in some engineering design codes (see e.g. RILEM Technical Committee TC-242-MDC (2015); Eurocode (2004); Fib (2012)). However, an exhaustive analysis of the data from the literature gathered by Bažant and Li (2008) shows that autogenous shrinkage never stops, as can be observed in Fig. 3.8: in the long term, autogenous shrinkage evolves linearly with the logarithm of time.

A physical explanation, proposed first by Hua et al. (1995), could be the following. The

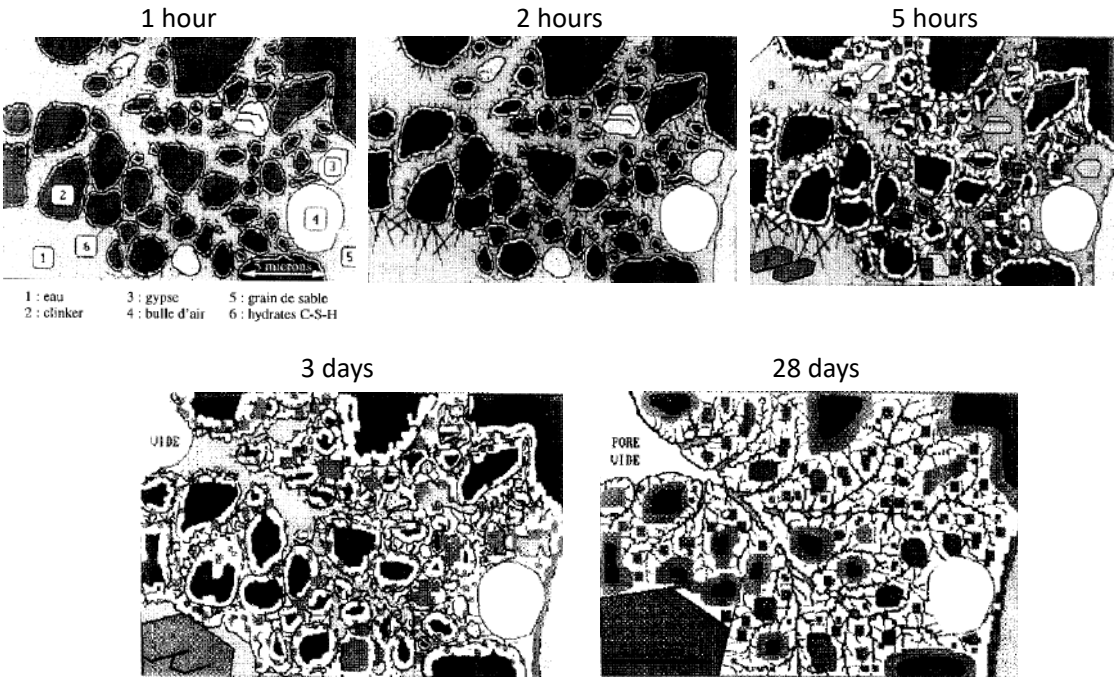

Figure 3.7 – Evolution of microstructure of cement paste over hydration. 1: water; 2: clinker; 3: gypsum; 4: air bubbles; 5: sand grains; 6: C-S-H. 'Vide' and 'pore vide' are vapor bubbles. Figures from Chanvillard (1999).

hydration reactions are such that the volume of the products is smaller than the volume of the reactants. When the cement paste (or the concrete) is still fluid, such difference of volume induces directly a contraction of the sample, called Le Chatelier's contraction. Even if the sample is sealed (i.e., exchanges no moisture with its surroundings), after setting has occurred (i.e., after the cement paste or concrete has become solid), hydration still goes on, and the system must geometrically accommodate this difference of volume: bubbles of vapor nucleate in the pore space, and grow as hydration progresses (see Fig. 3.7). The consumption of pore solution hence leads to the partial desaturation of the pore space, to the creation of curved interfaces (i.e., menisci) between the pore liquid and its vapor, and hence to a decrease of internal relative humidity: such phenomenon is called self-desiccation. Consequently, the pressure of the pore liquid becomes more and more negative (with respect to the atmospheric pressure), which translates into a compressive stress applied to the solid skeleton. Since the solid skeleton of cement-based materials is viscous, under the action of this stress induced by capillary effects, one expects the sample to shrink over time.

Such idea was proposed first by Hua et al. (1995) and used by others (see e.g. Gawin et al. (2006); Grasley and Leung (2011); Wyrzykowski et al. (2011); Luan and Ishida (2013); Hajibabaee et al. (2016); Li et al. (2017)). In particular, Ulm et al. (1999) verified for five concretes that differed in their water-to-cement ratio and for which basic creep and autogenous shrinkage were measured by Le Roy (1996) that this idea was compatible with experimental observations. Here, we aimed at exhaustiveness, by verifying on all possible tests on CEM I concrete or cement

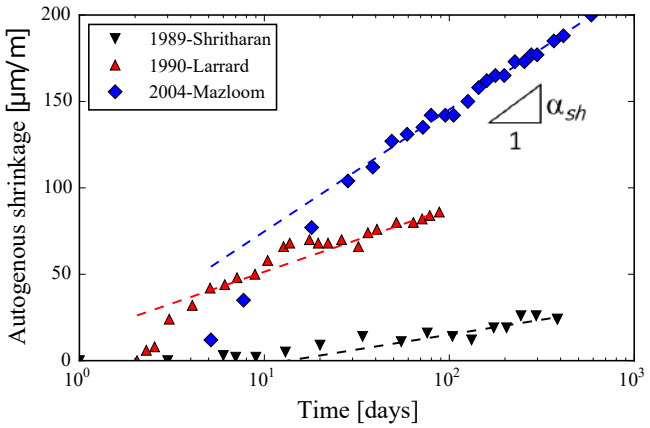

Figure 3.8 – Examples of autogenous shrinkage data. When autogenous shrinkage looks linear in a semi-log scale in the long term, as is the case here, the slope of the line is the parameter α_{sh} defined in Eq. 3.3. Figure from Aili et al. (2018).

paste samples in the literature (i.e., again, in the database gathered at Northwestern University (Bažant and Li, 2008)) whether indeed, the kinetics of long-term autogenous shrinkage could be explained by creep under the action of capillary forces induced by self-desiccation.

Main results

Sufficiently long autogenous shrinkage experiments exhibit a long-term kinetics that is logarithmic with respect to time. Consequently, in the long term, autogenous shrinkage strain $\varepsilon_{sh}(t)$ can be well approximated by:

$$\varepsilon_{sh}(t) = \alpha_{sh} \log(t/\tau_0) + \beta_{sh}, \tag{3.3}$$

so that the long-term kinetics is governed by the parameter α_{sh}, which we fitted for each sufficiently long experiment on concrete or cement paste available in the literature. The parameter α_{sh} is the slope of the line observed when plotting the autogenous shrinkage data on a semi-log scale (see Fig. 3.8). If the volumetric creep modulus C_c of the tested concrete or cement paste was known (see Eq. 3.1 for the definition of the creep modulus), we could calculate the equivalent mechanical stress σ_h to which the material should be subjected to explain this long-term kinetics of autogenous shrinkage, since linear viscoelastic calculations show that $\sigma_h = 3\alpha_{sh}C_c$. We could then check whether the back-calculated mechanical stress σ_h was consistent with the magnitude expected from stresses due to capillary forces. This is in short the procedure we followed, close to the fact that the creep properties of most of the concretes and cement pastes tested for autogenous shrinkage were not known, as they were not measured. Therefore, as a prerequisite to the procedure here proposed, we needed

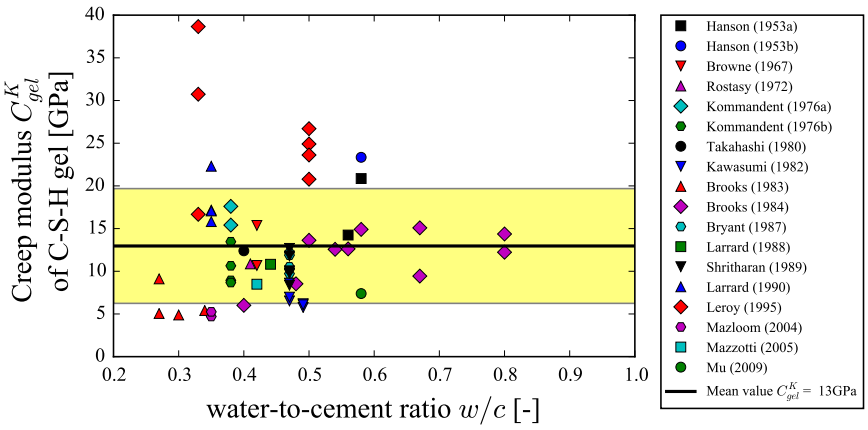

Figure 3.9 – Volumetric creep modulus $C_{\text{C-S-H}}$ of C-S-H as a function of water-to-cement ratio, computed from basic creep data available in the literature. The creep modulus controls the long-term kinetics of logarithmic creep (see Eq. 3.1). Figure adapted from Aili et al. (2018).

to estimate the creep properties (i.e., the creep modulus) of the concretes and cement pastes tested for autogenous shrinkage, based on their mix design.

We aimed at estimating the creep moduli of the concretes and cement pastes with upscaling, based on the creep modulus $C_{\text{C-S-H}}$ of C-S-H and the volume fraction of the various phases (known from the mix design), by using Mori-Tanaka schemes, under the assumption that no phase other than C-S-H could creep and that the various phases were perfectly bonded to each other. Such estimation by upscaling required the knowledge of the creep modulus of C-S-H. Consistently with our approach, the creep modulus $C_{\text{C-S-H}}$ of C-S-H was obtained by downscaling all basic creep measurements available in the literature that were sufficiently long to reach a logarithmic kinetics of creep. The results of this downscaling are displayed in Fig. 3.9. In spite of an evident scatter, the back-calculated volumetric creep modulus $C_{\text{C-S-H}}$ of C-S-H seems rather independent of the water-to-cement ratio: $C_{\text{C-S-H}} \approx 13$ GPa.

From the knowledge of the volumetric creep modulus of C-S-H and of the mix design, we could then estimate, for each concrete or cement paste on which autogenous shrinkage was measured, what its bulk creep modulus C_c was. For each of those concretes, the long-term kinetics of autogenous shrinkage is characterized by the parameter α_{sh} (see Fig. 3.8). We could hence calculate, for each concrete, to which equivalent mechanical stress $\sigma_h = 3\alpha_{sh}C_c$ the sample had to be submitted to explain the measured long-term kinetics of autogenous shrinkage. The results of this back-calculation are displayed in Fig. 3.10.

We then calculated, for each sample, the mechanical stress to which the sample was submitted under the action of capillary forces induced by self-desiccation. To do so, a simple version of partially saturated poromechanics yields that the volumetric stress induced by a capillary pressure P_c is equal to bS_LP_c, where b is the Biot coefficient of the material and S_L is the liquid saturation. Using Power's model (Powers and Brownyard, 1948) at an asymptotic degree of

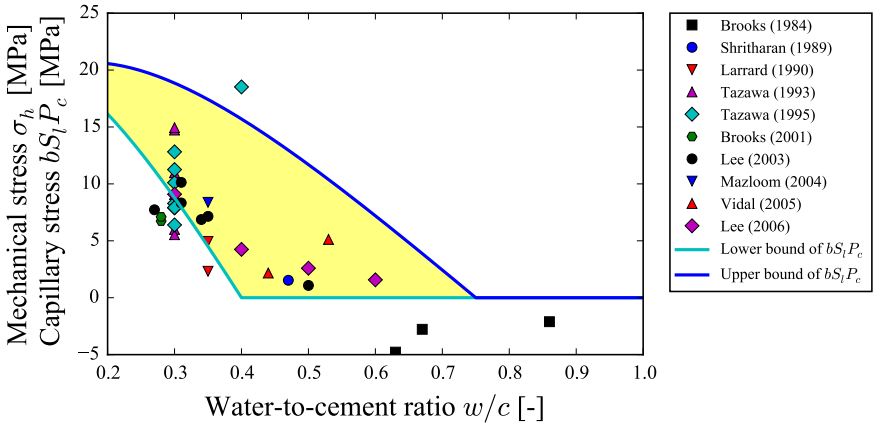

Figure 3.10 – Mechanical stress σ_h that should act on C-S-H gel to explain the long-term kinetics of autogenous shrinkage measured on concrete samples, displayed together with estimated bounds of the capillary stress bS_lP_c. Figure adapted from Aili et al. (2018).

hydration, the liquid saturation S_L can be estimated. Based on this same model, the volume fractions of the various phases can be estimated, which, in concatenation with Mori-Tanaka upscaling schemes, makes it possible to estimate the Biot coefficient b of the material. For the case of a Poisson's ratio of the C-S-H gel equal to 0.2, the viscoelastic Biot coefficient b of the material (i.e., cement paste or concrete) remains constant over time, and hence equal to its elastic value. The capillary pressure P_c is inferred from the long-term internal relative humidity h_R and the mole fraction x of ions in the pore solution (estimated to x =0.03, in accordance with results by Chen et al. (2013)) through Kelvin's law:

$$P_c = -\frac{RT}{V_w} \log \frac{h_R}{1-x}, \tag{3.4}$$

where V_w is the bulk molar volume of liquid water, R is the ideal gas constant, and T is the temperature.

Upper bounds and lower bounds for long-term relative humidity were estimated based on data available in the literature, and translated into respectively lower bounds and upper bounds of the capillary pressure P_c, and hence of the stress bS_LP_c due to capillary forces. The estimates of the bounds are displayed in Fig. 3.10, together with the back-calculated stress σ_h that should act on the concrete to explain their long-term kinetics of autogenous shrinkage. The fact that those back-calculated stresses lie in-between the estimated bounds indicates that the hypothesis that, in the long term, autogenous shrinkage is due to creep of the solid skeleton under the action of capillary forces is plausible.

Extension of the work

As mentioned in the presentation of the context of this study, we envisioned the derivation of a poromechanics-based model of a mature concrete, from which would naturally come out the various components of time-dependent deformations. In the framework of the Ph.D. of Aili (2017), we derived such poromechanics-based model (not presented in this manuscript), in which concrete was considered as a porous material with a solid skeleton which creeps, and is submitted to stresses induced by water and/or mechanical loading. The model is restricted to mature concrete, i.e., no aging induced by hydration is considered.

In its basic form, the model we derived is able to capture autogenous shrinkage, basic creep, and drying shrinkage, but fails at capturing drying creep: it predicts no drying creep. We remind that drying creep is the additional time-dependent strain of a loaded specimen exchanging water with its surroundings, with respect to the sum of autogenous shrinkage, basic creep and drying shrinkage (see Table 3.1). To capture drying creep, like Bažant and Xi (1994) and others, we had to enforce it phenomenologically in the model, in the spirit of what Sellier et al. (2015) did with their own poromechanical model: we needed to assume that the mechanical stress induced by capillary effects is augmented when the sample is loaded mechanically.

Conclusions and perspectives

The work here performed was based on an idea that had already been proposed in the literature, namely that autogenous shrinkage could be the viscous deformation of the solid skeleton under the action of capillary stresses induced by self-desiccation. The originality of our work rather lied in the exhaustiveness of the approach: we aimed at considering all sufficiently long autogenous shrinkage data available in the literature on CEM I (or equivalent) cement pastes or concretes. Since the study required an estimate of the creep properties of the tested concrete, to obtain this estimate, we analyzed all sufficiently long basic creep data in the literature on CEM I (or equivalent) cement pastes or concretes.

Our study is limited to the long-term kinetics of autogenous shrinkage. At early age, the picture is different: after mixing, the material is saturated and, once setting has occurred, relative humidity starts decreasing from unity, so that capillary stresses are initially very small. Therefore, the capillary stresses here identified as the driving force of long-term autogenous shrinkage may not drive early-age autogenous shrinkage. At early age, other phenomena enter the picture: on top of the well-known Le Chatelier's contraction, Abuhaikal et al. (2018) proposed a mechanism for autogenous shrinkage based on the evolution of colloidal eigenstresses. Such phenomena are likely to be more active at early age than in a mature concrete, as they are driven by hydration. Having a physical model of autogenous shrinkage that would be valid over the whole life of the material (i.e., from its early age up to its mature age) would present an interest, as it would make it possible to identify what physical process is dominating the evolutions of deformation at the various ages of the material.

As mentioned earlier, we envisioned a unified poromechanical physically-based model that could yield all components of time-dependent deformations naturally. Such model, that we derived for a mature concrete, would need to be extended to early age to include the effect of hydration. Even for mature concrete only, one weakness of the model is that drying creep could only be included in a phenomenological manner. Such phenomenological enforcement remains unsatisfactory, given our objective of deriving a unified poromechanical physically-based model that could capture all components of time-dependent deformations. The physical origin of drying creep remains quite debated. An interesting feature of drying creep is that it is not only observed for cement-based materials, but also for many other materials, including wood (for which it is called mechano-sorption) and Kevlar (Vlahinić et al., 2012). Therefore, drying creep appears to find its origin in what cement-based materials bear in common with those materials rather than in what distinguishes cement-based materials from them. A good candidate for this common origin seems to be the presence of micropores (see, e.g., Vlahinić et al. (2012) or Sinko et al. (2016)). Determining the physical origin of drying creep and how to implement it in a physical manner in a poromechanical model would be interesting.

3.5 Physical origin of long-term basic creep: two models based on local microscopic relaxations

Related journal article: Vandamme (2019)

Context and approach

This work was performed during my stay at the University of Cambridge in 2017-2018, as a French government by-fellow at Churchill College and as a visitor at the Department of Engineering.

As explained in section 3.1, a logarithmic kinetics of creep is observed for concrete in the long term. But such a logarithmic kinetics of creep is also observed for soils (Lambe and Whitman, 1969) and for some metallic alloys (Nabarro and DeVilliers, 1995). For those latter, two models have been proposed, which make it possible to retrieve such a logarithmic kinetics (Nabarro, 2001): those two models are called the exhaustion model and the work-hardening model. The goal of this work was to find out whether those two models yield evolutions of strains over time which are consistent with phenomenological observations of creep of concrete.

The two models

In the two models, the macroscopic deformation is initiated at sites whose activation requires some energy (i.e., an energy barrier needs to be overcome). The two models differ in how the activation energies are distributed and evolve during the creep process. We interpret the local

initiations of deformation as local microscopic relaxations.

We consider a material loaded with a macroscopic stress Σ (see Fig. 3.11). In the two proposed models, we consider that the material is subjected to a succession of local microscopic relaxations. If, in absence of any macroscopic stress, a local microscopic relaxation leads to an increment of macroscopic strain (which will happen if the microscopic volume to be relaxed is prestressed/eigenstressed), with respect to the terminology commonly used to describe time-dependent deformations of concrete, this increment is interpreted as autogenous shrinkage. Here, since we are interested in basic creep, the strain of interest for our problem is the one in excess of this autogenous shrinkage, i.e., the additional incremental strain occurring during the local microscopic relaxation, as a consequence of the presence of the macroscopic stress Σ (see Fig. 3.11).

We consider that each local microscopic relaxation requires an activation energy U. Classically, in the spirit of the transition state theory, the characteristic time τ_m for this local microscopic relaxation to occur should scale with the Boltzmann distribution $\exp(U/k_BT)$, where k_B is the Boltzmann constant and T is the absolute temperature: $\tau_m = \tau_0 e^{U/k_BT}$, where τ_0 is a microscopic characteristic time. We also assume that, under the action of a macroscopic stress Σ, the local relaxation will always lead to the release of the same elastic energy, on the order of $(\Sigma^2/2E)\Omega_m$, where E is the Young's modulus of the material and Ω_m is the characteristic microscopic volume relaxed at each local microscopic relaxation, and hence to the same small increment ε_{ind} of macroscopic strain: $\varepsilon_{ind} \sim (\Sigma/E)(\Omega_m/\Omega)$.

As we will see, the two models here proposed will yield a creep function $\varepsilon(t)/\Sigma$ that evolves logarithmically with time after a transient period, i.e., that can be approximated in the long term by:

$$\varepsilon(t)/\Sigma \approx \alpha \ln(t/\tau)\,. \tag{3.5}$$

The parameter τ will be referred as to the characteristic time of logarithmic creep, and the parameter α as to the prefactor to logarithmic creep. This prefactor, whose dimension is that of the inverse of a stiffness, governs the long-term logarithmic kinetics of creep since, in the long term: $\dot{\varepsilon}(t)/\Sigma \approx \alpha/t$.

In the exhaustion model (see Fig. 3.12-a), activation energies U_0 are distributed uniformly. The number of local microscopic relaxation sites with an activation energy comprised between U_0 and $U_0 + dU_0$ is noted $\bar{n}_0 dU_0$, where $\bar{n}_0$, whose dimension is the inverse of an energy, is constant. Under the action of a macroscopic stress Σ, the activation energies may be impacted. Hence, in first order, the activation energies are $U = U_0 - v_{exh}\Sigma$, where the dimension of v_{exh} is that of an energy divided by a stress, i.e., of a volume. The characteristic time for a given local relaxation to occur scales as $\tau_m = \tau_0 \exp((U_0 - v_{exh}\Sigma)/k_BT)$. Assuming a Poisson's process

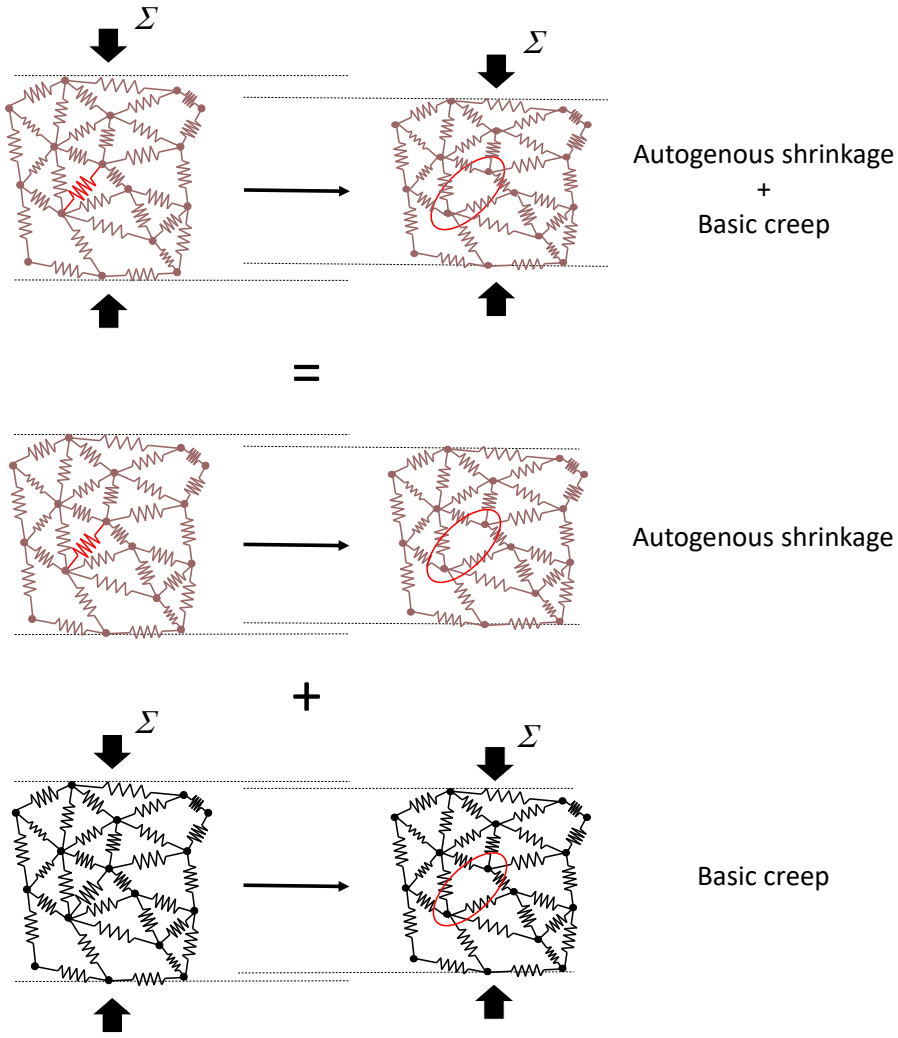

Figure 3.11 – Strain observed during a local microscopic relaxation in presence of a macroscopic stress Σ. With respect to the classical terminology used in concrete science, this strain is the sum of autogenous shrinkage and basic creep. Autogenous shrinkage is the macroscopic strain induced by the local microscopic relaxation of a prestressed/eigenstressed microscopic element (i.e., the red spring). Basic creep is the macroscopic strain induced by the local microscopic relaxation of a microscopic element in absence of any prestress/eigenstress (i.e., the black spring) but in presence of the macroscopic stress Σ. The meaning of the colors is the following: a red spring is a microscopic element subjected to a prestress/eigenstress (i.e., a microscopic element that is stressed even when no macroscopic stress is applied); a black spring is a microscopic element submitted to no prestress/eigenstress; a brown spring is a microscopic element which may or may not be prestressed/eigenstressed. Figure from Vandamme (2019).

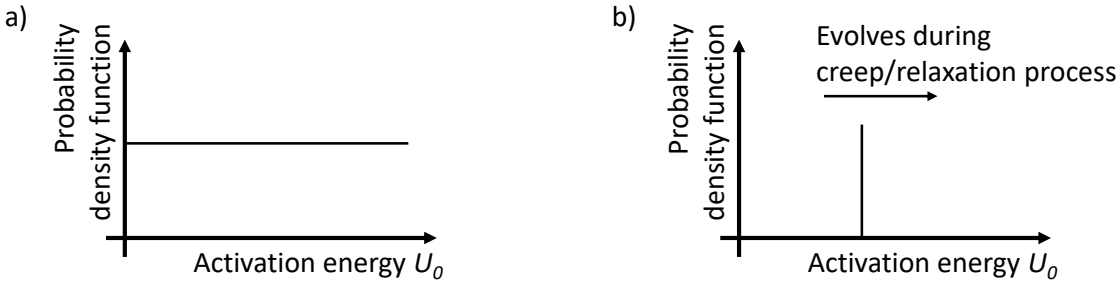

Figure 3.12 – Probability density functions of activation energies barriers a) in the exhaustion model and b) in the work-hardening model. The activation energy U_0 is that in absence of any macroscopic stress Σ and of any prestress/eigenstress σ. In the work-hardening model, the probability density function is a Dirac delta function. Figure from Vandamme (2019).

for the local microscopic relaxations of sites with an activation energy (in absence of any macroscopic stress) comprised between U_0 and $U_0 + dU_0$, after some manipulation, one finds out that, with the exhaustion model, in the long term, the creep function $\varepsilon(t)/\Sigma$ evolves as:

$$\frac{\varepsilon(t)}{\Sigma} \approx \frac{\bar{n}_0 k_B T \Omega_m}{E\Omega} \ln\left(\frac{t}{\tau_{exh}}\right), \text{ with } \tau_{exh} = \tau_0 \exp\left(-\left(\gamma + \frac{v_{exh}\Sigma}{k_B T}\right)\right), \tag{3.6}$$

where γ is the Euler-Mascheroni constant.

In the work-hardening model (see Fig. 3.12-b), the activation energy U is the same at all local microscopic relaxation sites, but evolves over time. In the version of the work-hardening model proposed by Nabarro (2001), the activation energies increase with strain. Here, in a dual version, we consider that there exists some microscopic prestress/eigenstress σ which impacts the energy barriers and is impacted by the local microscopic relaxations. In concrete science, this microscopic prestress/eigenstress can be the micro-prestress of Bažant et al. (1997) or the eigenstress of Abuhaikal et al. (2018) (hence the reference to a 'prestress/eigenstress' in the caption of Fig. 3.11). As was the case with the exhaustion model, we also consider here that the applied macroscopic stress Σ, as well as the prestress/eigenstress σ, can impact the activation energy U, hence expressed as $U = U_0 - v^{\Sigma}_{wor}\Sigma - v^{\sigma}_{wor}\sigma$, where U_0 is the activation energy of all local microscopic relaxation sites in absence of macroscopic stress Σ and of prestress/eigenstress σ, and where v^{Σ}_{wor} and v^{σ}_{wor} are two parameters whose dimension is that of an energy divided by a stress, i.e., a volume. The rate at which the prestress/eigenstress σ relaxes must be proportional to the rate at which local microscopic relaxation events occur. After some manipulation, one finds out that, with this adapted work-hardening model, the creep function $\varepsilon(t)/\Sigma$ evolves as:

$$\frac{\varepsilon(t)}{\Sigma} = \frac{k_B T \Omega_m}{v^{\sigma}_{wor} E \sigma_{ind} \Omega} \ln\left(1 + \frac{t}{\tau_{wor}}\right) \text{ with } \tau_{wor} = \frac{k_B T}{\dot{\sigma_0} v^{\sigma}_{wor}} \exp\left(\frac{U_0 - v^{\Sigma}_{wor}\Sigma - v^{\sigma}_{wor}\sigma_0}{k_B T}\right). \tag{3.7}$$

Consequently, both the exhaustion model and the adapted work-hardening model make it possible to retrieve a kinetics of creep that evolves logarithmically with respect to time in the long term.

Agreement of models with phenomenology of concrete creep

The two models will be confronted to the actual phenomenology on concrete creep. More specifically, confrontation will be performed with respect to the linearity of concrete creep with respect to stress, to the phenomenology known about the viscoelastic Poisson's ratio (see section 3.3), and to indentation creep measurements (see section 3.2). Both models agree equally well with the phenomenology, so that it is not possible to assess whether one model is better than the other.

But at the very early age (i.e., before 3 days), creep of concrete is known to be linear with respect to the applied stress, up to at least 30% of the compressive strength (Neville et al., 1983), which, for a typical concrete with a compressive strength of 60 MPa, translates into a linearity of the creep behavior up to about 20 MPa of applied stress. An observation of Eqs. 3.6 and 3.7 shows that, for the linearity of the creep function $\varepsilon(t)/\Sigma$ to be ensured, for each model, its characteristic time must be independent of the applied macroscopic stress, which is satisfied if the applied stress is sufficiently small to not impact significantly the activation energies. This constraint implies that, at least up to 20 MPa, the applied stress has no effect on the activation energies, and hence no effect on the probability for local microscopic sites to relax: said otherwise, local relaxations must occur in absence of macroscopic stress as often as when a macroscopic stress is applied (at least up to 20 MPa). If a macroscopic stress is applied, when those local relaxations occur, the relaxation translates into an additional increment of strain, which we interpret macroscopically as basic creep. But the applied macroscopic stress is not the reason for the local relaxation event (at least up to 20 MPa of applied macroscopic stress).

The phenomenology on the viscoelastic Poisson's ratio of concrete was discussed in section 3.3 (see Fig. 3.5). The two models here considered yield identical theoretical evolutions of viscoelastic Poisson's ratio with time. After some calculation, the asymptotic value ν_∞ of the viscoelastic Poisson's ratio in the long term is found to be related to the elastic Poisson's ratio ν_0 through $\nu_\infty = (5\nu_0 + 1)/(5\nu_0 + 9)$. This theoretical prediction, together with the experimental asymptotic values already displayed in Fig. 3.5, are displayed in Fig. 3.13: the two models capture reasonably well the asymptotic values of viscoelastic Poisson's ratio observed experimentally.

A final phenomenological observation relates to indentation creep experiments: as explained in section 3.2, indentation makes it possible to assess quantitatively the long-term kinetics of logarithmic creep of cement-based materials (i.e., the creep modulus C, see Eq. 3.1), but orders of magnitude faster than by macroscopic conventional testing. Using the terminology introduced for Eq. 3.5, indentation testing impacts the characteristic time τ of logarithmic

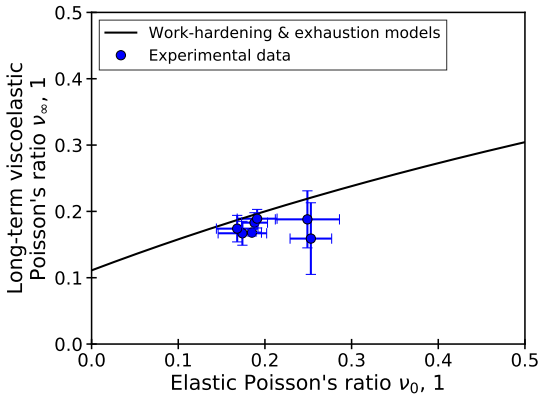

Figure 3.13 – Long-term asymptotic value of viscoelastic Poisson's ratio, as back-calculated from experiments and as predicted with the exhaustion model and with the adapted work-hardening model. The predictions with the two models overlap with each other. The values back-calculated from experiments come from Aili et al. (2016). Figure from Vandamme (2019).

creep, without impacting the prefactor α to logarithmic creep (or the creep modulus C, if we use the terminology of Eq. 3.1). The two models here proposed could explain why: indeed, Eqs. 3.6 and 3.7 show that the applied macroscopic stress Σ can impact the characteristic times τ_{exh} and τ_{wor} but do not impact the prefactors α to logarithmic creep. In indentation creep experiments, the stresses below the Berkovich indenter, which are on the order of a few hundred MPa, would be sufficiently large to significantly decrease the activation energy of the local microscopic relaxations. At the same time, the linearity of the creep behavior with respect to stress observed in standard macroscopic uniaxial creep experiments, which, as discussed before, implies that stresses up to a few dozen MPa do not impact the activation energies, makes it possible to estimate the magnitude of the characteristic stress above which stresses start impacting activation energies: this characteristic stress must be somewhere between a few dozen MPa and a few hundred MPa. Such order of magnitude is comparable with the magnitude of disjoining pressures which prevail in microporous materials such as cement-based materials (Bažant, 1972), which hints toward local microscopic relaxations in cement-based materials that are controlled by disjoining pressure effects (for stresses up to a few dozen MPa).

Concluding remarks

In this work, I discussed the applicability of two models imported from the literature on metallic alloys to explain basic creep of concrete. One model (i.e., the exhaustion model) was used as is, while another one (i.e., the work-hardening model) was adapted to incorporate the concept of microscopic prestress/eigenstress. The two models capture equally well the main phenomenological features of basic creep of concrete (i.e., linearity with respect to stresses, logarithmic kinetics in the long term, and asymptotic value of the viscoelastic Poisson's ratio) and can explain why indentation creep experiments make it possible to assess quantitatively

the long-term kinetics of logarithmic creep (i.e., the creep modulus C, see Eq. 3.1) orders of magnitude faster than regular macroscopic creep experiments.

The models here proposed are quite different, in terms of spirit, from the rate theory proposed to explain creep of concrete (Wittmann, 1982) or of geomaterials (Kwok and Bolton, 2010), although the rate theory also relies on activation of local sites. In that theory, particles constituting the solid skeleton are fixed to their position by interactions with surrounding particles: schematically, they are located in a potential trough. Under the application of a macroscopic stress, the energy landscape is modified, which favors the probability of jump of the particle in some specific directions, which translates into creep. In contrast, with our models based on local microscopic relaxations, the application of a macroscopic stress (at least up to a few dozen MPa) does not modify the activation energies: local microscopic relaxations occur at a rate that is independent of this macroscopic stress, and the macroscopic stress only enables the manifestation of the local microscopic relaxation into an infinitesimal increment of basic creep strain.

In contrast, the idea that the material evolves/relaxes even in absence of any applied load is consistent with the microprestress-solidification theory proposed by Bažant et al. (1997). The adapted work-hardening model relies on the existence and relaxation of a prestress/eigenstress σ, which is the microprestress in the microprestress-solidification theory of Bažant et al. (1997), and is the eigenstress observed by Abuhaikal et al. (2018). To some extent, the adapted work-hardening model can be interpreted as a discrete version of the microprestress-solidification theory, and may provide additional physical basis to this theory.

3.6 General conclusions and other perspectives

With our work on the time-dependent deformations of concrete, we aimed at tackling different challenges which I identified as important in section 3.1: 1) innovative testing methods which could provide indicators of long-term performance in a relatively fast manner, 2) accurate modeling of the long-term time-dependent behavior of concrete, 3) understanding of the physical origin of time-dependent deformations.

We contributed to those 3 challenges. 1) We showed that micro-indentation (in conjunction with analytical upscaling schemes) can provide in minutes an assessment of the long-term logarithmic kinetics of creep of concrete (see section 3.2). 2) We showed that, for engineering application, the viscoelastic Poisson's ratio can be considered constant over time (see section 3.3). 3) We showed that considering that the long-term kinetics of autogenous shrinkage is due to creep of the solid skeleton under the action of capillary forces is a plausible hypothesis (see section 3.4). We also discussed the relevance of two models based on local microscopic relaxations to explain basic creep of concrete (see section 3.5). When addressing each of those topics, I detailed some perspectives directly related to each of them. But I would like to underline next some other perspectives or interesting topics, which are also in relation with time-dependent deformations.

Some of the questions we addressed on time-dependent deformations of cement-based materials could prove relevant to a wider range of materials than just cement-based materials. Typically, the logarithmic feature of the kinetics of long-term creep is encountered in soils (e.g., clays, or sand) (Lambe and Whitman, 1969) as well as concrete. In all those materials, the origin of this logarithmic creep remains unknown, although a variety of processes have been proposed to explain it (see for instance Le et al. (2012) for a review of proposed mechanisms for clays, or Ye (2015) for a review of proposed mechanisms for C-S-H). We already mentioned some for cement-based materials in section 3.1. For clays, one can mention, among others: breakage of particles (Kwok and Bolton, 2013), reorganization of intermolecular bonds (Christensen and Wu, 1964), interparticle or interlayer sliding (Kuhn and Mitchell, 1993). In any case, the fact that such logarithmic trend is observed on a variety of geomaterials as well as on cement-based materials is quite puzzling. Therefore, considering a common origin for the logarithmic creep of all those materials is quite an appealing idea (although not a granted one). Consequently, as a reason for the logarithmic kinetics of long-term creep of concrete, I would rather look for a physical origin grounded in something that cement-based materials and geomaterials have in common (e.g., disorder, multiscale structure, porosity spanning several orders of magnitude down to the nanoscale, presence of water, heterogeneity,...), rather than in something that distinguishes cement from geomaterials (typically, its chemical composition, or the fact that cement is a material that is reactive).

In section 3.4, we explained how we modeled concrete as a visco-elastic solid skeleton submitted to capillary pressures. This approach could explain the long-term kinetics of autogenous shrinkage, as a consequence of creep under the action of capillary forces due to self-desiccation. However, one can wonder whether such a model (i.e. visco-elastic solid skeleton submitted to capillary effects) remains relevant for an unsealed sample exposed to drying. Indeed, not all water present in the sample deforms the material through capillary effects, as water is also adsorbed on surfaces or in the micropores of the C-S-H gel. At the relative humidities encountered in autogenous conditions (which are larger than 80%), considering only capillary effects may be relevant, but it is certainly not the case at relative humidities of 50%, at which very little capillary water is present. In Vandamme et al. (2010), for application to coal, we considered how surface adsorption deforms the material. And, as presented in section 2.2 and in Brochard et al. (2012), for application to coal again, we also considered the case of deformations induced by adsorption in generic pores, including micropores. However, we still lack a poromechanical model of the strains induced by variations of relative humidities on the full range of relative humidities, which distinguishes between capillary water, water adsorbed on surface, and water adsorbed in micropores. This perspective, which I mention here in this chapter on time-dependent deformations, is in fact not limited to time-dependent deformations only, but is relevant to drying-induced deformations in general, may they be delayed or instantaneous.

Finally, I wanted to mention the topic of transitional thermal creep (Parrott, 1979), which is an acceleration of load-induced creep when the load is concomitant with an increase or decrease of temperature. Cement-based materials exhibit thermal transient creep, as they

exhibit drying creep, which, we remind, is an acceleration of load-induced creep when the load is concomitant with an increase or decrease of relative humidity. I think the parallel between those 2 phenomena is quite puzzling, and I therefore wonder whether their physical origin does not overlap, at least partly.

4 Additional topics tackled

In this chapter, I want to describe in a briefer manner several other topics on which I worked. The description does not cover all topics addressed during the Ph.D. studies I co-advised: on top of the topics described in the sections below, I also worked on the optimization of the thermo-hydromechanical properties of concrete with wood aggregates (Ph.D. of Abdessamad Akkaoui, directed by S. Caré), and on the effect of fluids and temperature on creep of geo-materials (Ph.D. of Hugo Troupel, directed by J.-M. Pereira). Presently, I am also co-advising the Ph.D. project of Ginger El Tabbal (directed by P. Dangla, co-advised with S. Granet and M. Bottoni) on the modeling of the behavior of a concrete for a nuclear waste package.

4.1 Freeze-thaw resistance of cement-based materials

Ph.D. student: Nathan MAYERCSIK
(Ph.D. student at GeorgiaTech under the supervision of Kim KURTIS)
Related journal article: Mayercsik et al. (2016)
Colleagues involved: Sébastien BRISARD, Kim KURTIS (GeorgiaTech)

Context and approach

This study was performed in the framework of a collaboration between GeorgiaTech and École des Ponts ParisTech. Such collaboration was made possible by a NSF IRES funding on Coupled Geomechanical Processes and Energy Technologies, obtained by Chloé Arson (GeorgiaTech). Thanks to this funding, for several years in a row, I had the opportunity to welcome students of Kim Kurtis (GeorgiaTech). Among those students, 2 years in a row I welcomed Nathan Mayercsik, to work on freeze-thaw resistance of cement-based materials.

Concrete can be damaged by freezing, but its ability to resist freeze-thaw cycles can be greatly improved by the inclusion of entrained air voids, as shown by Powers (1945, 1949) in his pioneering works. Upon freezing, the effect of air voids is twofold (Coussy, 2005): 1) they serve as reservoir of expansion to accommodate water that is pressurized by the formation of ice (whose density is lower than that of liquid water) in the surrounding paste, and 2) they serve as cryo-pumps. The pressurization of the remaining liquid water by the forming ice is called hydraulic pressure effect (Powers, 1945). What 'cryo-pumps' means is explained next. At negative temperatures, once liquid water is pushed into the air void, it is no more confined and hence freezes. Consequently, liquid water in the capillary pores in the vicinity of the air voids is in contact with ice at atmospheric pressure. Under the hypothesis of local thermodynamic equilibrium, since temperature is negative, this liquid water must be at a pressure lower than the atmospheric pressure, which pulls liquid water from the cement paste toward the air void, hence the term of 'cryo-suction' used to describe this effect and of 'cryo-pump' to describe the role of air voids. Those two effects (i.e., reservoir of expansion and cryo-pump) made possible by the presence of air voids help alleviate the buildup of pore pressure in the paste (or can even lead to the contraction of the air void, as was observed experimentally (Piltner

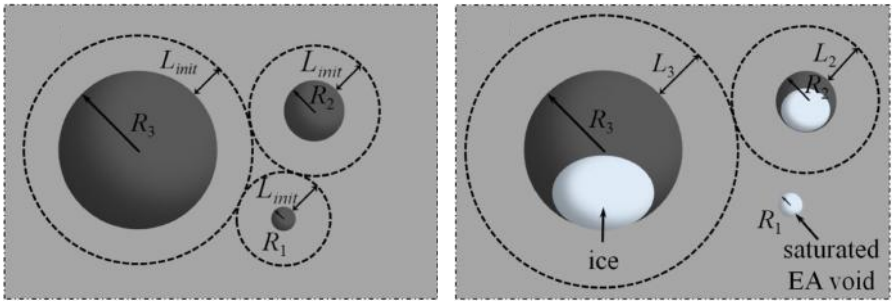

Figure 4.1 – Schematic describing the distribution of entrained air voids and the shell of cement paste surrounding them. (left) Before the first freeze-thaw cycle, the thickness of the shell of cement paste from which water flows toward the air void upon freezing is assumed to be the same for all air voids. (right) After a given number of freeze-thaw cycles, air voids have absorbed some water, to such extent that the smallest air voids are now filled and all water in the cement paste around those air voids must flow to other air voids, resulting in an increasing shell thickness around those latter air voids. Figures from Mayercsik et al. (2016).

and Monteiro, 2000)) and hence make the material more resistant to freezing.

The resistance of a specific concrete to freezing can be assessed with the ASTM C666 standard (ASTM International, 2003). One of the procedures proposed in this standard consists in immersing the sample, performing 300 freeze-thaw cycles, and measuring its dynamic Young's modulus regularly throughout the procedure. The procedure is stopped if the dynamic Young's modulus decreases below 60% of its initial value.

When the sample is immersed at the beginning of the procedure, water quickly invades the capillary porosity by capillary suction, but traps air in the air voids (Fagerlund, 1993), which explains why they can still play their role even if the sample is under water[1]. However, over time, concomitantly with a diffusion of the air outside of the sample, water will invade the air voids (a process that we will call 'absorption'). Consequently, cycle after cycle, an increasing number of air voids will become saturated and lose their ability to protect the material against frost damage (see Fig. 4.1). The rate of absorption, and how absorption occurs (e.g., in an equal manner in all air voids, or not), has been studied extensively by Fagerlund (1993).

One of the first attempts to characterize the distribution of air voids in the paste was done by Powers (1949), which led to the so-called $\bar{L}$ parameter, which is calculated as the distance from the center of a cubic cell to the periphery of an air void, under the assumption that the air void system consists of monosized and regularly spaced porosity. ASTM C457 (ASTM International, 2013) proposed that concrete should withstand freeze-thaw cycles if $\bar{L} < 250$ μm. In his Ph.D. work, Nathan Mayercsik proposed an alternative microstructural parameter, the $\bar{M}$ parameter, defined such that 95% of the paste is at a distance smaller than $\bar{M}$ from the periphery of an air void (Mayercsik et al., 2014). This parameter was envisioned as potentially able to outperform

[1] My thoughts go to Gilles Chanvillard, who replied so kindly, quickly, and friendly (as always) to a naive question of mine, and pointed that out.

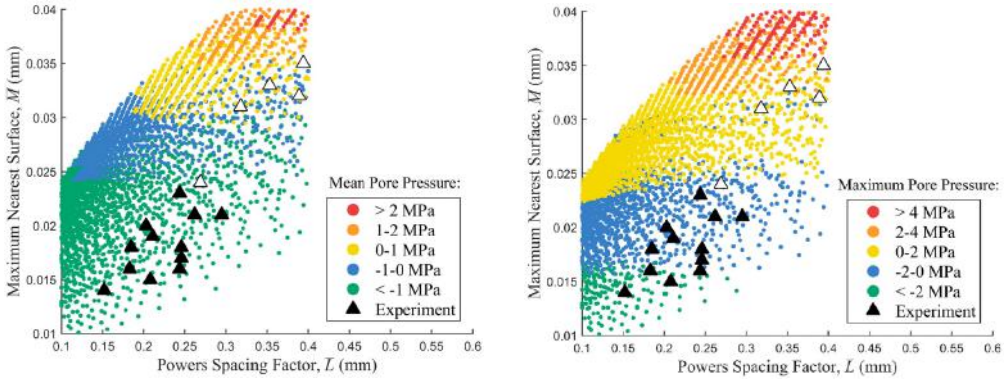

Figure 4.2 – Maximum spacing factor $\bar{M}$ versus Powers' spacing factor $\bar{L}$ for arbitrary air void systems. Color corresponds to maximum pore pressure. Figures from Mayercsik et al. (2016).

the Powers' spacing factor $\bar{L}$, as it takes into account the size distribution of the air voids.

The aim of this collaboration was to use poromechanical modeling to provide some theoretical insight into the relevance of the original $\bar{M}$ parameter in comparison with the more classical Powers' spacing factor $\bar{L}$. To do so, based on virtual arrangements of air voids, we calculated the evolution of pore pressure in the paste around each air void during a freeze-thaw cycle, by using the poroelastic approach proposed by Coussy and Monteiro (2008), which takes into account the effects of hydraulic pressure and cryo-suction. Modeling results were compared with experimental data of concrete samples, whose distribution of air voids was assessed by image analysis and which were submitted to the ASTM C666 standard. For those samples, Fig. 4.2 shows that, although $\bar{L}$ and $\bar{M}$ parameters are correlated, there exist samples with identical $\bar{L}$ but quite different $\bar{M}$, and conversely.

Main results

A large number of virtual microstructures were generated, with various size distributions of air voids, which were then discretized into four size classes, and for which both parameters $\bar{L}$ and $\bar{M}$ were calculated. The evolutions of pore pressure in the shell of paste around each class of air voids during one freeze-thaw cycle were calculated. Results of these calculations are displayed in Fig. 4.2, on which the experimental results are also visible. There appears to exist a threshold mean pore pressure (around -1 to 0 MPa approximately) or maximal pore pressure (around 0 to 2 MPa approximately), above which the samples failed, and below which the samples did not[2]. Mean or maximal pore pressures depend more clearly on $\bar{M}$ than on $\bar{L}$, which supports the idea that the parameter $\bar{M}$ is more relevant physically than Powers' spacing factor $\bar{L}$.

We also aimed at characterizing the evolution or pore pressure over the full ASTM C666

[2]The case of one sample which failed in spite of exhibiting $\bar{L}$ and $\bar{M}$ values close to the ones of samples which did not fail is discussed in Mayercsik et al. (2016).

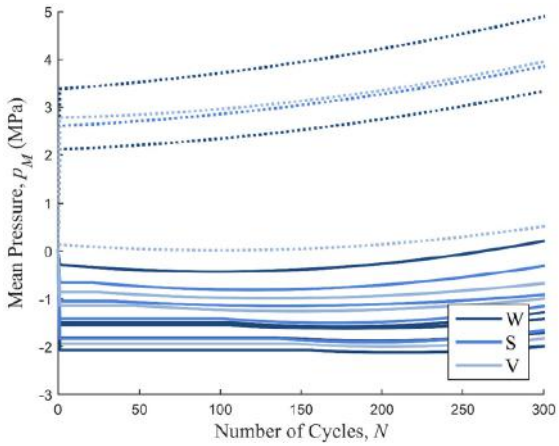

Figure 4.3 – Evolution of mean pore pressure over freeze-thaw cycles, for the various concrete samples tested, as predicted by the model in the case of a low rate of water absorption. The mean pore pressure is calculated at the end of the freezing, i.e., at the lowest temperature of the freeze-thaw cycle. Figure from Mayercsik et al. (2016).

procedure, i.e., over the 300 freeze-thaw cycles. To do so, upon gradual filling of the air voids, when the volume of air remaining in the air void was too small to accommodate all water that needed to be expelled from the paste shell during freezing, we numerically redistributed the shell surrounding this air void around other air voids, with the physical idea that, if water could not flow toward a specific air void because this specific air void was filled with water, it had to flow toward another one (see Fig. 4.1). The air void distribution of the nine concrete samples tested and displayed in Fig. 4.2 was discretized in four size classes. Filling of the air voids was considered to happen first in the smallest air voids, which is one of the mechanism of void filling proposed by Fagerlund (1993). At the lowest absorption rate considered, when significant variations of mean pore pressures were observed over time, the mean pore pressure increased[3]. However, quantitatively, results were quite sensitive to the absorption rate, while Fagerlund (1993) proposes that its magnitude can vary on at least two orders of magnitude.

Perspectives

As just explained, results of the modeling were quite dependent on the absorption rate assumed, while this rate is quite unknown. Better understanding how the air voids become saturated over time would be beneficial. Also, since saturation occurs by diffusion of air toward the surroundings, it is likely that the saturation process is heterogeneous (i.e., that air voids close to the surface of the sample saturate faster than those in the core of the sample), while, in the model, saturation of the air voids was assumed to occur homogeneously throughout the sample.

[3]For some samples, a slight decrease was observed: for some sizes of air voids and cooling rates, slightly increasing the thickness of the shell around the air void led to a decrease of mean pore pressure during cooling.

The model we employed is poroelastic, like most modeling attempts of freeze-thaw resistance based on poromechanics (see, e.g., Coussy and Monteiro (2008) or Zeng et al. (2011)). However, as soon as significant positive pore pressures will develop, one can expect some local damage or micro-cracking in the microstructure, which in turn could provide some additional accessible volume to the fluid, and hence help relieve those positive pore pressures. Such negative feedback loop is not captured by the model.

A more fundamental question related to freeze-thaw damage is that of its physical origin, which is still debated. In our study, we considered both the effects of hydraulic pressure and of cryo-suction, but neglected any osmotic effects, which are known to play a role (Powers, 1955). Such debate on the physical origin of frost damage is not limited to internal freezing (i.e., damage due to freezing of the bulk of the material, as was considered in our study), but is also relevant for salt scaling (i.e., superficial damage of concrete that occurs in presence of water containing salts). Indeed, for salt scaling, on top of the effect of hydraulic pressure and of the osmotic effect already mentioned, another theory called the glue-spall mechanism (Valenza and Scherer, 2006) gained significant traction[4] recently, but remains still debated (see, e.g., Yuan et al. (2017), who argue on the necessity of still considering the pressure of the solution during its freezing). Much still needs to be done to capture the full complexity of frost-induced damage and quantify the role of each of the proposed physical mechanisms at its origin.

4.2 Crystallization-induced expansion of cement-based materials

Ph.D. student: Nam Nghia BUI
Colleagues involved: Jean-Michel PEREIRA, Rémi BARBARULO (LafargeHolcim)

Context

Sulfate attacks (observed for instance when a civil engineering structure is exposed to seawater or groundwater) can severely limit the durability of cement-based materials (Skalny et al., 2002). Upon the diffusion of sulfate ions through the porosity of the concrete, chemical reactions occur which lead to the formation of gypsum and/or ettringite (Taylor, 1997). These crystallizations make the concrete expand and damage it. To assess the resistance of a mix to sulfate attacks, the American standard C1012/C1012M-13 consists in immersing mortar bars and cubes in a sulfate solution and measuring their change in length over time (ASTM International, 2015). Such immersion experiments are long (significant expansion is usually only observed after several months) and complex to analyze (since sulfate ions diffuse into the

[4] In the glue-spall mechanism, a layer of saline water needs to freeze above the surface of the concrete. Because of mismatches in coefficients of thermal dilation, further decrease of temperature will lead to tensile stresses in the ice layer, which will make the layer crack. Under certain conditions of temperature and of mechanical properties of ice and concrete, those cracks can propagate into the concrete and bifurcate below the surface of the concrete, thus leading to the removal of thin pieces of concrete, i.e., spalling.

sample from its surface, chemical composition and expansion are heterogeneous throughout the sample), so that the process through which sulfate attacks damage a concrete remains not fully understood. For instance, whether gypsum formation contributes to the expansion or not remains controversial (Tian and Cohen, 2000).

More generally, the physical origin of how in-pore crystallization translates into an expansion or a damage remains well debated. This question is of interest not only for concrete science and durability of concrete structures, but also for geotechnical engineering (see, e.g., Oldecop and Alonso (2012)), geophysics (see, e.g., Wellman and Wilson (1965)) or conservation science (see e.g., Espinosa-marzal and Scherer (2010) or Flatt et al. (2014)). The most widespread theory to explain how a crystal can 'push' on the pore walls is the theory of crystallization pressure (Correns, 1949), which relates the pressure that a crystal can exert in excess of the pressure of the pore solution to the supersaturation. This relation, first proposed by Correns (1949) in an erroneous form and then corrected (Ping and Beaudoin, 1992; Steiger, 2005), is derived based on a condition of local thermodynamic equilibrium. However, the theory of crystallization pressure remains debated (Désarnaud et al., 2013). Moreover, when comparing different salts, the one with a larger crystallization pressure is not always the one with the larger potential to induce damage (Shahidzadeh-Bonn et al., 2010). The pressure exerted by a crystal on a wall seems to not depend on the supersaturation only, but also on the nature of the salt and of the solid wall, making this pressure system-specific (Desarnaud et al., 2016). One complexity in studying the relation between crystallization and expansion/damage is that crystal growth is, by definition, an out-of-equilibrium process, and the pressure exerted by a crystal appears to involve various kinetics (Shahidzadeh-Bonn et al., 2010; Naillon et al., 2018).

Approach

The aim of this study was to better understand the process through which sulfate-induced crystallization leads to a pressure or an expansion in cement-based materials. To answer this question, we aimed at designing and using original experiments which were faster and induced a less heterogeneous response of the sample than with standard immersion experiments. To this purpose, we chose to work with cylindrical samples prepared from hydrated cement-based materials which were ground and recompacted. Such samples were about two orders of magnitude more permeable than regular cement paste samples, which made it possible to flush them with a sodium sulfate solution in about half an hour[5].

Samples were tested in oedometric cells and isochoric cells designed by Tang et al. (2011). In oedometric cells, which prevent lateral deformations, the axial stress was applied and the axial deformation was measured. In isochoric cells (see Fig. 4.4), both lateral and axial deformations are prevented and the pressure exerted by the sample on the walls of the cell were measured[6].

[5] When injections were repeated, flushing the sample with the same volume of solution and at the same pressure required more and more time, as a consequence of the crystallization.

[6] As a consequence of the way how pressures were measured in the isochoric cell, while the absolute magnitude

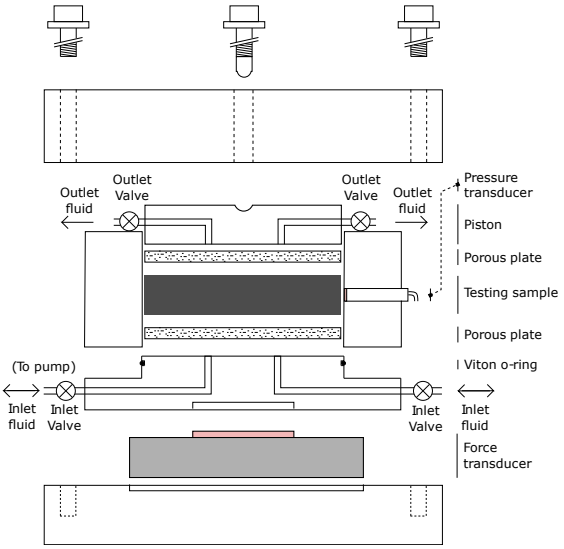

Figure 4.4 – Isochoric cell used for the measurement of crystallization-induced pressures in ground and recompacted cement paste samples.

Therefore, the isochoric cell provided a direct measurement of the macroscopic stress resulting from crystallization pressure. The isochoric cell was also designed such that the fluid flushed through the sample could be recovered.

Various samples were tested, among which ordinary Portland cement pastes. The samples were flushed with sodium sulfate solutions at 3 mM, 66 mM, and 1190 mM to induce crystallization of ettringite and/or gypsum. The rationale for using solutions at 3 mM was that this concentration was sufficiently low to ensure that the injection would only lead to precipitation of ettringite, not gypsum (Damidot and Glasser, 1993). The saturation index with respect to ettringite was equal to 5.67 when flushing the sample with a solution at 3 mM, while it was equal to 7.19 when flushing the sample with solutions at 66 mM or 1190 mM[7]. Each experiment consisted in repeating injections of sulfate once an equilibrium had been reached.

In parallel to the experimental campaign, thermodynamic modeling was performed (with the model CHESS of speciation (van der Lee, 1998) combined with the database Cemdata14 (Lothenbach et al., 2012)), to calculate how the phase assembly evolved over the injections. We verified that, based on the knowledge of the initial phase assembly, the thermodynamic modeling was able to predict satisfactorily the phase assembly after the injections.

of the axial stress was measured, only the variation of the radial stress with respect to a state of reference could be measured.

[7] At the larger 2 concentrations of sulfate, the saturation index was in fact limited by the solubility of gypsum.

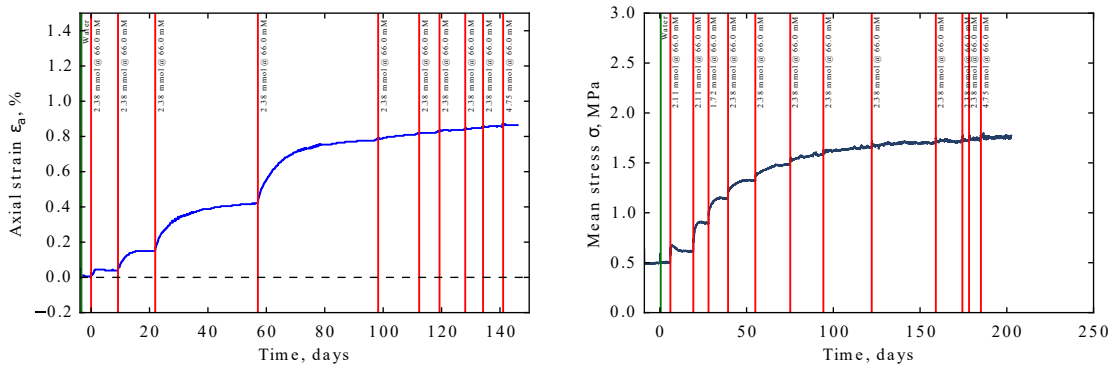

Figure 4.5 – Typical results obtained upon flushing of ground and recompacted cement paste samples with sodium sulfate solution: (left) axial strain measured during an experiment performed in an oedometric cell, and (right) volume stress measured during an experiment performed in an isochoric cell. Each vertical red or green line represents a flushing of the sample with the sodium sulfate solution or with water, respectively. Figure adapted from Bui (2016).

Main results

Figure 4.5 displays typical results of the experiments performed on regular Portland cement samples, with the oedometric and isochoric cells. After each injection of sulfate, strains (for what concerns the oedometric cell) and stresses (for what concerns the isochoric cell) started evolving immediately after the injection and stabilized after about a week (for the first injections) or more (for the latter injections). In any case, in accordance with our expectations, we succeeded in designing an experiment that induced an expansion (or a stress) much faster than with standard testing. Our results thus show that, if standard experiments by immersion in sulfate solutions only make it possible to observe an expansion after several months, this is not because of the kinetics of the chemical reaction per se, whose characteristic time must be much shorter than several months.

As already stated, the isochoric cells were designed to make it possible to recover the fluid flushed through the sample. The concentration in sulfate in the output fluid was measured after each injection and compared with the predictions of the thermodynamic model. A good match was found between measured output concentrations (which remained close to 0 mM while monosulfoaluminates were available for reaction, and then increased to either the input concentration or the solubility of gypsum) and predicted ones[8]. Together with the ability of the thermodynamic model to predict the final phase assembly, this good match proves that the thermodynamic model could predict the evolution of the phase assembly over the injections.

The pressures exerted on the walls of the isochoric cell were measured, so that we can display the volume stress versus the volume of crystals formed in Fig. 4.6. We observed a linear

[8] To obtain a good match of evolutions of output concentrations for the sample flushed with solution at 3 mM, we needed to consider that about half of the monosulfoaluminates present in the sample did not react.

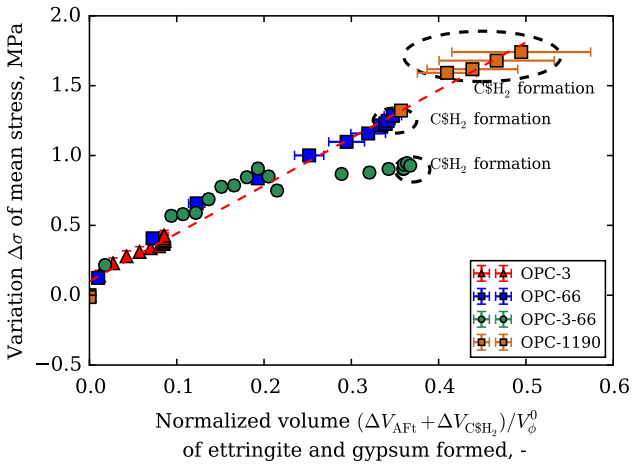

Figure 4.6 – Evolution of volume stress versus normalized volume of formed ettringite and gypsum, for cement paste samples in isochoric conditions and flushed with sodium sulfate solutions of various concentrations. The evolutions of the phase assemblage were calculated through thermodynamic modeling, based on the measured amounts of sulfates that remained in the sample. The volumes ΔV_{AFt} and $\Delta V_{C\$H_2}$ of respectively ettringite and gypsum formed are normalized with the volume V_ϕ^0 of pores. The slope of the dashed line is 3.42 MPa. Figure adapted from Bui (2016).

relationship between those two parameters, which was the same for the three experiments performed (i.e., for the experiments performed with the sulfate solutions at the three concentrations). Therefore, the macroscopic crystallization-induced pressure did not depend on the saturation index (or, equivalently, on the supersaturation) or on the type of crystal formed, but on the volume of crystal (i.e., ettringite or gypsum) formed.

Our interpretation of the observation of a linear relation between macroscopic crystallization-induced pressure and volume of crystal is based on an analogy with the expansion of a perfectly plastic hollow sphere injected with an incompressible fluid: the fluid must be pushed sufficiently hard to deform the hollow sphere irreversibly, but if it was pushed sufficiently hard, once the injection is stopped, the expansion of the sphere must be equal to the volume of liquid that was injected. This interpretation does not contradict the notion of crystallization pressure induced by supersaturation, which must be sufficiently large to deform the sample irreversibly. But this interpretation also recognizes that supersaturation is by nature transient and must vanish once equilibrium is reached.

Perspectives

Many questions related to our experimental results still need to be answered. Why do crystallizations of gypsum and of ettringite appear to have identical effects (see Fig. 4.6)? Why is the development of stress non-monotonic and quite fast during the first injections, but then

monotonic and slower during the latter injections (see Fig. 4.6-right)? Why is a significant fraction of the monosulfoaluminates initially present in the sample non reactive when injections are performed at the lowest concentration? The interpretation of our data is made complex by the fact that, in contrast to our expectations, the response of the sample was in fact quite heterogeneous: indeed, during the first injections, the output concentration was close to 0 mM, so that gradients of sulfate concentration throughout the sample were significant.

An important question is whether our results, obtained on samples prepared from a material that was ground and recompacted, can be extrapolated to ordinary cement paste samples obtained by hydration. Indeed, one can argue that the cohesion of our samples, and hence their strength, were quite low (in comparison with regular cement paste samples, which are not ground or recompacted), so that not much stress was needed to deform our samples irreversibly. In particular, even if gypsum crystallization contributed to the expansion of our samples (see Fig. 4.6), one can still wonder whether gypsum contributes to the expansion of regular (i.e., not ground and recompacted) cement-based materials.

In any case, the experimental setup which we designed made it possible to observe expansion or development of stresses much faster than with conventional testing by immersion. This innovation is of value for the cement and concrete industry, which can envision to use our setup to quickly estimate whether a given mix design is resistant to sulfate attacks, faster than by immersing samples in a sulfate solution. For this purpose, LafargeHolcim has implemented oedometric cells at its research center, with encouraging results.

4.3 Use of shrinkage-reducing admixtures to reduce drying shrinkage of cement-based materials

Ph.D. student: Hafsa RAHOUI
Related journal article: Maruyama et al. (2019)
Colleagues involved: Ippei MARUYAMA (Nagoya University), Martin MOSQUET (LafargeHolcim), Jean-Michel PEREIRA

Context and approach

Upon drying, cement-based materials shrink, which can cause their cracking. One way to mitigate drying shrinkage is to add shrinkage-reducing admixtures (SRAs) to the mix. Although SRAs have proven beneficial to reduce drying shrinkage (as well as autogenous shrinkage and plastic shrinkage), their mechanisms of action are still debated. In particular, the ability of a SRA to reduce drying shrinkage is often attributed to its ability to decrease the surface tension of the pore solution, but such explanation alone is not satisfactory, as the efficiency of a SRA has been shown experimentally to not be correlated to its ability to decrease surface tension (Maruyama et al., 2018).

SRAs typically consist of glycol ethers. In this study, we studied one specific SRA, namely hexylene glycol, which is among the main components of some commercialized SRAs, can be found in a pure state, and has already been extensively characterized in terms of physico-chemical properties. The approach combined an extensive experimental campaign (mostly performed at Nagoya University, but also at LafargeHolcim Centre de Recherche), together with poromechanical modeling.

In terms of experiments, drying shrinkage isotherms were obtained by measuring the deformation of thin cement paste slabs (3 mm x 13 mm x 100 mm), each equilibrated at various relative humidities for several months. The experiments were performed on a full desorption-adsorption cycle, so as to assess the irreversibility of the first drying shrinkage. With the aim of optimizing the amount of SRA to be added to a mix for various compositions of this mix, experiments were performed with cement pastes containing 3 different alkali contents. Other experiments performed were: measurement of drying shrinkage isotherms after short-term drying (measured with a thermo-mechanical analyzer, after equilibration of 0.5mm-thick samples for several hours), characterization of the microstructure at various ages (i.e., the solid phase assembly was assessed with X-ray diffraction and thermo-gravimetry analysis, and the pore size distribution was measured with nitrogen sorption, water sorption, and mercury intrusion porosimetry), pore solutions extraction and characterization, leaching experiments (to characterize the ability of the SRA to adsorb on the cement paste or not).

In terms of modeling, first a purely phenomenological model was developed, which makes it possible to predict drying shrinkage for a cement paste that contains a given content of alkali and SRA and at a given relative humidity: the goal of such model was to provide a tool readily usable by the engineer to tailor the amount of SRA that he needs to add to the mix, depending on the alkali content. A second modeling approach proposed was more physical: it consisted in modeling drying shrinkage by explicitly considering the various types of water contained in a cement paste (i.e., capillary water, water adsorbed on solid surfaces, and water adsorbed in micropores) and how each of those types of water deforms the sample. To the light of this model, the effect of the SRA was then discussed.

Main results

Typical drying shrinkage isotherms are displayed in Fig. 4.7, which shows that the SRA considered is most efficient in the range of relative humidities ranging from 33% to 75%. In this range of relative humidities, in presence of SRA, roughly, we observed a plateau: drying induced no additional shrinkage. The SRA was found to make the pore structure of the paste before drying coarser, and to alter how the pore structure evolves upon drying. The SRA was also found to slow down hydration. Leaching experiments showed that, in saturated conditions, the SRA is not adsorbed on the cement paste. Significant differences in microstructure (specific surface area in particular) were observed, depending on whether the material was dried for a short time (i.e., several hours) or for a long time (i.e., several months): there appears to exist some slow kinetics of evolution of the microstructure within the representative elementary volume

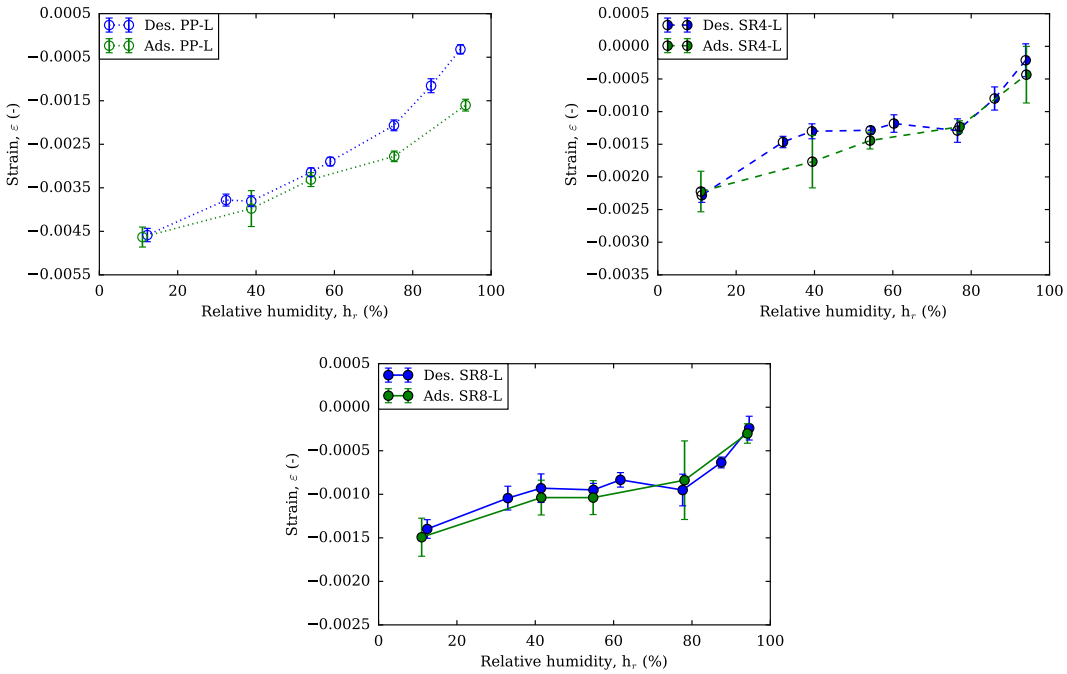

Figure 4.7 – Drying shrinkage isotherms of cement paste samples with low alkali content, with no SRA (PP-L) and with SRA at a content of 4% (SR4-L) and 8% (SR8-L). Blue and green symbols indicate drying and rehumidification, respectively. Figures from Rahoui (2018).

(REV), which is consistent with the fact that, within the REV, you need at least several days to reach local thermodynamic equilibrium (Gajewicz et al., 2016).

We proposed 2 models to estimate the water content in a cement paste versus relative humidity and resolve how the water is separated into various types: a model called '2W' relies on water sorption isotherms and resolves water into water present in the capillary porosity and water adsorbed on solid surfaces, and a model called '3W' relies on nitrogen sorption isotherms and resolves water into water present in the capillary porosity, water adsorbed on solid surfaces, and water adsorbed in the micropores of the C-S-H gel. We find that the adsorption isotherm of the water in micropores (i.e., the amount of water in the micropores versus relative humidity) is independent of the amount of alkali or SRA in the paste.

In the framework of linear poroelasticity, we modeled how each type of water contributes to the deformation of the material: capillary water was assumed to deform the material following the model of Coussy et al. (2004), water adsorbed on solid surfaces was assumed to deform the material following Bangham's law (Bangham and Razouk, 1938), and the deformation due to water in micropores was assumed to be related linearly to the water content in the micropores (as is roughly observed in a variety of microporous materials, see e.g. Carrier et al. (2013) for clay or Hol and Spiers (2012) for coal). The models 2W and 3W were fitted on the rehumidification branch (for model 2W, the only fitting parameter is the proportionality

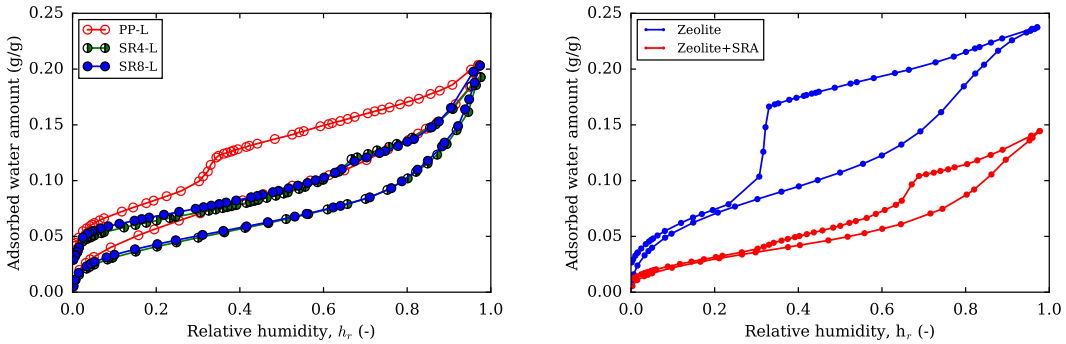

Figure 4.8 – Water adsorption isotherms obtained on (left) cement pastes and (right) zeolites, which contain SRA or not. The sharp decrease of adsorbed amounts on the desorption branch occurs at a relative humidity which is independent of the adsorbent and is attributed to cavitation. Cavitation is seen to occur at a relative humidity of about 35% in absence of SRA, and of about 65% in presence of SRA. The cement pastes contain no SRA (PP-L) or SRA at a content of 4% (SR4-L) or 8% (SR8-L). Figures adapted from Rahoui (2018).

factor between variations of surface energy and strain, while, for model 3W, a second fitting parameter is the proportionality factor between variations of water content in micropores and strain) and a blind prediction of the first drying shrinkage was performed, which was in reasonable agreement with the data, and captured in particular most of the irreversibility observed during first drying shrinkage in absence of SRA. From this observation, we inferred that most of this irreversibility stems from a hysteresis of the sorption isotherm, rather than from a mechanical irreversibility. Models 2W and 3W were as good as each other to predict drying shrinkage.

As expected, the SRA decreased the surface tension of the pore solution, which impacted capillary effects. Through fit of the models, the SRA was also found to impact the proportionality factor between variations of surface tension and strain (for both models 2W and 3W), and the proportionality factor between variations of water content in micropores and strain (for model 3W). Finally, another interesting way through which the SRA impacts drying shrinkage is by modifying the relative humidity at which cavitation of the pore solution occurs. Indeed, in absence of SRA, cavitation of water (i.e., the fact that all bulk water present in the sample is transformed into vapor, as a consequence of the high tensile stresses due to capillary effects) occurs at a relative humidity around 35% (Maruyama et al., 2019). As can be observed in Fig. 4.8, the presence of SRA increases the relative humidity at which such cavitation occurs up to about 65%: Consequently, upon drying, capillary effects can deform the material over a smaller range of relative humidities in presence of SRA than in absence of it.

Perspectives

In this work, we showed that, on top of acting on surface tension, the SRA considered (i.e., hexylene glycol) reduces drying shrinkage by increasing the relative humidity at which cavitation of the pore solution occurs. The modeling also suggests that the SRA modifies how adsorption of the pore solution translates into a strain. However, this last effect is only suggested: a definite experimental proof of this effect is still needed. For instance, even though we showed that, in saturated conditions, the SRA is not being adsorbed on the solid surfaces of the cement paste, as proposed by late Ellis Gartner, a double-isotherm experiment could be designed to check whether, upon drying, the SRA can be adsorbed on those solid surfaces: such experiment would consist, after equilibration of the sample at various relative humidities, in measuring the partial pressure of the SRA in the vapor in equilibrium with the sample.

In terms of modeling, we aimed at predicting drying shrinkage by considering the various types of water present in a paste (i.e., capillary, adsorbed on solid surfaces, and/or adsorbed in micropores). The model was obtained by simple concatenation of the model by Coussy et al. (2004) with phenomenological laws (i.e., Bangham's model (Bangham and Razouk, 1938) and a linear relation between adsorption in micropores and the strain it induces), but a proper thermodynamic derivation of such a model is still missing.

4.4 Wetting-induced collapse of partially saturated sand

Ph.D. student: Jean-François BRUCHON
Related journal articles: Bruchon et al. (2013a,b)
Colleagues involved: Michel BORNERT, Pierre DELAGE, Nicolas LENOIR, Jean-Michel PEREIRA

Context and approach

The idea of this study germinated concomitantly with the project of acquisition of a federative X-ray microtomography equipment platform at Laboratoire Navier. One of the originality of this platform was that it was designed specifically to simplify the use of solicitation devices (may the solicitation be mechanical, hydric, or thermal), while performing the image acquisition. This study was the first Ph.D. project to use this X-ray microtomography platform.

Wetting-induced collapse (or capillary collapse) designates the irreversible and sudden deformation of a soil upon provision of water (Dudley, 1970). Collapse occurs in a variety of loose soils (e.g., clay, loess, or sand) and is a cause of concern in geotechnical engineering, as it caused for instance excessive settlements along the high-speed railway in Northern France (Delage et al., 2005).

Wetting-induced collapse has been extensively studied macroscopically, in clays (Barden et al.,

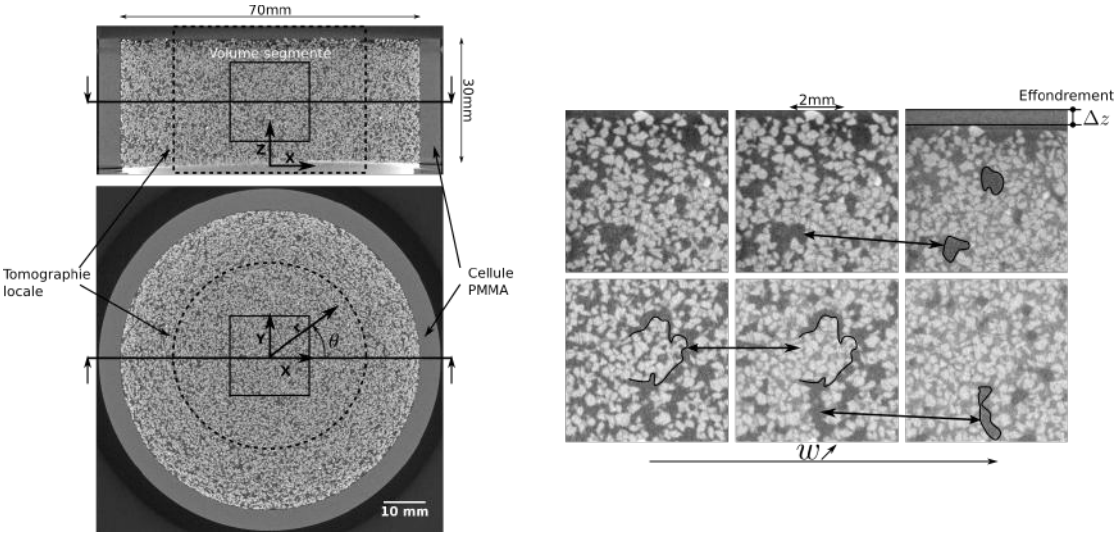

Figure 4.9 – Sets of X-ray microtomography scans performed on sand sample: (left) horizontal slice and vertical slice of a global tomography, and (right) vertical slices of local tomographies acquired at three imbibition steps and from two regions of the specimen: (top) close to the free surface and (bottom) in the center of the specimen. Figures from Bruchon et al. (2013a).

1973), loess (Muñoz-Castelblanco et al., 2011), and sands (Lins and Schanz, 2005). The aim of the study was to perform a full 3-dimensional characterization of wetting-induced collapse with X-ray microtomography, to better understand the mechanisms leading to the collapse.

We focused on a clean loose sand placed in an oedometric cell (but with no top cap, so that the top surface of the sample was free), which was progressively saturated from its bottom surface by controlling the water pressure with the negative water column technique. At each saturation level, both a global tomography with a voxel size of 50 μm and a local tomography with a voxel size of 25 μm were acquired (see Fig. 4.9). With those voxel sizes, we chose to focus the study at a mesoscopic scale, at which, in combination with volumetric digital image correlation (Bornert et al., 2004), the use of continuum mechanics still remains relevant. However, the scale of study was too large to observe and study quantitatively the various interfaces at stake, and in particular the air-water menisci.

Main results

A first result, obtained at the global scale of the sample, was that the collapse process is progressive when the imbibition is progressive, while at the time several had wondered whether the collapse process could indeed be controlled (see, e.g. Buscarnera and Nova (2011)).

An in-depth analysis of the notion of representative elementary volume (REV) was performed on the set of local tomographies. Based on the asymptotic behavior method (Lantuéjoul, 1991), we showed that the size of the REV depends on the quantity of interest (for instance, the volume fraction occupied by the air, or the characteristic size of the volumes occupied by the

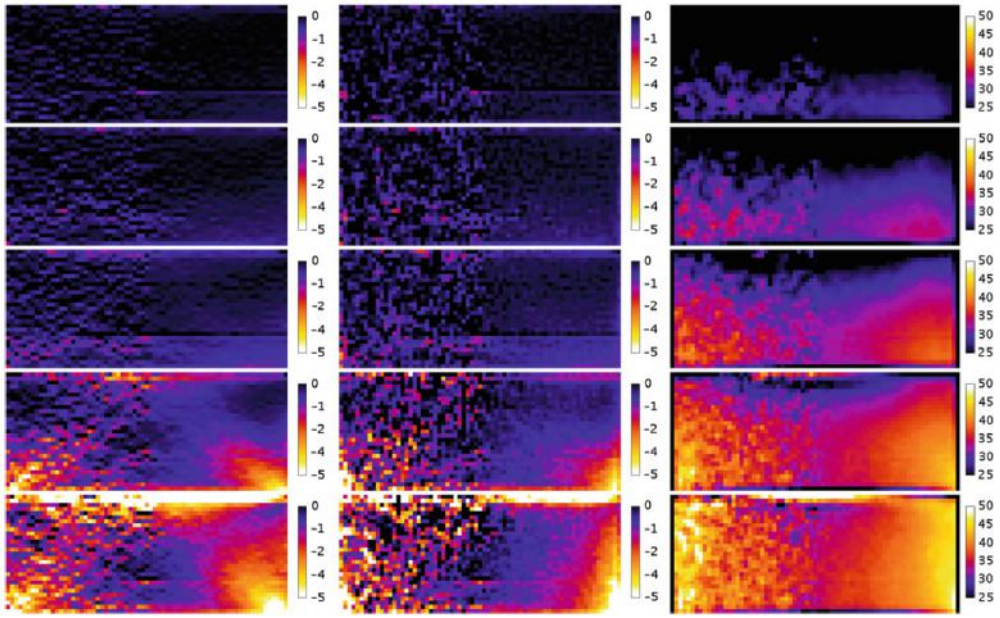

Figure 4.10 – Maps of (left) vertical strains, (center) volumetric strains and (right) water content at increasing levels of imbibition. The level of imbibition increases when moving from top to bottom. Each map is the juxtaposition of a half vertical slice in the xz plan (left half of the map) and the θ-average of all half vertical slices (right half of the map). Scale of color bars is percentage values. The central vertical axis of the maps coincides with the central axis of the specimen. Figure from Bruchon et al. (2013a).

air) and evolves during the saturation.

Volumetric digital image correlation (Bornert et al., 2004) applied to the set of global tomographies made it possible to characterize the local strains within the sample during the imbibition process (see Fig. 4.10). Given the symmetries of the problem, one would have expected the strains to exhibit a heterogeneity only in the vertical direction. However, Fig. 4.10 shows that heterogeneities are in fact both vertical and radial. In particular, strains are larger in the bottom corners, from which shear bands originate: those heterogeneities of strains could be the result of an initial heterogeneous density of the sample (i.e., in spite of the care dedicated to the preparation of the specimen), sand in the bottom corners could have been looser) or of the provision of water along preferential paths (as the oedometric cell was made of polymethyl methacrylate (PMMA) to facilitate the penetration of X-rays).

Because of gravity effects, the difference in capillary pressures was of 0.3 kPa between the bottom and the top of the specimen, which can lead to non-negligible differences in water content for a sand. Considering, on top of this difference, the observed heterogeneities of strain, one could wonder whether properties measured at the macroscopic scale of the sample are representative of the local properties of the material at the scale of the representative elementary volume. To answer this question, we calculated the retention curve and the relation between volume strain and water content, at both the global scale of the sample and

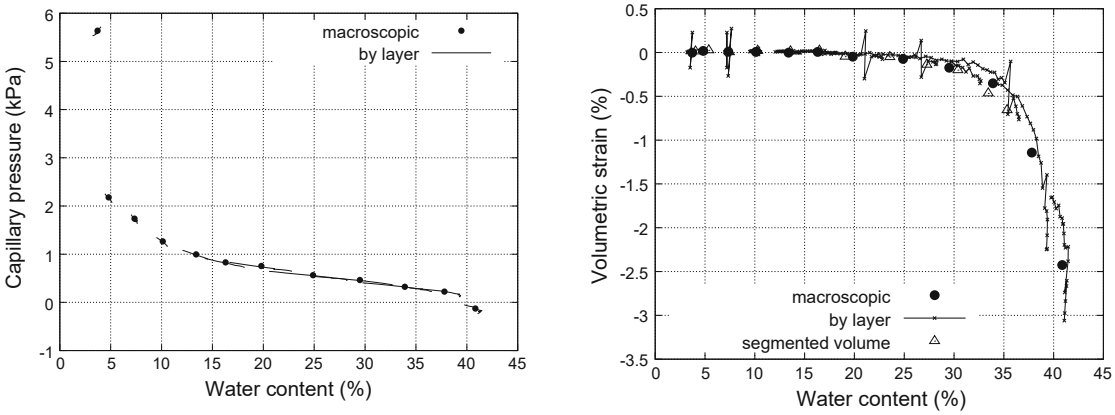

Figure 4.11 – Comparison of relations measured at the macroscopic scale of the sample and at the more local scale of a 1-voxel-thick layer of material: (left) retention curve and (right) relation between volumetric strain and water content. Local relations are obtained by averaging parameters over all voxels of a horizontal slice. Sub-figures from Bruchon et al. (2013a).

at the more local scale of a 1-voxel-thick layer of material. To calculate those relations at the local scale, we used the imposed local pressure of water, the local volume strain obtained with volume digital image correlation, and the local water content, which was estimated with an original method based on the local volume strain and the local variation of gray levels. For the two relations considered (i.e., retention curve and relation between volume strain and water content), we found out that measuring them at the global scale of the sample or at the local scale of the representative elementary volume yielded quite similar results (see Fig. 4.11), which we attributed to the fact that the non-linearity of those relations was small.

Perspectives

The methodology here proposed can be applied to study the hydro-mechanical collapse of other materials (e.g., loess) or more generally the irreversible or reversible deformations of soils under hydro-mechanical loading (e.g., swelling/shrinkage upon cycles of drying and imbibition (Alonso et al., 2005), or collapse when the imbibition is performed under mechanical load (Muñoz-Castelblanco et al., 2011)). However, for what concerns wetting-induced collapse of sand, an interesting scientific perspective would be to work at the lower scale of the grain, to understand how the movement of the individual grains (Bornert et al., 2010; Kaddhour et al., 2013) and the evolution of the capillary bridges (Scheel et al., 2008) over the imbibition process translate into the observed macroscopic collapse.

4.5 Impact of moisture on mechanical properties of clay

Ph.D. student: Benoit CARRIER

Related journal articles: Carrier et al. (2013, 2014, 2016)

Colleagues involved: Henri VAN DAMME (IFSTTAR), Michel BORNERT, Roland J.-M. PELLENQ (UMI MIT-CNRS, Aix-Marseille Université)

Context of study

A better understanding of the hydro-mechanical behavior of clays is of interest for a variety of applications, such as underground nuclear waste storage[9] (Andra, 2005), stability of soils[10] (USGS, 2004), or petroleum engineering[11] (Anderson et al., 2010), which can all involve soils or rocks with a significant fraction of clay. Clay-based composite soils or rocks are heterogeneous multiscale porous materials (see Fig. 1.1 and Bobko and Ulm (2008)), whose macroscopic mechanical behavior is significantly impacted by the microscopic scale. In particular, the sensitivity of their mechanical behavior to water is a consequence of the clay fraction and its sub-nanometer scale porosity.

For clays like for virtually all families of materials, bottom-up approaches are attractive: scientists aim at predicting the macroscopic behavior based on the knowledge of the microstructure and of the properties at the smallest scales. Several aimed at doing so by starting explicitly from the sub-nanometric scale of the clay layer, either by employing continuum micro-mechanics techniques (e.g., Ortega et al. (2007) and Cariou et al. (2012)), or molecular simulations (e.g., Ebrahimi et al. (2014)). However, given the multiscale and complex microstructure of clay-based natural materials, validate each step of such bottom-up approaches remains challenging, in spite of the existence of small-scale experimental techniques such as nano-indentation (e.g., Ebrahimi et al. (2014) used nano-indentation to validate their coarse-grained simulations).

[9] For the repository of its Long-Lived and High-Level or Intermediate-Level waste (which can present a significant radiological risk for up to 100,000 years), France envisions deep geological disposal (République Française, 2006). The site presently being designed by the French national agency for the management of radioactive waste ANDRA is located in a rock. In the long term, confinement of the radionuclides will be ensured by the rock and by the bentonite plug used to seal the underground disposable cells. Both rock and plug contain significant proportions of clay.

[10] Stability of building foundations can be impaired by the shrinkage and swelling of expansive clays, consecutive to respectively drought and rain. Indeed, in France, the economic consequences of the impact of shrinkage-swelling phenomenon of expansive clays on buildings represent the second item of insurance compensation for natural disaster in France, after floods. For France, the Commissariat Général au Développement Durable estimated the total cost of shrinking and swelling to 3.5 billion euros between 1995 and 2006 (Commissariat Général au Développement Durable, 2010).

[11] Shales are rocks which contain a significant fraction of clay and are commonly encountered during exploration and production of oil and gas. During drilling operations, when the well goes through a layer of shale, in contact with the aqueous drilling fluid the clay swells, which can lead to well-bore instabilities. The cost of well-bore instabilities in general is estimated to up to 1 billion US dollars per year worldwide (Aadnoy and Ong, 2003).

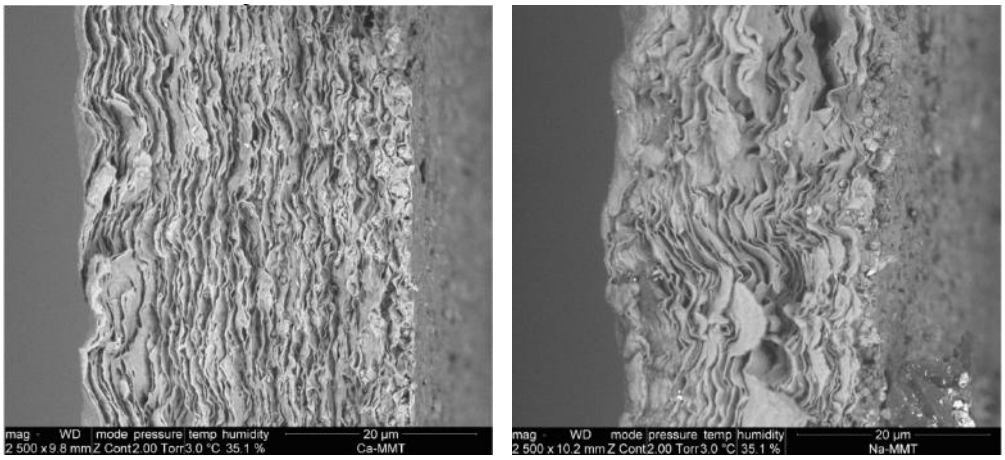

Figure 4.12 – ESEM observation at a relative humidity of 35% of the edges of SWy-2 clay films containing (left) calcium as an interlayer cation, or (right) sodium as an interlayer cation. Figures from Carrier et al. (2013).

In this study we aimed at having a critical look at this challenge, by finding out whether the properties of the clay layer could be upscaled to a mesoscale system that should be as simple and small as possible (so that the upscaling would remain simple) while remaining sufficiently large so that it could be tested with classical experimental means. Consequently, the approach here proposed consisted in: 1) molecular simulations to characterize the properties of the clay layer, and 2) experiments on 'simple' pure clay systems. The 'simple' clay systems that we chose to work with are self-standing clay films (Zabat et al., 1997). Those films were manufactured by evaporation of a SWy-2 montmorillonite clay suspension (see Fig. 4.12), yielding films with thicknesses around 50 μm to 100 μm and anisotropic microstructures in which the clay layers were roughly parallel to the plane of the film, as observed visually (see Fig. 4.12) and from their order parameters that ranged from 0.66 to 0.79. We therefore saw the clay films as systems that were sufficiently simple and small to serve as 'mesoscale' elements of study, as intermediates between the scale of the clay layer and the macroscopic scale of natural clay-based rocks.

The clay could be homoionized before the films were manufactured, so that the role of the interlayer cation could be investigated. The clay films could be cut and handled like a sheet of paper, and could be solicited mechanically with a regular tensile apparatus (see Fig. 4.14-left). The following properties of the film were characterized experimentally upon moisture variations and compared with results obtained by molecular simulations at the scale of the clay layer: adsorption, swelling, stiffness, creep.

Main results on adsorption and swelling

Water adsorption isotherms were measured on the films. Molecular simulations helped interpret evolutions of basal spacing with relative humidity found in the literature (Cases et al., 1997; Ferrage et al., 2005), to calculate the amount of interlayer water as a function of relative humidity. Fig. 4.13-left shows that water in the films was mostly adsorbed in the clay nanometric interlayer.

We characterized the swelling/shrinkage of the films with moisture by using environmental scanning electron microscopy, in conjunction with digital image correlation (Doumalin and Bornert, 2000): the dimensions of the films varied mostly in the direction perpendicular to the plane of the film. Hysteresis was larger when plotting the thickness of the films versus relative humidity than versus water content. Strains at the scale of the film (perpendicular to the plane of the film) compared well with strains at the scale of the clay layer (perpendicular to the plane of the clay layer), as calculated from data on basal spacing available in the literature (see Fig. 4.13-right) (Cases et al., 1997; Ferrage et al., 2005). This good agreement is a consequence of the significant anisotropy of the films. The fact that adsorption and swelling behavior of the film can be directly inferred from those of the clay layer suggests that clay films are good model systems to aim at performing a first step of upscaling from the scale of the clay layer.

Main results on stiffness

The stiffness (i.e., Young's modulus in the direction of the film) of the films was measured with a regular tensile testing machine (see Fig. 4.14-left), but which was enclosed in a transparent box in which relative humidity could be controlled, and through which we could observe the film to measure the strains by digital image correlation. Results are displayed in Fig. 4.15-right. The elastic properties depended significantly on relative humidity. Like for swelling, hysteresis of the stiffness was larger when the stiffness of the films was displayed versus relative humidity than when displayed versus water content.

The full stiffness tensor of the stack of clay layers was obtained with molecular simulations. Simulations were performed in the $N\Sigma T$ ensemble (i.e., imposed number of molecules of water, stress, and temperature) in LAMMPS (Plimpton, 1995), and stiffness coefficients were obtained from fluctuations of the dimensions of the box, with a Parinello-Rahman fluctuation formula (Parrinello and Rahman, 1982). Given the strong contrast of stiffness properties parallel to the clay layers and perpendicular to the clay layer, an anisotropic version of the elastic bath method (Van Workum and de Pablo, 2003) needed to be implemented. This method consists in virtually immersing the simulated system into a material of known stiffness, to increase or decrease strain fluctuations and improve convergence of the calculation of the thermodynamic variables. Results of the calculation are displayed in Fig. 4.15-left and show the importance of performing calculations at realistic temperatures (typically, 300K), rather than at 0K, in particular for stiffness coefficients significantly impacted by the interlayer water. The decrease of in-plane stiffness coefficients (i.e., C_{11} or C_{22}) is due to evolutions of geometry,

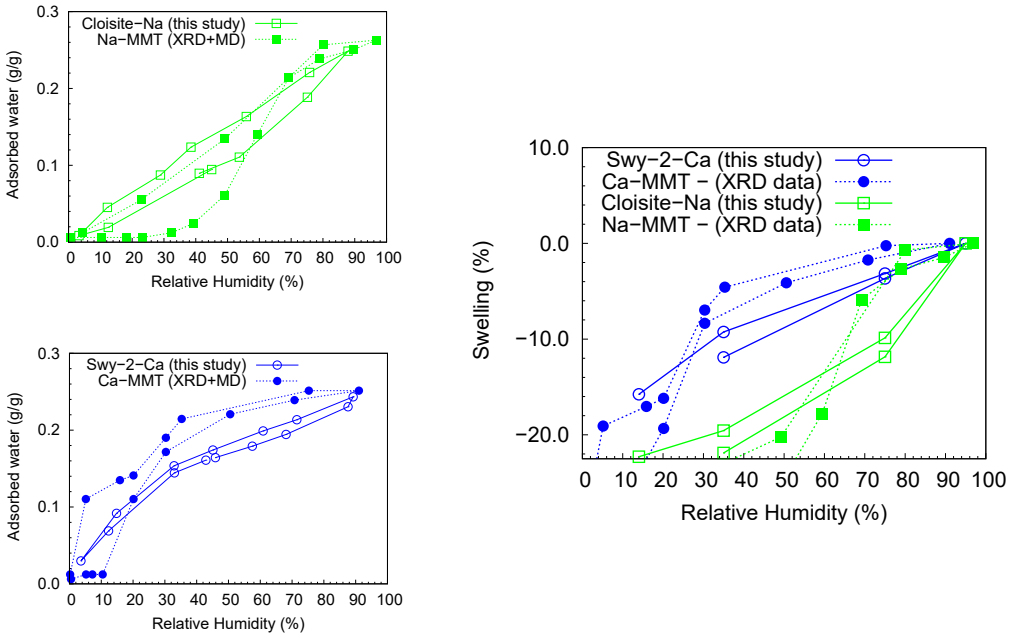

Figure 4.13 – Comparison of results at the scale of the dozens-of-microns-thick clay films and of the nanometric clay layers: (left) adsorption and (right) swelling. Results at the scale of the clay films and at the scale of the clay layers are displayed with open symbols and closed symbols, respectively. 'Cloisite-Na' and 'Na-MMT' indicate a montmorillonite with Na^+ as interlayer cation. 'Cloisite-Na' and 'Na-MMT' indicate a montmorillonite with sodium as interlayer cation. 'SWy-2-Ca' and 'Ca-MMT' indicate a montmorillonite with Ca^{2+} as interlayer cation. Figures from Carrier et al. (2013).

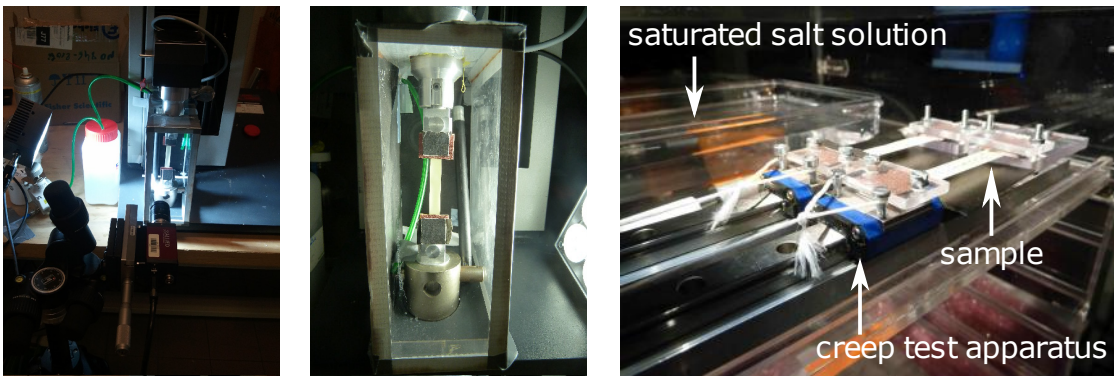

Figure 4.14 – Pictures of the experimental setups for the tensile tests: (left 2 figures) overall view and sample in the grips of the tensile test machine for the measurement of stiffness, (right) experimental setup for the measurement of creep. Figures from Carrier et al. (2016).

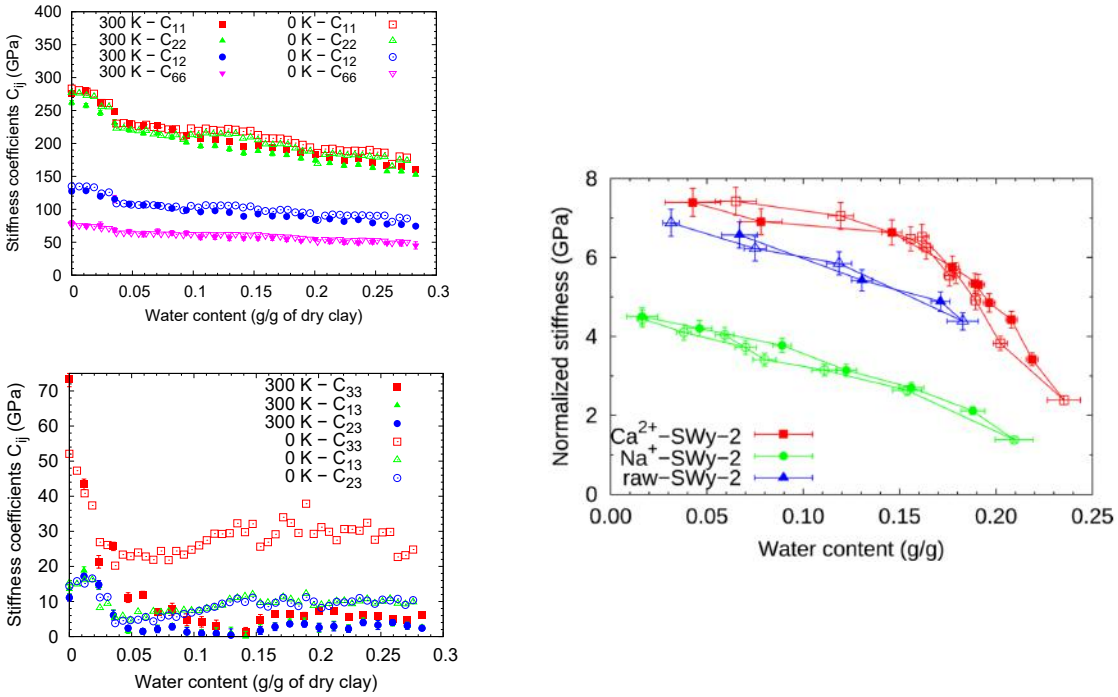

Figure 4.15 – Elastic properties of (left) a stack of clay layers as predicted by molecular simulations and of (right) clay films as measured experimentally. (top left) In-plane stiffness coefficients and (bottom left) out-of-plane stiffness coefficients. Figures from (left) Carrier et al. (2014) and (right) Carrier et al. (2016).

and is a consequence of the fact that layers are further apart from each other when the amount of water in the interlayer increases.

The comparison between experiments and molecular simulations remained qualitative. One observation is that, at all water contents, the stiffness of the films depended on the interlayer cation, while the stiffness of the clay layers did not. Another observation is related to how the stiffness properties decreased with relative humidity / water content. Given the microstructure of the films, upon tension, we could imagine that, at the scale of the clay particles, response would be governed by in-plane stiffness (i.e., coefficients C_{11} or C_{22}), or by shear of layers over each other (i.e., coefficients C_{13} or C_{23}). Once corrected for geometrical effects, in-plane stiffness showed no dependence on water content, while shear stiffness decreased dramatically at low water content. How a combination of those coefficients could result in a smooth decrease of stiffness at the scale of the film over the water contents of interest is a priori not obvious. However, we did not go further in our attempt to retrieve the stiffness properties at the scale of the clay film from those at the scale of the clay layer.

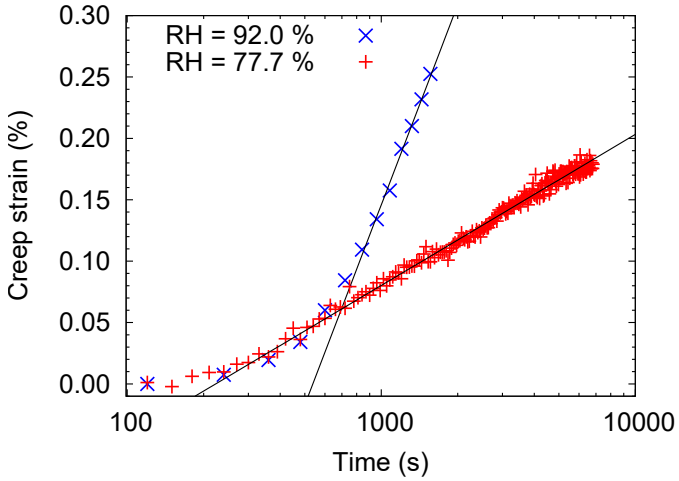

Figure 4.16 – Evolution of creep strain of a film made of clay SWy-2 with Ca^{2+} as an interlayer cation. Figure from Carrier et al. (2016).

Main results on creep

At the scale of the stack of clay layers, creep was characterized by molecular simulations in a 'brute force' manner, i.e., by applying a shear stress to force sliding of adjacent clay layers over each other. For all stresses considered, strain increased linearly over time. But, to obtain exploitable simulation results, we needed to apply irrealistically high stresses (i.e., on the order of a few dozen MPa) and obtained irrealistically high strains (i.e., on the order of a few hundreds of percents). Consequently, one can reasonably wonder whether the observed linear kinetics is representative of the creep kinetics of the clay layer at more realistic levels of stresses and strains. To tackle creep (and the long time scales it involves) with molecular simulations, more sophisticated methods exist (typically, activation-relaxation techniques (Mousseau et al., 2012)), but we did not attempt to use them.

To measure creep properties of the films, we developed a setup with which a constant load could be applied to the film, by using a dead weight (see Fig. 4.14-right). The system was enclosed in a transparent box, so that relative humidity could be controlled and strains could be measured in a contact-less manner by digital image correlation. Moisture had a tremendous impact on creep kinetics: at the largest relative humidity, the film containing Ca^{2+} interlayer cations crept about three orders of magnitude faster than at the lowest relative humidity. The variation was of about two orders of magnitude for the film containing Na^{+} interlayer cations.

I want to emphasize one interesting qualitative observation: after a few seconds, all films, at all relative humidities, crept logarithmically with respect to time (see Fig. 4.16), as natural soils macroscopically do (Lambe and Whitman, 1969). Such kinetics is not observed in the molecular simulations. Maybe the logarithmic kinetics of creep observed experimentally does not originate in the sliding of clay layers over each other (which is what we simulated), or originates from a scale larger than that of the simulation box, or the process at the physical

origin of creep is not reachable in the duration of the molecular simulation.

Discussions and perspectives

We performed a comprehensive experimental characterization of self-standing clay films. Adsorption and swelling properties of the dozens-of-microns-thick films can readily be inferred from those of the nanometric clay layers. However, understanding elastic and creep properties from those of the nanometric clay layers appears to be much less straightforward. On top of the physical properties mentioned, we also measured order parameters, thus providing to the community an interesting set of data which can be used by researchers interested in bottom-up approaches to test their upscaling schemes by starting from the scale of the clay layer.

For what concerns elastic properties, one reason for the discrepancy between scales could lie in the nature of the characterized stiffnesses at the two scales. Indeed, since the molecular simulations were performed in the $N\Sigma T$ ensemble, the stiffness coefficients displayed in Fig. 4.15-left are undrained coefficients. In contrast, the tensile experiments were performed at controlled relative humidity, i.e., yielded a measurement of drained stiffness coefficients. At the scale of clay layers, inferring drained coefficients from the undrained ones obtained by molecular simulations is theoretically possible, but the error bars obtained on those calculated drained coefficients were very large. Another reason why the stiffness of the films depended on the interlayer cation while the stiffness of the clay layers did not could be the mesostructure of the films (i.e., how clay particles are arranged in space), which is very likely to depend on the interlayer cation, since the cohesion between layers containing Ca^{2+} interlayer cations is known to be greater than that between layers containing Na^{+} interlayer cations (Pellenq et al., 1997), resulting in tactoids containing a larger number of clay layers in the former case than in the latter (Schramm and Kwak, 1982). In any case, explaining the elastic properties of the films from those of the clay layers remains a challenge.

The fact that a logarithmic creep was observed while the films were in tension (i.e., in an experiment in which the volume of the sample must have increased over time) is interesting to me. Any physical explanation for the observation of logarithmic creep in clay must be consistent with this observation. In particular, it now seems to me unlikely that free-volume dynamics, which I proposed as a potential explanation for the logarithmic kinetics of long-term creep of concrete (Vandamme and Ulm, 2013), could be a valid explanation for creep of clay. Indeed, I do not see how a theory based on the idea that creep rate would decrease because of the compaction (i.e., decrease of free volume) of the material could explain logarithmic creep in a material under tension.

The clay films could be a valuable system to find out the physical origin of creep in clay. While creeping, the films could be observed with a variety of techniques of complementary scales, such as environmental scanning electron microscopy, X-ray radiography and transmission X-ray microscopy, small angle X-ray scattering, and/or nuclear magnetic resonance. The

combination of these observations could yield information on the micro/meso-structure (see e.g. Brisard et al. (2012) or Michot et al. (2013)) and/or the porosity of the films, and on their evolution concomitant to their creep. A post-doctoral project will start in 2019 in this direction.

In terms of bottom-up modeling, numerical upscaling through coarse-grained simulations (typically like the ones presently developed by my colleague Laurent Brochard in the framework of his ANR project TEAM2ClayDesicc) could be very valuable. Such simulations could for instance be used to assess the role of the flexibility (in bending) of the clay particles on the macroscopic behavior of the clay systems. Indeed, the bending stiffness of individual clay layers can be significant, as was observed with large-scale molecular simulations (Suter et al., 2007) or experimentally (e.g., see Fig. 2 in Atanasova et al. (2016)). Flexibility of the clay layer is therefore likely to play a role on the macroscopic mechanical behavior, but taking it into account through analytical Eshelby-based homogenization techniques could be difficult, hence the interest of coarse-grained simulations.

5 Synthesis and perspectives

5.1 Personal synthesis

I have worked on a variety of materials (namely concrete, coal, clay, and sand) and a variety of processes (among which adsorption-induced deformations, drying and autogenous shrinkage, creep, crystallization-induced expansion, freezing-induced damage, or wetting-induced collapse): all topics that I addressed are related to porous materials that deform. Most of my projects combined experiments and modeling, although my main expertise lies in poromechanical modeling.

Several of my projects focused on the understanding of physical processes (adsorption, creep, crystallization) and on how those physical processes impact the macroscopic behavior. To model those processes and their macroscopic manifestation, when appropriate, I aimed at using thermodynamics, as it is the perfect lingua franca to tackle complex coupled phenomena occurring in porous materials.

My various projects, through their multidisciplinary character, gave me the great opportunity to interact with colleagues from a variety of disciplines (typically physicists and physical chemists, while I am a mechanician) or working on a variety of materials. I appreciate very much the fruitful exchanges to which those interactions can lead. I am always amazed (in a good sense) by how related problems can be tackled in very different manners by different communities.

Several of my projects have been undertaken in collaboration with the industry (in particular the cement and concrete industry, and the oil and gas industry). I appreciate very much working on such projects, as the industrial context requires to remain dedicated to provide well-balanced modeling solutions, for instance models that capture the complexity of the physical processes at stake while remaining sufficiently simple to be calibrated and used. I also noted that the industry is appealed by innovative ways of characterizing their materials with respect to a specific issue, especially if this innovative characterization is significantly faster than more classical characterizations.

5.2 Perspectives

Since I have, along the manuscript, provided individual perspectives to the various topics I addressed, here I will only provide some more general thoughts.

With years, I have become more sensitive to the social purpose of my work, and hence appreciate working for the building industry, or toward nuclear waste storage or CO_2 storage. In this spirit, even though I never had a chance to do so, I think I would appreciate very much working on conservation science, a part of which focuses on porous materials, and for which several of the physical processes that I already tackled are relevant.

Scientifically speaking, I see myself going on working on the topics described below, all

related to microscopic processes and their impact on the macroscopic behavior of the porous material:

- **In-pore crystallization**. In-pore crystallization includes salt crystallization and freezing. I appreciate the fact that those topics present an applicative interest while raising some very fundamental questions on the physical origin of the processes at stake, as I detailed in sections 4.1 and 4.2 for freezing and salt crystallization, respectively.
- **Deformations induced by capillarity and adsorption**. For this topic as well, I appreciate the combination of applicative and fundamental scientific interests. I also appreciate the extensive requirement to thermodynamics that their study requires.
- **Time-dependent deformations**, for which I remain puzzled by the fact that some phenomenological features (i.e., logarithmic kinetics of long-term creep, Pickett effect) are robustly observed on a variety of materials, while their physical origin remains debated.

Bibliography

Aadnoy, B. S. and Ong, S. (2003). Introduction to special issue on borehole stability. *Journal of Petroleum Science and Engineering*, 38(3-4):79–82. *Cited page 71*

Abuhaikal, M., Ioannidou, K., Petersen, T., Pellenq, R. J., and Ulm, F. J. (2018). Le Châtelier's conjecture: Measurement of colloidal eigenstresses in chemically reactive materials. *Journal of the Mechanics and Physics of Solids*, 112:334–344. *Cited pages 43, 47, and 50*

ACI Committee 209 (2008). Guide for modeling and calculating shrinkage and creep in hardened concrete (ACI 209.2R-08). Technical report, American Concrete Institute, Farmington Hills, MI. *Cited page 38*

Aili (2017). *Shrinkage and Creep of Cement-Based Materials under Multiaxial Load: Poromechanical Modeling for Application in Nuclear Industry*. PhD thesis. *Cited page 43*

Aili, A., Vandamme, M., Torrenti, J.-M., and Masson, B. (2015). Theoretical and practical differences between creep and relaxation Poisson's ratios in linear viscoelasticity. *Mechanics of Time-Dependent Materials*, 19(4):537–555. *Cited page 33*

Aili, A., Vandamme, M., Torrenti, J.-M., and Masson, B. (2018). Is long-term autogenous shrinkage a creep phenomenon induced by capillary effects due to self-desiccation? *Cement and Concrete Research*, 108:186–200. *Cited pages 38, 40, 41, and 42*

Aili, A., Vandamme, M., Torrenti, J.-M., Masson, B., and Sanahuja, J. (2016). Time evolutions of non-aging viscoelastic Poisson's ratio of concrete and implications for creep of C-S-H. *Cement and Concrete Research*, 90:144–161. *Cited pages 33, 36, 37, and 49*

Alonso, E. E., Romero, E., Hoffmann, C., and García-Escudero, E. (2005). Expansive bentonite-sand mixtures in cyclic controlled-suction drying and wetting. *Engineering Geology*, 81(3):213–226. *Cited page 70*

Anderson, R., Ratcliffe, I., Greenwell, H., Williams, P., Cliffe, S., and Coveney, P. (2010). Clay swelling — A challenge in the oilfield. *Earth-Science Reviews*, 98(3-4):201–216. *Cited page 71*

Andra (2005). Evaluation of the feasability of a geological repository in an argillaceous formation. Technical report, Andra. *Cited page 71*

ASTM International (2003). *ASTM C666. Standard Test Method for Resistance of Concrete to Rapid Freezing and Thawing*, volume 03. ASTM International, West Conshohocken, PA. *Cited page 55*

ASTM International (2013). *ASTM C457. Standard Test Method for Microscopical Determination of Parameters of the Air-Void System in Hardened Concrete 1*, volume 05. *Cited page 55*

ASTM International (2015). *ASTM C1012/C1012M-15. Standard Test Method for Length Change of Hydraulic-Cement Mortars Exposed to a Sulfate Solution*, volume 11. Publication Title: ASTM International. *Cited page 58*

Atanasova, M. T., Vyalikh, A., Scheler, U., and Focke, W. W. (2016). Characterization of rectorite from the Beatrix Gold Mine in South Africa. *Applied Clay Science*, 126:7–16. *Cited page 78*

Bangham, D. H. and Razouk, R. I. (1938). The swelling of charcoal. Part V. The saturation and immersion expansions and the heat of wetting. *Proceedings of the Royal Society A: Mathematical, Physical and Engineering Sciences*, 166(927):572–586. *Cited pages 65 and 67*

Barden, L., McGown, A., and Collins, K. (1973). The collapse mechanism in partly saturated soil. *Engineering Geology*, 7(1):49–60. *Cited page 67*

Bažant, Z. P. (1972). Thermodynamics of interacting continua with surfaces and creep analysis of concrete structures. *Nuclear Engineering and Design*, 20(2):477–505. *Cited page 49*

Bažant, Z. P., Hauggaard, A. B., Baweja, S., and Ulm, F.-J. (1997). Microprestress-solidification theory for concrete creep. I: Aging and drying effects. *Journal of Engineering Mechanics*, 123(11):1188–1194. *Cited pages 28, 47, and 50*

Bažant, Z. P., Hubler, M. H., and Yu, Q. (2011). Pervasiveness of excessive segmental bridge deflections: Wake-up call for creep. *ACI Structural Journal*, 108(6):766–774. *Cited page 27*

Bažant, Z. P. and Wittman, F. H. (1982). Mathematical models for creep and shrinkage of concrete. In *Creep and Shrinkage in Concrete Structures*. John Wiley & Sons. *Cited page 36*

Bažant, Z. P. and Xi, Y. (1994). Drying creep of concrete: Constitutive model and new experiments separating its mechanisms. *Materials and Structures*, 27(1):3–14. *Cited page 43*

Bažant, Z. P., Xi, Y., Baweja, S., and Carol, I. (1993). Preliminary guidelines and recommendations for characterizing creep and shrinkage in structural design codes. In *Proceedings of the 5th International RILEM Symposium on Creep and Shrinkage of Concrete (ConCreep 5)*, pages 805–829. *Cited page 35*

Bažant, Z. R. and Li, G. H. (2008). Comprehensive database on concrete creep and shrinkage. *ACI Materials Journal*, 105(6):635–637. *Cited pages 36, 38, and 40*

Beurthey, S. and Zaoui, A. (2000). Structural morphology and relaxation spectra of viscoelastic heterogeneous materials. *European Journal of Mechanics - A/Solids*, 19(1):1–16. *Cited page 31*

Bobko, C. P. and Ulm, F.-J. (2008). The nano-mechanical morphology of shale. *Mechanics of Materials*, 40(4-5):318–337. *Cited page 71*

Bornert, M., Chaix, J.-M., Doumalin, P., Dupré, J.-C., Fournel, T., Jeulin, D., Maire, E., Moreaud, M., and Moulinec, H. (2004). Mesure tridimensionnelle de champs cinématiques par imagerie volumique pour l'analyse des matériaux et des structures. *Instrumentation, Mesure, Métrologie*, 4(3-4):43–88. *Cited pages 68 and 69*

Bornert, M., Lenoir, N., Bésuelle, P., Pannier, Y., Hall, S., Viggiani, G., and Desrues, J. (2010). Discrete and continuum analysis of localised deformation in sand using X-ray μCT and volumetric digital image correlation. *Géotechnique*, 60(5):315–322. *Cited page 70*

Brisard, S., Chae, R. S., Bihannic, I., Michot, L., Guttmann, P., Thieme, J., Schneider, G., Monteiro, P. J. M., and Levitz, P. (2012). Morphological quantification of hierarchical geomaterials by X-ray nano-CT bridges the gap from nano to micro length scales. *American Mineralogist*, 97(2-3):480–483. *Cited page 78*

Brochard, L. (2011). *Poromécanique et Adsorption : Application Au Gonflement Du Charbon Lors Du Stockage Géologique Du Carbone*. PhD thesis. *Cited pages 7 and 8*

Brochard, L., Vandamme, M., and Pellenq, R. J.-M. (2012). Poromechanics of microporous media. *Journal of the Mechanics and Physics of Solids*, 60(4):606–622. *Cited pages 10 and 51*

Bruchon, J.-F., Pereira, J.-M., Vandamme, M., Lenoir, N., Delage, P., and Bornert, M. (2013a). Full 3D investigation and characterisation of capillary collapse of a loose unsaturated sand using X-ray CT. *Granular Matter*, 15(6):783–800. *Cited pages 67, 68, 69, and 70*

Bruchon, J.-F., Pereira, J.-M., Vandamme, M., Lenoir, N., Delage, P., and Bornert, M. (2013b). X-ray microtomography characterisation of the changes in statistical homogeneity of an unsaturated sand during imbibition. *Géotechnique Letters*, 3(2):84–88. *Cited page 67*

Bui, N. N. (2016). *Expansion and Stresses Induced by Crystallization in Cement-Based Materials in Presence of Sulfates*. PhD thesis, Université Paris-Est. *Cited pages 61 and 62*

Burgoyne, C. and Scantlebury, R. (2006). Why did Palau bridge collapse? *The Structural Engineer*, (June):30–37. *Cited page 27*

Buscarnera, G. and Nova, R. (2011). Modelling instabilities in triaxial testing on unsaturated soil specimens. *International Journal for Numerical and Analytical Methods in Geomechanics*, 35(2):179–200. *Cited page 68*

Cariou, S., Duan, Z., Davy, C., Skoczylas, F., and Dormieux, L. (2012). Poromechanics of partially saturated COx argillite. *Applied Clay Science*, 56:36–47. *Cited page 71*

Carrier, B., Vandamme, M., Pellenq, R. J.-M., Bornert, M., Ferrage, E., Hubert, F., and Van Damme, H. (2016). Effect of water on elastic and creep properties of self-standing clay films. *Langmuir: the ACS Journal of Surfaces and Colloids*, 32(5):1370–1379. *Cited pages 71, 74, 75, and 76*

Carrier, B., Vandamme, M., Pellenq, R. J.-M., and Van Damme, H. (2014). Elastic properties of swelling clay particles at finite temperature upon hydration. *The Journal of Physical Chemistry C*, 118(17):8933–8943. *Cited pages 71 and 75*

Carrier, B., Wang, L., Vandamme, M., Pellenq, R. J.-M., Bornert, M., Tanguy, A., and Van Damme, H. (2013). ESEM study of the humidity-induced swelling of clay film. *Langmuir: the ACS Journal of Surfaces and Colloids*, 29(41):12823–33. *Cited pages 65, 71, 72, and 74*

Cases, J. M., Bérend, I., François, M., Uriot, J. R., Michot, L. J., and Thomas, F. (1997). Mechanism of adsorption and desorption of water vapor by homoionic montmorillonite: 3. The Mg2+, Ca2+, Sr2+ and Ba2+ exchanged forms. *Clays and Clay Minerals*, 45(1):8–22. *Cited page 73*

Ceglarska-Stefańska, G. and Czapliński, A. (1993). Correlation between sorption and dilatometric processes in hard coals. *Fuel*, 72(3):413–417. *Cited page 8*

Chanvillard, G. (1999). *Le Matériau Béton: Connaissances Générales*. ENTPE-Aléas. *Cited pages 26 and 39*

Chen, H., Wyrzykowski, M., Scrivener, K., and Lura, P. (2013). Prediction of self-desiccation in low water-to-cement ratio pastes based on pore structure evolution. *Cement and Concrete Research*, 49:38–47. *Cited page 42*

Cheng, A. H. D. (1997). Material coefficients of anisotropic poroelasticity. *International journal of rock mechanics and mining sciences & geomechanics abstracts*, 34(2):199–205. *Cited page 14*

Christensen, R. M. (1982). *Theory of Viscoelasticity: An Introduction*. Academic Press, New York. *Cited pages 34 and 35*

Christensen, R. W. and Wu, T. H. (1964). Analysis of clay deformation as a rate process. *Journal of the Soil Mechanics and Foundations Division*, 90(6):125–160. *Cited page 51*

Clarkson, C.R., B. R. (2000). Binary gas adsorption / desorption isotherms: Effect of moisture and coal composition upon carbon dioxide selectivity over methane. *International Journal of Coal Geology Bustinr International Journal of Coal Geology*, 42(42):241–271. *Cited page 13*

Cody, G. D., Larsen, J. W., and Siskin, M. (1988). Anisotropic solvent swelling of coals. *Energy and Fuels*, 2(3):340–344. *Cited page 14*

Commissariat Général au Développement Durable (2010). Le régime d'assurance des catastrophes naturelles en France métropolitaine entre 1995 et 2006. Technical report. *Cited page 71*

Connell, L. D., Lu, M., and Pan, Z. (2010). An analytical coal permeability model for tri-axial strain and stress conditions. *International Journal of Coal Geology*, 84(2):103–114. *Cited page 9*

Correns, C. W. (1949). Growth and dissolution of crystals under linear pressure. *Discussions of the Faraday Society*, 5:267. *Cited page 59*

Cour des Comptes (2016). Rapport public annuel 2016, Tome 1 : La maintenance des centrales nucléaires : Une politique remise à niveau, des incertitudes à lever. Technical report. *Cited page 33*

Coussy, O. (2004). *Poromechanics*. John Wiley & Sons. *Cited page 14*

Coussy, O. (2005). Poromechanics of freezing materials. *Journal of the Mechanics and Physics of Solids*, 53(8):1689–1718. *Cited page 54*

Coussy, O., Dangla, P., Lassabatère, T., and Baroghel-Bouny, V. (2004). The equivalent pore pressure and the swelling and shrinkage of cement-based materials. *Materials and Structures*, 37(1):15–20. *Cited pages 65 and 67*

Coussy, O. and Monteiro, P. (2008). Poroelastic model for concrete exposed to freezing temperatures. *Cement and Concrete Research*, 38(1):40–48. *Cited pages 56 and 58*

Cowin, S. C. (2004). Anisotropic poroelasticity: Fabric tensor formulation. *Mechanics of Materials*, 36(8):665–677. *Cited page 14*

Cui, X. and Bustin, R. M. (2005). Volumetric strain associated with methane desorption and its impact on coalbed gas production from deep coal seams. *AAPG Bulletin*, 89(9):1181–1202. *Cited page 9*

Damidot, D. and Glasser, F. P. (1993). Thermodynamic investigation of the CaO-Al2O3-CaSO4-H2O system at 25°C and the influence of Na2O. *Cement and Concrete Research*, 23(1):221–238. *Cited page 60*

Dangla, P. (2017). Bil-2.4, a modeling platform based on finite volume/element method. *Cited page 21*

Day, S., Fry, R., Sakurovs, R., and Weir, S. (2010). Swelling of coals by supercritical gases and its relationship to sorption. *Energy and Fuels*, 24(4):2777–2783. *Cited page 22*

Delage, P., Cui, Y. J., and Antoine, P. (2005). Geotechnical problems related with loess deposits in Northern France. In *Proceedings of International Conference on Problematic Soils*, pages 517–540. *Cited page 67*

Desarnaud, J., Bonn, D., and Shahidzadeh, N. (2016). The pressure induced by salt crystallization in confinement. *Scientific Reports*, 6. *Cited page 59*

Désarnaud, J., Grauby, O., Bromblet, P., Vallet, J. M., and Baronnet, A. (2013). Growth and dissolution of crystal under load: New experimental results on KCl. *Crystal Growth and Design*, 13(3):1067–1074. *Cited page 59*

Doumalin, P. and Bornert, M. (2000). Micromechanical applications of digital image correlation techniques. In *Interferometry in Speckle Light*, pages 67–74. Springer Berlin Heidelberg, Berlin, Heidelberg. *Cited page 73*

Dudley, J. H. (1970). Review of collapsing soils. *Journal of Soil Mechanics & Foundations Division*, 97(SM1):925–947. *Cited page 67*

Duke, C. M. and Davis, H. E. (1944). Some properties of concrete under sustained combined stresses. *ASTM Proceedings*, 44. *Cited page 34*

Ebrahimi, D., Whittle, A. J., and Pellenq, R. J.-M. (2014). Mesoscale properties of clay aggregates from potential of mean force representation of interactions between nanoplatelets. *The Journal of Chemical Physics*, 140(15):154309. *Cited page 71*

Enever, J. R. and Hennig, A. (1997). The relationship between permeability and effective stress for Australian coals and its implications with respect to coalbed methane exploration and reservoir modelling. In *1997 International Coalbed Methane Symposium*, Tuscaloosa, AL. *Cited pages 9 and 10*

Espinosa-marzal, R. M. and Scherer, G. W. (2010). Advances in understanding damage by salt crystallization. *Accounts of Chemical Research*, 43(6):897–905. *Cited page 59*

Espinoza, D. N., Pereira, J.-M., Vandamme, M., Dangla, P., and Vidal-Gilbert, S. (2015). Desorption-induced shear failure of coal bed seams during gas depletion. *International Journal of Coal Geology*, 137:142–151. *Cited pages 16 and 20*

Espinoza, D. N., Shovkun, I., Makni, O., and Lenoir, N. (2016). Natural and induced fractures in coal cores imaged through X-ray computed microtomography — Impact on desorption time. *International Journal of Coal Geology*, 154-155:165–175. *Cited page 14*

Espinoza, D. N., Vandamme, M., Dangla, P., Pereira, J.-M., and Vidal-Gilbert, S. (2013). A transverse isotropic model for microporous solids: Application to coal matrix adsorption and swelling. *Journal of Geophysical Research: Solid Earth*, 118(12):6113–6123. *Cited pages 13 and 14*

Espinoza, D. N., Vandamme, M., Pereira, J.-M., Dangla, P., and Vidal-Gilbert, S. (2014). Measurement and modeling of adsorptive–poromechanical properties of bituminous coal cores exposed to CO2: Adsorption, swelling strains, swelling stresses and impact on fracture permeability. *International Journal of Coal Geology*, 134-135:80–95. *Cited pages 13, 14, 15, 16, 17, 18, and 19*

Eurocode (2004). EN 1992-1-1, Eurocode 2: Design of concrete structures - Part 1-1: General rules and rules for buildings. Technical report. *Cited pages 27 and 38*

Fagerlund, G. (1993). The long time water absorption in the air-pore structure of concrete. Technical report, Lund Institute of Technology. Publication Title: Report TVBM. *Cited pages 55 and 57*

Ferrage, E., Lanson, B., Sakharov, B. A., and Drits, V. A. (2005). Investigation of smectite hydration properties by modeling experimental X-ray diffraction patterns: Part I. Montmorillonite hydration properties. *American Mineralogist*, 90(8-9):1358–1374. *Cited page 73*

Fib (2012). Fib Model Code 2010. Technical report. *Cited pages 27 and 38*

Flatt, R. J., Caruso, F., Sanchez, A. M. A., and Scherer, G. W. (2014). Chemo-mechanics of salt damage in stone. *Nature communications*, 5:4823. *Cited page 59*

Furr, H. L. (1967). Creep tests of two-way prestressed concrete. *ACI Journal Proceedings*, 64(6):288–294. *Cited page 34*

Gajewicz, A., Gartner, E., Kang, K., McDonald, P., and Yermakou, V. (2016). A 1H NMR relaxometry investigation of gel-pore drying shrinkage in cement pastes. *Cement and Concrete Research*, 86:12–19. *Cited page 65*

Gale, J. (2004). Geological storage of CO2: What do we know, where are the gaps and what more needs to be done? *Energy*, 29(9-10):1329–1338. *Cited page 6*

Gartner, E. (2004). Industrially interesting approaches to "low-CO2" cements. *Cement and Concrete Research*, 34(9):1489–1498. *Cited page 27*

Gartner, E. (2017). What are BYF cements , and how do they differ from CSA cements ? In *The Future of Cement, 200 Years after Louis Vicat*. *Cited page 27*

Gawin, D., Pesavento, F., and Schrefler, B. A. (2006). Hygro-thermo-chemo-mechanical modelling of concrete at early ages and beyond. Part II: Shrinkage and creep of concrete. *International Journal for Numerical Methods in Engineering*, 67(3):332–363. *Cited page 39*

Gopalakrishnan, K., Neville, A., and Chali, A. (1969). Creep Poisson's ratio of concrete under multiaxial compression. *ACI Journal*, (December):1008–1020. *Cited pages x, 35, and 36*

Gor, G. Y., Huber, P., and Bernstein, N. (2017). Adsorption-induced deformation of nanoporous materials—A review. *Applied Physics Reviews*, 4(1):011303. *Cited page 12*

Granger, L. and Torrenti, J.-M. (1995). Evaluation of the lifespan of a nuclear PC vessel in terms of delayed behaviour and loss prestress. In *IABSE Symposium on Extending the Lifespan of Structures*. *Cited page 34*

Grasley, Z. C. and Leung, C. K. (2011). Desiccation shrinkage of cementitious materials as an aging, poroviscoelastic response. *Cement and Concrete Research*, 41(1):77–89. *Cited page 39*

Hajibabaee, A., Grasley, Z., and Ley, M. T. (2016). Mechanisms of dimensional instability caused by differential drying in wet cured cement paste. *Cement and Concrete Research*, 79:151–158. *Cited page 39*

Hilton, H. H. (2017). Elastic and viscoelastic Poisson's ratios: The theoretical mechanics perspective. *Materials Sciences and Applications*, 08(04):291–332. *Cited page 34*

Hol, S., Peach, C. J., and Spiers, C. J. (2011). Applied stress reduces the CO2 sorption capacity of coal. *International Journal of Coal Geology*, 85(1):128–142. *Cited page 12*

Hol, S. and Spiers, C. J. (2012). Competition between adsorption-induced swelling and elastic compression of coal at CO2 pressures up to 100 MPa. *Journal of the Mechanics and Physics of Solids*, 60(11):1862–1882. *Cited pages 8, 14, and 65*

Hu, D., Zhou, H., Zhang, F., and Shao, J. (2010). Evolution of poroelastic properties and permeability in damaged sandstone. *International Journal of Rock Mechanics and Mining Sciences*, 47(6):962–973. *Cited page 14*

Hua, C., Acker, P., and Ehrlacher, A. (1995). Analyses and models of the autogenous shrinkage of hardening cement paste. I. Modelling at macroscopic scale. *Cement and Concrete Research*, 25(7):1457–1468. *Cited pages 38 and 39*

Kaddhour, G., Ando, E., Salager, S., Bésuelle, P., Viggiani, C., Hall, S., and Desrues, J. (2013). Application of X-ray tomography to the characterisation of grain-scale mechanisms in sand. pages 195–200. *Cited page 70*

Kosmatka, S. H., Panarese, W. C., and Kerkhoff, B. (2002). *Design and Control of Concrete Mixtures*, volume 5420. Portland Cement Association Skokie, IL. *Cited page 2*

Kowalczyk, P., Ciach, A., and Neimark, A. V. (2008). Adsorption-induced deformation of microporous carbons: Pore size distribution effect. *Langmuir*, 24(13):6603–6608. *Cited page 8*

Kuhn, M. R. and Mitchell, J. K. (1993). New perspectives on soil creep. *Journal of Geotechnical Engineering*, 119(3):507–524. *Cited page 51*

Kulasinski, K., Guyer, R., Derome, D., and Carmeliet, J. (2015). Poroelastic model for adsorption-induced deformation of biopolymers obtained from molecular simulations. *Physical Review E*, 92(2):022605. *Cited pages 12 and 13*

Kwok, C.-Y. and Bolton, M. D. (2010). DEM simulations of thermally activated creep in soils. *Géotechnique*, 60(6):425–433. *Cited page 50*

Kwok, C. Y. and Bolton, M. D. (2013). DEM simulations of soil creep due to particle crushing. *Géotechnique*, 63(16):1–12. *Cited page 51*

Laird, D. A. (2006). Influence of layer charge on swelling of smectites. *Applied Clay Science*, 34(1-4):74–87. *Cited page 2*

Lake, L. W. and Srinivasan, S. (2004). Statistical scale-up of reservoir properties: Concepts and applications. *Journal of Petroleum Science and Engineering*, 44(1-2):27–39. *Cited page 22*

Lambe, T. W. and Whitman, R. W. (1969). *Soil Mechanics*. Wiley, New York, NY. *Cited pages 44, 51, and 76*

Lantuéjoul, C. (1991). Ergodicity and integral range. *Journal of Microscopy*, 161(3):387–403. *Cited page 68*

Laubach, S. E., Marrett, R. A., Olson, J. E., and Scott, A. R. (1998). Characteristics and origins of coal cleat: A review. *International Journal of Coal Geology*, 35(1-4):175–207. *Cited pages 6 and 22*

Le, T. M., Fatahi, B., and Khabbaz, H. (2012). Viscous behaviour of soft clay and inducing factors. *Geotechnical and Geological Engineering*, 30(5):1069–1083. *Cited page 51*

Le Roy, R. (1996). Déformations instantanées et différées des bétons à hautes performances. Technical report, Laboratoire Central des Ponts et Chaussées. *Cited pages ix, 29, 30, and 39*

Le Roy, R., Le Maou, F., and Torrenti, J.-M. (2017). Long term basic creep behavior of high performance concrete: Data and modelling. *Materials and Structures*, 50(1). *Cited page 33*

Levine, J. R. (1996). Model study of the influence of matrix shrinkage on absolute permeability of coal bed reservoirs. *Geological Society, London, Special Publications*, 109(1):197–212. *Cited page 8*

L'Hermite, R. (1959). What do we know about the plastic deformation and creep of concrete? *RILEM Bulletin*, 1:888–896. *Cited page 34*

Li, X., Grasley, Z. C., Bullard, J. W., and Garboczi, E. J. (2017). Irreversible desiccation shrinkage of cement paste caused by cement grain dissolution and hydrate precipitation. *Materials and Structures*, 50(2):1–14. *Cited page 39*

Lins, Y. and Schanz, T. (2005). Determination of hydro-mechanical properties of sand. In *Unsaturated Soils: Experimental Studies. Proceedings of the International Conference "From Experimental Evidence towards Numerical Modeling of Unsaturated Soils"*, pages 15–32, Berlin/Heidelberg. Springer-Verlag. *Cited page 68*

Liu, H.-H. and Rutqvist, J. (2010). A new coal-permeability model: Internal swelling stress and fracture-matrix interaction. *Transport in Porous Media*, 82(1):157–171. *Cited page 18*

Liu, J., Spiers, C. J., Peach, C. J., and Vidal-Gilbert, S. (2016). Effect of lithostatic stress on methane sorption by coal: Theory vs. experiment and implications for predicting in-situ coalbed methane content. *International Journal of Coal Geology*, 167:48–64. *Cited page 12*

Liu, J., Wang, J., Chen, Z., Wang, S., Elsworth, D., and Jiang, Y. (2011). Impact of transition from local swelling to macro swelling on the evolution of coal permeability. *International Journal of Coal Geology*, 88(1):31–40. *Cited page 22*

Lothenbach, B., Pelletier-chaignat, L., and Winnefeld, F. (2012). Stability in the system CaO-Al2O3-H2O. *Cement and Concrete Research*, 42(12):1621–1634. *Cited page 60*

Luan, Y. and Ishida, T. (2013). Enhanced shrinkage model based on early age hydration and moisture status in pore structure. *Journal of Advanced Concrete Technology*, 11(12):360–373. *Cited page 39*

Maruyama, I., Gartner, E., Beppu, K., and Kurihara, R. (2018). Role of alcohol-ethylene oxide polymers on the reduction of shrinkage of cement paste. *Cement and Concrete Research*, (April):0–1. *Cited page 63*

Maruyama, I., Rymeš, J., Vandamme, M., and Coasne, B. (2019). Cavitation of water in hardened cement paste under short-term desorption measurements. *Materials and Structures*. *Cited pages 63 and 66*

Mayercsik, N. P., Felice, R., Ley, M. T., and Kurtis, K. E. (2014). A probabilistic technique for entrained air void analysis in hardened concrete. *Cement and Concrete Research*, 59:16–23. *Cited page 55*

Mayercsik, N. P., Vandamme, M., and Kurtis, K. E. (2016). Assessing the efficiency of entrained air voids for freeze-thaw durability through modeling. *Cement and Concrete Research*, 88:43–59. *Cited pages 54, 55, 56, and 57*

Mazumder, S., Karnik, A. A., and Wolf, K.-H. A. (2006). Swelling of coal in response to CO2 sequestration for ECBM and its effect on fracture permeability. *SPE Journal*, 11(03):390–398. *Cited pages 6 and 8*

Michot, L. J., Bihannic, I., Thomas, F., Lartiges, B. S., Waldvogel, Y., Caillet, C., Thieme, J., Funari, S. S., and Levitz, P. (2013). Coagulation of Na-montmorillonite by inorganic cations at neutral pH. A combined transmission X-ray microscopy, small angle and wide angle X-ray scattering study. *Langmuir*, 29(10):3500–3510. *Cited page 78*

Miller, M., Bobko, C. P., Vandamme, M., and Ulm, F.-J. (2008). Surface roughness criteria for cement paste nanoindentation. *Cement and Concrete Research*, 38(4):467–476. *Cited page 2*

Moore, R. L., Loftin, D., and Palmer, I. (2011). History matching and permeability increases of mature coalbed methane wells in San Juan basin. In *Asia Pacific Oil & Gas Conference and Exhibition*, pages 1–12, Jakarta, Indonesia. *Cited pages 6 and 7*

Morcote, A., Mavko, G., and Prasad, M. (2010). Dynamic elastic properties of coal. *Geophysics*, 75(6):E227–E234. *Cited page 22*

Mori, T. and Tanaka, K. (1973). Average stress in matrix and average elastic energy of materials with misfitting inclusions. *Acta metallurgica*, 21(5):571–574. *Cited pages 31 and 36*

Mousseau, N., Béland, L. K., Brommer, P., Joly, J.-F., El-Mellouhi, F., Machado-Charry, E., Marinica, M.-C., and Pochet, P. (2012). The Activation-Relaxation Technique: ART Nouveau and Kinetic ART. *Journal of Atomic, Molecular, and Optical Physics*, 2012:1–14. *Cited page 76*

Muñoz-Castelblanco, J., Delage, P., Pereira, J.-M., and Cui, Y.-J. (2011). Some aspects of the compression and collapse behaviour of an unsaturated natural loess. *Géotechnique Letters*, 1(2):17–22. *Cited pages 68 and 70*

Müller, H. S., Anders, I., Breiner, R., and Vogel, M. (2013). Concrete: Treatment of types and properties in fib Model Code 2010. *Structural Concrete*, 14(4):320–334. *Cited page 27*

Myers, A. L. and Prausnitz, J. M. (1965). Thermodynamics of mixed-gas adsorption. *AIChE Journal*, 11(1):121–127. *Cited page 23*

Nabarro, F. R. N. (2001). The time constant of logarithmic creep and relaxation. *Materials Science and Engineering A*, 309-310:227–228. *Cited pages 44 and 47*

Nabarro, F. R. N. and DeVilliers, H. L. (1995). *The Physics of Creep: Creep and Creep-Resistant Alloys*. Taylor & Francis, London. OCLC: 832576348. *Cited page 44*

Naillon, A., Joseph, P., and Prat, M. (2018). Ion transport and precipitation kinetics as key aspects of stress generation on pore walls induced by salt crystallization. *Physical Review Letters*, 120(3):034502. *Cited page 59*

Neimark, A. V., Coudert, F.-X., Boutin, A., and Fuchs, A. H. (2010). Stress-based model for the breathing of metal-organic frameworks. *The Journal of Physical Chemistry Letters*, 1(1):445–449. *Cited page 13*

Neville, A. M., Dilger, W. H., and Brooks, J. J. (1983). *Creep of Plain and Structural Concrete*. Construction Press. *Cited pages 26, 34, and 48*

Nikoosokhan, S., Vandamme, M., and Dangla, P. (2014). A poromechanical model for coal seams saturated with binary mixtures of CH4 and CO2. *Journal of the Mechanics and Physics of Solids*, 71(1):97–111. *Cited pages 13 and 23*

Nonat, A. (2004). The structure and stoichiometry of C-S-H. *Cement and Concrete Research*, 34(9):1521–1528. *Cited page 2*

Okotie, V. U. and Moore, R. L. (2010). Well production challenges and solutions in a mature , very low-pressure coalbed methane reservoir. In *Canadian Unconventional Resources & International Petroleum Conference*, pages 1–17, Calgary, Canada. *Cited page 16*

Oldecop, L. and Alonso, E. (2012). Modelling the degradation and swelling of clayey rocks bearing calcium-sulphate. *International Journal of Rock Mechanics and Mining Sciences*, 54:90–102. *Cited page 59*

Ortega, J. A., Ulm, F.-J., and Abousleiman, Y. N. (2007). The effect of the nanogranular nature of shale on their poroelastic behavior. *Acta Geotechnica*, 2(3):155–182. *Cited page 71*

Pachon-Rodriguez, E. A., Guillon, E., Houvenaghel, G., and Colombani, J. (2011). Pressure solution as origin of the humid creep of a mineral material. *Physical Review E*, 84(6):066121. *Cited page 28*

Pachon-Rodriguez, E. A., Guillon, E., Houvenaghel, G., and Colombani, J. (2014). Wet creep of hardened hydraulic cements — Example of gypsum plaster and implication for hydrated Portland cement. *Cement and Concrete Research*, 63:67–74. *Cited page 28*

Palmer, I. and Mansoori, J. (1998). How permeability depends on stress and pore pressure in coalbeds: A new model. *SPE Reservoir Evaluation and Engineering*, pages 539–544. *Cited page 8*

Pan, Z. and Connell, L. D. (2012). Modelling permeability for coal reservoirs: A review of analytical models and testing data. *International Journal of Coal Geology*, 92:1–44. *Cited page 9*

Pan, Z. J. and Connell, L. D. (2007). A theoretical model for gas adsorption-induced coal swelling. *International Journal of Coal Geology*, 69(4):243–252. *Cited page 6*

Parrinello, M. and Rahman, A. (1982). Strain fluctuations and elastic constants. *The Journal of Chemical Physics*, 76(5):2662. *Cited page 73*

Parrott, L. J. (1979). A study of transitional thermal creep in hardened cement paste. *Magazine of Concrete Research*, 31(107):99–103. *Cited page 51*

Pellenq, R. J.-M., Caillol, J. M., and Delville, A. (1997). Electrostatic attraction between two charged surfaces: A (N,V,T) Monte Carlo simulation. *The Journal of Physical Chemistry B*, 101(42):8584–8594. *Cited page 77*

Peng, Y., Liu, J., Wei, M., Pan, Z., and Connell, L. D. (2014). Why coal permeability changes under free swellings: New insights. *International Journal of Coal Geology*, 133:35–46. *Cited page 22*

Perrier, L., Pijaudier-Cabot, G., and Grégoire, D. (2015). Poromechanics of adsorption-induced swelling in microporous materials: A new poromechanical model taking into account strain effects on adsorption. *Continuum Mechanics and Thermodynamics*, 27(1-2):195–209. *Cited page 12*

Pickett, G. (1942). The effect of change in moisture-content on the creep of concrete under a sustained load. In *ACI Journal Proceedings*, volume 38. *Cited page 27*

Pijaudier-Cabot, G., Vermorel, R., Miqueu, C., and Mendiboure, B. (2011). Revisiting poromechanics in the context of microporous materials. *Comptes Rendus Mécanique*, 339(12):770–778. *Cited page 12*

Piltner, R. and Monteiro, P. J. M. (2000). Stress analysis of expansive reactions in concrete. *Cement and Concrete Research*, 30(6):843–848. *Cited page 54*

Ping, X. and Beaudoin, J. (1992). Mechanism of sulphate expansion I. Thermodynamic principle of crystallization pressure. *Cement and Concrete Research*, 22(4):631–640. *Cited page 59*

Pini, R. (2009). *Enhanced Coal Bed Methane Recovery Finalized to Carbon Dioxide Storage*. PhD thesis, ETH Zürich. *Cited page 9*

Plimpton, S. (1995). Fast parallel algorithms for short-range molecular dynamics. *Journal of Computational Physics*, 117(1):1–19. *Cited page 73*

Polivka, M., Pirtz, D., and Adams, R. F. (1963). Studies of creep in mass concrete. *ACI Special Publication*, 6:257–286. *Cited page 34*

Powers, T. C. (1945). A working hypothesis for further studies of frost resistance of concrete. *Journal of the American Concrete Institute*, 41(4):245–272. *Cited page 54*

Powers, T. C. (1949). The air requirement of frost-resistant concrete. *Highway Research Board Proceedings*, 29:184–211. *Cited pages 54 and 55*

Powers, T. C. (1955). Basic considerations pertaining to freezing and thawing tests. *Portland Cement Association Journal Research and Development Laboratories*. *Cited page 58*

Powers, T. C. (1968). *Mechanisms of Shrinkage and Reversible Creep of Hardened Portland Cement Paste*. London, England. Publication Title: International Conference on the Structure of Concrete. *Cited page 28*

Powers, T. C. and Brownyard, T. L. (1948). Studies of the physical properties of hardened Portland cement paste. *Journal of the American Concrete Institute*, 22(Bulletin 22):22. *Cited page 41*

Pusch, R. and Yong, R. N. (2006). *Microstructure of Smectite Clays and Engineering Performance*. Taylor & Francis, New York, NY. *Cited page 2*

Rahoui, H. (2018). *Contribution to Understanding the Action of SRA in Cementitious Materials: Experiments and Modeling*. PhD thesis, Université Paris-Est. *Cited pages 65 and 66*

Ravikovitch, P. I. and Neimark, A. V. (2006). Density functional theory model of adsorption deformation. *Langmuir*, 22(26):10864–8. *Cited page 11*

République Française (2006). Loi n° 2006-739 du 28 juin 2006 de programme relative à la gestion durable des matières et déchets radioactifs. *Cited page 71*

Reucroft, P. J. and Sethuraman, A. R. (1987). Effect of pressure on carbon dioxide induced coal swelling. *Energy and Fuels*, 1(1):72–75. *Cited page 8*

RILEM Technical Committee TC-242-MDC (2015). RILEM draft recommendation: TC-242-MDC multi-decade creep and shrinkage of concrete: Material model and structural analysis. *Materials and Structures*, 48(4):753–770. *Cited pages 27, 35, and 38*

Robertson, E. (2005). Modeling permeability in coal using sorption-induced strain data. *Proceedings of SPE Annual Technical Conference and Exhibition*, pages 1–10. *Cited page 8*

Ross, A. D. (1954). Experiments on the creep of concrete under two-dimensional stressing. *Magazine of Concrete Research*, 6(16):3–10. *Cited page 34*

Scheel, M., Seemann, R., Brinkmann, M., Di Michiel, M., Sheppard, A., Breidenbach, B., and Herminghaus, S. (2008). Morphological clues to wet granular pile stability. *Nature materials*, 7(3):189–93. *Cited page 70*

Schramm, L. L. and Kwak, J. C. T. (1982). Influence of exchangeable cation composition on the size and shape of montmorillonite particles in dilute suspension. *Clays and Clay Minerals*, 30(1):40–48. *Cited page 77*

Scott, M., Mazumder, S., and Jiang, J. (2012). Permeability increase in Bowen basin coal as a result of matrix shrinkage during primary depletion. In *SPE Asia Pacific Oil and Gas Conference and Exhibition*, volume 4, pages 1–21, Perth, Australia. *Cited page 22*

Scrivener, K. L., Crumbie, A. K., and Laugesen, P. (2004). The interfacial transition zone (ITZ) between cement paste and aggregate in concrete. *Interface Science*, 12(4):411–421. *Cited page 31*

Seidle, J., Jeansonne, M., and Erickson, D. (1992). Application of matchstick geometry to stress dependent permeability in coals. In *SPE Rocky Mountain Regional Meeting*. Society of Petroleum Engineers. *Cited page 8*

Sellier, A., Multon, S., Buffo-Lacarrière, L., Vidal, T., Bourbon, X., and Camps, G. (2015). Concrete creep modelling for structural applications: Non-linearity, multi-axiality, hydration, temperature and drying effects. *Cement and Concrete Research*, pages 1–15. *Cited pages 38 and 43*

Selvadurai, A. P. S. and Suvorov, A. P. (2016). Thermo-poromechanics: Applications and developments. In *Thermo-Poroelasticity and Geomechanics*, pages 1–44. Cambridge University Press, Cambridge. *Cited page 9*

Shahidzadeh-Bonn, N., Desarnaud, J., Bertrand, F., Chateau, X., and Bonn, D. (2010). Damage in porous media due to salt crystallization. *Physical Review E - Statistical, Nonlinear, and Soft Matter Physics*, 81(6):1–6. *Cited page 59*

Shi, J.-Q. and Durucan, S. (2005). A model for changes in coalbed permeability during primary and enhanced methane recovery. *SPE Reservoir Evaluation & Engineering*, 8(04):291–299. *Cited page 9*

Sinko, R., Vandamme, M., Bažant, Z. P., and Keten, S. (2016). Transient effects of drying creep in nanoporous solids: Understanding the effects of nanoscale energy barriers. *Proceedings of the Royal Society A: Mathematical, Physical and Engineering Science*, 472(2191):20160490. *Cited page 44*

Skalny, J., Marchand, J., and Odler, I. (2002). *Sulfate Attack on Concrete*. Spon Press. *Cited page 58*

Steiger, M. (2005). Crystal growth in porous materials - I: The crystallization pressure of large crystals. *Journal of Crystal Growth*, 282(3-4):455–469. *Cited page 59*

Suter, J. L., Coveney, P. V., Greenwell, H. C., and Thyveetil, M. A. (2007). Large-scale molecular dynamics study of montmorillonite clay: Emergence of undulatory fluctuations and determination of material properties. *Journal of Physical Chemistry C*, 111(23):8248–8259. *Cited page 78*

Tadros, M. K., Al-Omaishi, N., Seguirant, S. J., and Gallt, J. G. (2003). NCHRP Report 496, Prestress Losses in Pretensioned High-Strength Concrete Bridge Girders. Technical report, Transportation Research Board. *Cited page 27*

Tang, C. S., Tang, A. M., Cui, Y. J., Delage, P., Schroeder, C., and De Laure, E. (2011). Investigating the swelling pressure of compacted crushed-Callovo-Oxfordian claystone. *Physics and Chemistry of the Earth*, 36(17-18):1857–1866. *Cited page 59*

Taylor, H. F. W. (1997). *Cement Chemistry*. Thomas Telford, London, 2nd edition. Publication Title: Inorganic Chemistry. *Cited page 58*

Tian, B. and Cohen, M. D. (2000). Does gypsum formation during sulfate attack on concrete lead to expansion? *Cement and Concrete Research*, 30(1):117–123. *Cited page 59*

Torrenti, J.-M. and Le Roy, . R. (2017). Analysis of some basic creep tests on concrete and their implications for modeling. (November 2016):1–6. *Cited page 29*

Ulm, F.-J., Le Maou, F., and Boulay, C. (1999). Creep and shrinkage coupling: New review of some evidence. *Revue Française de Génie Civil*, 3:21–37. *Cited page 39*

USGS (2004). Landslide types and processes. Technical report, USGS. *Cited page 71*

Valenza, J. J. and Scherer, G. W. (2006). Mechanism for salt scaling. *Journal of the American Ceramic Society*, 89(4):1161–1179. *Cited page 58*

Van Damme, H. (2018). Concrete material science: Past, present, and future innovations. *Cement and Concrete Research*, (April):0–20. *Cited page 26*

van der Lee, J. (1998). Thermodynamic and mathematical concepts of CHESS. Technical report, Ecole des Mines de Paris. *Cited page 60*

Van Workum, K. and de Pablo, J. J. (2003). Improved simulation method for the calculation of the elastic constants of crystalline and amorphous systems using strain fluctuations. *Physical Review E*, 67(1):011505. *Cited page 73*

Vandamme, M. (2019). Two models based on local microscopic relaxations to explain long-term basic creep of concrete. *Proceedings of the Royal Society A: Mathematical, Physical and Engineering Science*. *Cited pages 44, 46, 47, and 49*

Vandamme, M., Brochard, L., Lecampion, B., and Coussy, O. (2010). Adsorption and strain: The CO2-induced swelling of coal. *Journal of the Mechanics and Physics of Solids*, 58(10):1489–1505. *Cited page 51*

Vandamme, M., Dangla, P., Nikoosokhan, S., and Brochard, L. (2014). Modeling the poromechanical behavior of microporous and mesoporous solids: Application to coal. In *Nonlinear Elasticity and Hysteresis*, pages 105–126. Wiley-VCH Verlag GmbH & Co. KGaA, Weinheim, Germany. *Cited page 21*

Vandamme, M., Tweedie, C. C. A., Constantinides, G., Ulm, F.-J., and Van Vliet, K. J. (2012). Quantifying plasticity-independent creep compliance and relaxation of viscoelastoplastic materials under contact loading. *Journal of Materials Research*, 27(1):302–312. *Cited page 29*

Vandamme, M. and Ulm, F.-J. (2009). Nanogranular origin of concrete creep. *Proceedings of the National Academy of Sciences of the United States of America*, 106(26):10552–10557. *Cited pages 28 and 29*

Vandamme, M. and Ulm, F.-J. (2013). Nanoindentation investigation of creep properties of calcium silicate hydrates. *Cement and Concrete Research*, 52:38–52. *Cited pages 31 and 77*

Vermorel, R. and Pijaudier-Cabot, G. (2014). Enhanced continuum poromechanics to account for adsorption induced swelling of saturated isotropic microporous materials. *European Journal of Mechanics, A/Solids*, 44:148–156. *Cited page 12*

Vlahinić, I., Thomas, J. J., Jennings, H. M., and Andrade, J. E. (2012). Transient creep effects and the lubricating power of water in materials ranging from paper to concrete and Kevlar. *Journal of the Mechanics and Physics of Solids*, 60(7):1350–1362. *Cited page 44*

Wellman, H. W. and Wilson, A. T. (1965). Salt weathering, a neglected geological erosive agent in coastal and arid environments. *Nature*, 205(4976):1097–1098. *Cited page 59*

Wittmann, F. H. (1982). Creep and shrinkage mechanisms. In *Creep and Shrinkage in Concrete Structures*, pages 129–161. *Cited pages 28 and 50*

Worrell, E., Price, L., Martin, N., Hendriks, C., and Meida, L. O. (2001). Carbon dioxide emissions from the global cement industry. *Annual Review of Energy and the Environment*, 26(1):303–329. *Cited pages 26 and 27*

Wu, Y., Liu, J. S., Elsworth, D., Chen, Z. W., Connell, L., and Pan, Z. J. (2010). Dual poroelastic response of a coal seam to CO2 injection. *International Journal of Greenhouse Gas Control*, 4(4):668–678. *Cited page 9*

Wyrzykowski, M., Lura, P., Pesavento, F., and Gawin, D. (2011). Modeling of internal curing in maturing mortar. *Cement and Concrete Research*, 41(12):1349–1356. *Cited page 39*

Ye, H. (2015). Creep mechanisms of calcium–silicate–hydrate: An overview of recent advances and challenges. *International Journal of Concrete Structures and Materials*. *Cited page 51*

York, G. P., Kennedy, T. W., Perry, E. S., and Thompson, J. N. (1972). Experimental determination of Poisson's ratio for creep. *ACI Special Publication*, 34:535–546. *Cited page 34*

Yuan, J., Lu, H., Yang, Q., and Ling, J. (2017). Mechanisms on the salt-frost scaling of concrete. *Journal of Materials in Civil Engineering*, 29(3):D4015002. *Cited page 58*

Zabat, M., Vayer-Besançon, M., Harba, R., Bonnamy, S., and Van Damme, H. (1997). Surface topography and mechanical properties of smectite films. *Progress in Colloid & Polymer Science*, 105(1):96–102. *Cited page 72*

Zeng, Q., Fen-Chong, T., Dangla, P., and Li, K. (2011). A study of freezing behavior of cementitious materials by poromechanical approach. *International Journal of Solids and Structures*, 48(22-23):3267–3273. *Cited page 58*

Zhang, Q., Le Roy, R., Vandamme, M., and Zuber, B. (2014). Long-term creep properties of cementitious materials: Comparing microindentation testing with macroscopic uniaxial compressive testing. *Cement and Concrete Research*, 58:89–98. *Cited pages 28, 30, and 32*